Development and Characterization of Novel Bioluminescent Reporters of Cellular Activity

By

Derrick C. Cumberbatch

Dissertation

Submitted to the Faculty of the

Graduate School of Vanderbilt University

in partial fulfillment of the requirements

for the degree of

DOCTOR OF PHILOSOPHY

in

Biological Sciences

May 10, 2019

Nashville, Tennessee

Approved:

C. David Weaver, Ph.D.

Douglas McMahon, Ph.D.

Qi Zhang, Ph.D.

Carl Johnson, Ph.D.

To my beloved and supportive wife Alicia,

and

to my parents Cameron and Marcia Cumberbatch.

ACKNOWLEDGEMENTS

This work was made possible by financial support from the NIMH grants MH107713 and MH116150 awarded to Carl Johnson, Ph.D. as well as funds provided by the Vanderbilt University Dissertation Enhancement Grant, graciously awarded to me by the Graduate School. I appreciate Dr. Carl Johnson for taking me into his lab and providing me with ample tools that aided in the successful completion of my Ph.D. I would like to express gratitude to my committee members Drs. David Weaver, Douglas McMahon, Qi Zhang, and the late Dr. Donna Webb for guiding me through the process of becoming a competent researcher.

I would also like to make special mention of Jie Yang, Ph.D. whose persistent efforts and sage advice were an ever-present help during my graduate studies. His one-on-one training provided me with many skills that will serve me well as a molecular biologist. Meaningful contributions from the other current and past members of the Johnson lab group, Yao Xu, Ph.D., Tetsuya Mori, Ph.D., Shuqun Shi, Ph.D., Chi Zhao, Ph.D., Peijun Ma, Ph.D., He Huang, Ph.D., Kathryn Campbell, Briana Wyzinski, Kevin Kelly, Maria Luisa Jabbur, Carla O'Neale and Ian Dew deserve to be highlighted here as well.

I am thankful for the many professors, fellow graduate students and undergraduate students who have given me helpful insights and suggestions on my Ph.D. journey, making special mention of Hu Lan, Ph.D., Jeff Jones Ph.D., Siwei He, Ph.D., Xiaohan Wang, Ph.D., Sam Centanni, Ph.D., Kim Kwangho, Ph.D., Gary Sulikowski, Ph.D., Paige Vinson, Ph.D., and Emily Days.

TABLE OF CONTENTS

LIST OF FIGURES

LIST OF SUPPLEMENTARY FIGURES

LIST OF ABBREVIATIONS

AAV	adeno-associated virus
ACSF	artificial cerebrospinal fluid
ANEP	aminonaphthylethenyl-pyridinium
ANOVA	analysis of variance
ATP	adenosine triphosphate
a.u.	arbitrary units
BF	brightfield
BRET	Bioluminescence resonance energy transfer
$[Ca^{2+}]$	calcium ion concentration
cAMP	cyclic adenosine monophosphate
Cbcl	carbachol
CheR	CheRiff
CHO	Chinese hamster ovary
ChR	channelrhodopsin
CM	cardiomyocyte
CRC	concentration response curve
DIV	day *in vitro*
DNA	deoxyribonucleic acid
EB-CCD	electron bombardment charged-coupled device
EDTA	Ethylenediaminetetraacetic acid
EGTA	ethylene glycol-bis(β-aminoethyl ether)-N,N,N′,N′-tetraacetic acid
EM	emission
EM-CCD	electron multiplying charged-coupled device
EX	excitation
FBS	fetal bovine serum
FLuc	firefly luciferase
FRET	Förster Resonance Energy Transfer
GECI	genetically encoded calcium indicator
GFP	green fluorescent protein
GLuc	Gaussia luciferase
HEPES	4-(2-hydroxyethyl)-1-piperazineethanesulfonic acid
hIPSC	human induced pluripotent stem cell

hM_1R	human muscarinic receptor 1
His6	6-histadine
HTS	high throughput screen
K_d	dissociation constant
kDa	kiloDalton
LP	longpass
MOPS	3-(N-morpholino)-propanesulfonic acid
NLuc	NanoLuc luciferase
NpHR	halorhodopsin
Opn4	melanopsin
PBS	phosphate buffered saline
pCAG	CAG promoter
pCMV	CMV promoter
PCR	polymerase chain reaction
PMT	photon multiplier tube
pMyo2	Myo2 promoter
RLuc	Renilla luciferase
ROI	region of interest
SNR	signal to noise ratio
SOC	store operated calcium
TG	thapsigargin
TnC	troponin C
VGCC	voltage gated calcium channel
YFP	yellow fluorescent protein

CHAPTER I

GENERAL INTRODUCTION

The aim of this Ph.D. dissertation thesis is to explore novel methods for imaging living cells and tissues in the hopes that the tools developed here could be used to push the boundaries of research in a variety of fields including: neuroscience, small molecule drug discovery, and microscopic diagnostic techniques. This introductory chapter will cover the historical significance and the use of bioluminescence in cell biological optical methods, the efficacy of data acquisition using optogenetics, and the ever-expanding repertoire of reporters that can monitor specific cellular events.

Bioluminescence

The glow of a firefly on a summer's evening is the result of a remarkable chemical reaction. This type of light production by an organism is called bioluminescence and it is exhibited by a large variety of species, including bacteria, fungi, insects, and fish (Wilson & Hastings, 1998; Haddock, 2010). In its most basic form, bioluminescence occurs when an enzyme (called a luciferase) catalyzes an oxygen-dependent reaction with its substrate (called a luciferin) and produces light (DeLuca & McElroy, 1974; Baldwin, 1996). The high-energy, oxidized intermediate is the entity that releases a photon of light. Aside from oxygen dependency and the need for a luciferin substrate, few of the luciferases from different taxonomic families of organisms resemble each other, and therefore are hypothesized to have evolved separately, and at different times throughout evolutionary history (Wilson & Hastings, 1998). Bioluminescence occurs in a

variety of colors (Viviani, 2002) and each luciferase-luciferin reaction differs with respect to the reaction's conditions. For some luciferases, the temperature and pH can change the spectrum of their bioluminescence emission (Zhao et al., 2005; Liang et al., 2012; Ugarova et al., 2005).

While many of us are most familiar with firefly bioluminescence, the vast majority of bioluminescent organisms live in the ocean (Fig. 1.1) (Widder, 2010; Haddock, 2010). There are many physiological structures and unique behaviors that organisms have developed to take advantage of the emitted light. Some have specialized organs whose sole function is light emission (e.g. sea pansies). Others, that are not intrinsically bioluminescent, have created a symbiotic relationship with bioluminescent microorganisms, and can culture them in their bodies under conditions that are ideal for the microorganism's growth (e.g. angler fish) (Wilson & Hastings,

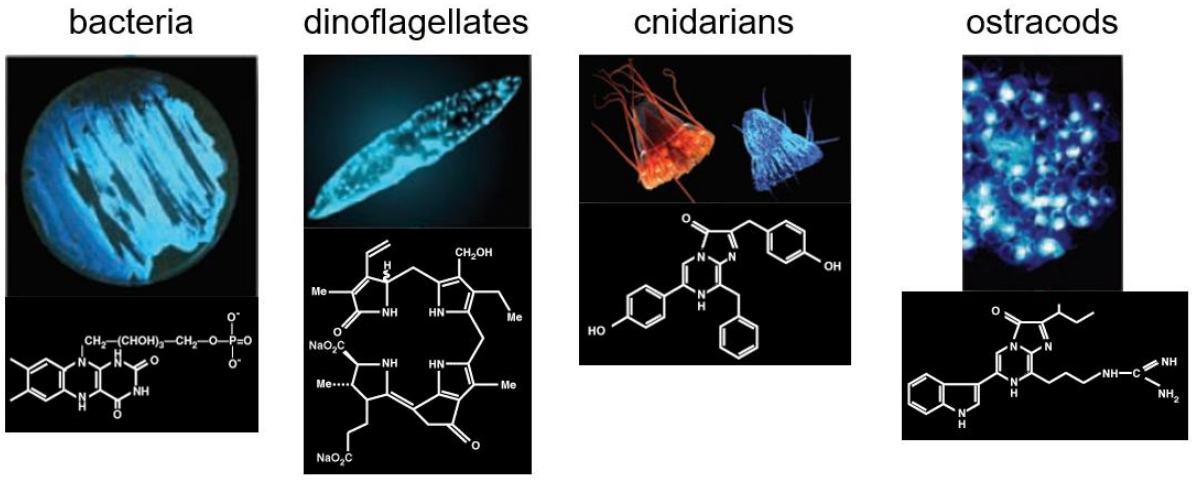

Figure 1.1. The diversity of bioluminescence exhibited by marine organisms. The photographs depict the labeled group of organisms with the luciferin each uses to produce light displayed underneath. Adapted from Widder, 2010.

1998). There is even a fish that spits its bioluminescence into the water around it, which some

scientists speculate might be to startle would-be predators (Wilson & Hastings, 2013). After witnessing naturally-occurring bioluminescence, it did not take scientists very long to hypothesize ways to harness that light to measure cellular processes.

Illuminating the Cell Through Microscopy

One of the most important pillars of modern molecular biology is built on the scientist's ability to observe phenomena at the single cell level. In this field, the "cell" is the ultimate model system, so analytical methods for detecting microscopic, cell-level phenomena in real-time are invaluable. As early as the 17th century, light microscopy gave scientists unprecedented access into the microbial world (reviewed extensively by Amos, 2000). Cellular light microscopy takes advantage of the contrasting textures created by the absorption, reflection and diffraction of light as it passes through different materials inside the cell. Components within the such as the cell membrane, nucleus, and cytoplasm each have different optical properties and a microscope makes them visible once magnified. However, most cells do not possess multicolored natural pigments that delineate discrete cellular mechanisms from each other so it is difficult to determine whether two similar-looking structures may have different origins. Cells are dynamic environments, and visualizing pathways and reactions within cells in real time is very important. Recent advances in imaging technology have not only allowed scientists to visualize these processes, but also to control these processes using light.

Contributions of the humble jellyfish *Aequorea victoria*

The green fluorescent protein from the jellyfish *Aequorea victoria* (AvGFP) is well-known to most scientists. The role that the AvGFP played in modern microscopy is cemented in the fact

that researchers Osamu Shimomura, Martin Chalfie, and Roger Tsien shared the 2008 Nobel Prize in Chemistry for its discovery and subsequent development (Shimomura et al., 1962). Briefly, this GFP's protein structure is composed of a beta-barrel structure that forms between the N- and C-termini of the protein, with a chromophore nestled in the middle of the beta-barrel. The chromophore is formed by a cyclization reaction between three of the structural groups on amino acids within the barrel. These amino acids can be serine, threonine, tyrosine, and/or glycine (Tsien, 1998). The chromophore can absorb 470 – 490 nm light and emit 500 – 520 nm light (wavelengths of lower energy than that which was absorbed). The excited electrons use the absorbed energy to enter a higher energy-state and their subsequent return to a ground state forces them to release the energy as photons of light (Jabloński, 1933). This describes the basic premise of fluorescence phenomena and AvGFP absorbs blue light (~490 nm) and emits green light (~510 nm).

AvGFP, and proteins like it, are now ubiquitous in the cellular microscopy field, but when AvGFP was originally discovered, it was actually just an unintended by-product of aequorin purification. Shimomura and colleagues (Shimomura et al., 1962) spent many years studying the bioluminescence mechanisms of marine invertebrates and were able to deduce that some of these organisms used a GFP as an energy carrier for its bioluminescent protein. This photoprotein was named aequorin and catalyzes the oxidation of coelenterazine to produce light, but only when Ca^{2+} ions are present (Fig. 1.2) (Inoue et al., 1976). The light emitted in the intact jellyfish is green, but when the aequorin is purified from the animals, its intrinsic emission is blue. The two proteins become separated during the purification process but the jellyfish naturally uses bioluminescence

resonance energy transfer (BRET) from aequorin to GFP to produce the green light (Morin & Hastings, 1971).

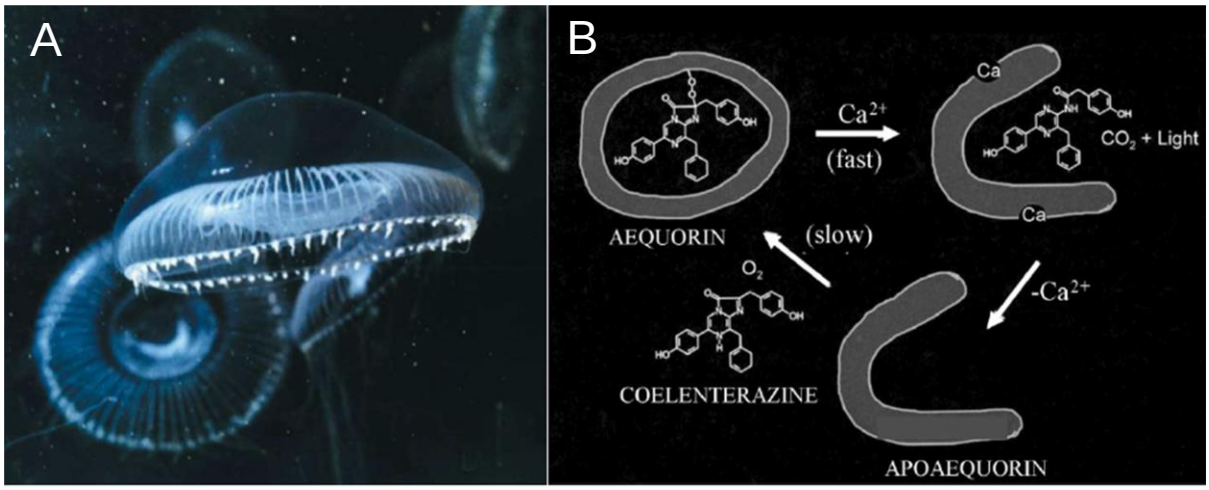

Figure 1.2. The bioluminescent jellyfish *Aequorea victoria*. (**A**) photograph of the jellyfish swimming in its natural habitat. The bioluminescent aequorin and GFP reside in the small protrusions on the underside of the bell-shaped body. (**B**) Illustration of the Ca^{2+}-dependent bioluminescence mechanism of aequorin including the relative reaction speeds. Adapted from Shimomura, 2005.

First glimpses of intracellular Ca^{2+} neural activity using Aequorin bioluminescence

From about the 1970's through to the early 1990s, photoprotein biology was increasingly used by researchers in many fields. Since Ca^{2+} is one of the major secondary messengers within cells the Ca^{2+}-dependent luciferase aequorin proved highly valuable to understanding intracellular Ca^{2+} dynamics. Scientists were first able to see how Ca^{2+} is directly involved in muscle function by microinjecting purified aequorin into the muscle fibers of the barnacle *Balanus nubilus* allowing researcher to observe calcium transients (Ridgway & Ashley, 1967). Aequorin also gave us the first visualizations of Ca^{2+}'s waves in vertebrate egg fertilization (Ridgway et al., 1977; Gilkey et

al., 1987). After the DNA sequence of aequorin was deciphered and cloned, more articles were published outlining its use in measuring intracellular Ca^{2+} (Inouye et al., 1985) and even allowed the first observations of the circadian rhythm of cytosolic Ca^{2+} in plants like tobacco and *Arabidopsis* (Johnson et al., 1995).

Changes in cytosolic Ca^{2+} concentration regulate a wide variety of mechanisms within most cell types. Extracellular and endoplasmic reticulum calcium levels are very high relative to the cytosol. This creates a large concentration gradient between these two Ca^{2+} stores and the cytosol. When cytosolic Ca^{2+} levels increase, it can be a signal to respond in a variety of ways including increasing DNA transcription via the transcription factor cAMP response element binding protein (CREB) (Montminy & Bilezikjian, 1987). Proper regulation of intracellular Ca^{2+} is also integral to neural function and heart health (Fearnley et al., 2011). Additionally, cytosolic Ca^{2+} fluxes can trigger even more release from intracellular Ca^{2+} stores through store operated Ca^{2+} channels (SOCC) and this in turn can lead to downstream effects ranging from cell motility to immune responses (Lewis, 2007). In summary, the intracellular regulation of calcium ion concentration is very important.

Even though aequorin was useful in the early days of Ca^{2+} research, it has practical constraints that limit its supremacy as an optical tool. Aequorin is a Ca^{2+} sensitive protein and as such, needs to be purified with buffers that are completely free of even minuscule amounts of Ca^{2+} (requires buffers containing the chelators EDTA/EGTA). Initially, before aequorin could be expressed in cells genetically, only a few labs were able to perform the necessary micro injection protocol. Furthermore, in order for aequorin purified from bacteria to luminesce, it first has to be incubated with its luminescent substrate coelenterazine for many hours, and as soon as a molecule reacts with Ca^{2+}, the coelenterazine is oxidized and the apo-aequorin would need more hours to

recharge. Even the ability to genetically encode aequorin could not circumvent the issues relating to the swift decline in luminescence intensity once Ca^{2+} is introduced and the long time needed to recharge apo-aequorin to active aequorin (Prasher et al., 1985). For the aequorin-coelenterazine complex to emit light, a covalent, peroxide bond has to first be formed between the two and this takes a significant amount of time (Head et al., 2000).

In contrast to the technical difficulties experienced with aequorin, once the DNA sequence of AvGFP was known, it became clear that it was relatively easy to use for reporting gene expression and was not dependent on any other secondary element like a substrate (Prasher et al., 1992, Chalfie et al., 1994). Additionally, instead of reliance on an enzymatic luminescence reaction, the light emitted from GFP results from fluorescence and is therefore proportional to the excitation light supplied by the researcher. Therefore, the light output can be better controlled. I suspect this is the main reason why fluorescent-proteins research and the tools used to detect fluorescence experienced a much faster rate of development when compared with bioluminescence techniques (Tsien, 1998; Day & Davidson, 2009).

The Rise of GFP and Fluorescence-based imaging

Since the discovery and application of AvGFP in cell biology, fluorescent proteins from many other organisms have been characterized and implemented. These new proteins also have a host of different absorption and excitation spectra, and therefore we currently have fluorescent proteins that emit light of colors throughout the visible spectrum (~400 – 700 nm). There are multiple examples of blue, green, yellow, red and far-red fluorescent proteins, each with properties that are more amenable to some physiological applications compared with others (Rizzo et al.,

2004; Heim et al., 1994; Yang et al., 1996; Shaner et al., 2013; Kremers et al., 2006; Nguyen et al., 2005; Lam et al., 2012; Shaner et al., 2004; Piatkevich et al., 2013; Chu et al., 2014).

Scientists have also mutated the natural amino acid structure of fluorescent proteins to create even more color variants. Moreover, they have created some mutant proteins that change color or turn off or turn on depending on the wavelength of excitation light (Patterson & Lippincott-Schwartz, 2002; Ando et al., 2002). These fluorescent proteins are called photo-switchable or photo-activatable molecules.

The development of functional variants of bioluminescent proteins has progressed at a much slower rate compared with fluorescence proteins. Most mutations in photoprotein chromophore structure produce non-active enzymes and therefore only a limited number of luminescence proteins exist. Development of new luciferases depends on both the luciferase and the luciferin, while new fluorescent proteins only rely on the structure of the protein itself thus decreasing the molecular complexity of fluorescence-based techniques. Furthermore, the fact that GFP does not usually have a significant effect on a protein's endogenous function when fused to it is crucial to its ubiquitous use (Crivat & Taraska, 2012). Microscopy techniques evolved to take advantage of the properties of GFP for both live and fixed samples. Fluorescence microscopy is one such microscopic technique. It entails using an excitation light source which elicits fluorescence emission from a sample, then passes that light through a series of filters to collect the maximum amount of light emitted by the fluorescent protein. Any non-specific light is blocked by the filters and only the optimal wavelength is focused onto the detector (Webb & Brown, 2013). Whether the detector is image-forming (like a camera) or solely for total light collection (like a photomultiplier tube (PMT)), the light emitted by the sample is collected and measured.

One of the drawbacks of the fluorescence microscope is that sometimes too much emission of light can be a bad thing. Being able to see minute details in an image is related to the resolution of the image. This can depend on a variety of factors including, but not limited to, the detector's properties for image acquisition. But resolution can also be affected by light itself. To form images, light has to be focused onto a surface, and the better the focus, the better the image. Since detectors such as cameras can form images using the lenses in the microscope to refract the light towards it, having the right focus is paramount. This is a real challenge because a cell is a three-dimensional object and therefore some fluorescence will occur above and/or below the plane of focus. However, even epifluorescence objectives with the most precisely aligned lenses allow some unfocused light to reach the camera and as such, decrease the resolution and the signal-to-noise ratio of images. Clearly, epifluorescence is good for some applications but not ideal for others.

The invention of confocal microscopy was one of the ways around this particular problem (Minsky, 1988). A confocal microscope has all of the basic components that a simple, epifluorescence microscope would have, but with one added feature. Confocal microscopes, and their various iterations, pass the collected light through a pin-hole. The pin-hole reduces the total amount of light gathered and by extension, significantly reduces the amount of unfocused light that reaches the detector, allowing for limited collections of light outside of the focal plane and much more precisely focused imaging. This type of imaging has given us greater appreciation of the complexity of the three-dimensional structure inside cells. Furthermore, the high-intensity light sources that were developed in tandem with confocal microscopy methods had a variety of added benefits for cellular imaging. However, with all things, every new method has its pros and cons.

Drawbacks and limitations of optical methods

In the late 1990's, when there was a boon in the interest in fluorescence imaging, scientists were just beginning to pioneer real-time, cellular imaging. Now, it is routine for a GFP-tagged protein of interest to be genetically targeted to a cell of choice. Multiple forms of microscopy have been advancing rapidly over the last few decades because innovators have been in a never-ending search to find the best trade-offs to increase the signal-to-noise ratio while maximizing the spatial and temporal resolution of any images captured.

For any imaging application, the brightest signal possible per unit of time is desirable as well as maintaining the largest difference between background noise and true signal. The faster an image is recorded, the better the process can be understood kinetically because fewer intermediate events are left out. But it takes time for a detector to capture a certain amount of light to achieve adequate signal-to-noise ratio (SNR) and the number of photons that trigger the detector depends on the sensitivity of the detector. So, if the total light output is increased, then the imaging speed can be increased. If light output is low, image acquisition time will have to be slowed down to allow for enough photons of light to hit and register in the detector. When using fluorescence microscopy, scientists can simply increase the light intensity being introduced to the system to overcome this problem, up to the limits of phototoxicity and/or photobleaching. But with bioluminescence, the chemistry of the luciferase / luciferin must be modified for increased photo output. There is only so much substrate that can be added before the reaction reaches saturation.

The adenosine triphosphate (ATP)-dependent luciferase from *Photinus pyralis* (firefly luciferase, or FLuc) has been used for a variety of applications (e.g. cell viability assays, ATP concentration measurements, and gene expression) and over the years, scientists have continued to push the limits of what luciferases can assay. However, luciferases generally suffer from

complications that fluorescent proteins do not have – namely, (1) substrate-dependence and (2) low photon output.

On the other hand, fluorescence imaging also has its drawbacks. Fluorescence depends on atomic changes within bonds that allow electrons to move between multiple excited states once they have been exposed to certain wavelengths of light. And while this occurs very efficiently in fluorescence sensors, many living tissues also contain compounds that can fluoresce – termed autofluorescence. This extra background light, unavoidable because of the excitation light of the external light source, can diminish the signal-to-noise ratio while imaging (to be addressed in Chapter II). Fluorescence imaging can also lead to photobleaching effects, because the excessive incident light can negatively and irreversibly change the chemical bond structure in the fluorescence chromophore (Magidson & Khodjakov, 2013). Confocal and multiphoton fluorescence microscopy can alleviate some of these issues (Denk et al., 1990), but they still cause cell-damaging phototoxicity and photobleaching (Wäldchen et al., 2015) and cannot be used to image photosensitive tissues like plants and the retina. Also, the high photon flux of multiphoton microscopy can cause temperature increases in the tissue being imaged so many precautions need to be taken into consideration when using this technique for constant imaging (Benninger & Piston, 2013). Furthermore, overlapping fluorescence spectra and/or crosstalk while using optogenetics methods creates ambiguous imaging results.

Optogenetics

With the increase in microscopic techniques came improvements to excitatory light devices (e.g. lasers) and the added bonus of using light as an actuator instead of just as an excitatory tool for observations. Researchers cloned one of the light sensitive ion channels responsible for

phototaxis in the alga *Chlamydomonas reinhardtii* and expressed it in a variety of cells from other organisms (Nagel et al., 2002; Nagel et al., 2003; Nagel et al., 2005). They noticed that the channel would open and let positive ions pass through the membrane and depolarize the cell as long as light of an appropriate wavelength and intensity was shone on the transgenic cells. The modulation of ion fluxes in and out of cells forms the basis for regulating neurological cellular activity. The field of biology where light is used to experimentally manipulate the activity state of cells was born and is called "Optogenetics" (Deisseroth et al., 2006).

The cationic channel originally cloned from *Chlamydomonas* was called channelrhodopsin (ChR). Channelrhodopsins have since been isolated from other organisms, but they all exist as transmembrane proteins and bind the chemical retinal to create a chromophore within its structure (Nagel et al., 2002; Ardevol & Hummer, 2018; Kato et al., 2012). When the appropriate wavelength of light shines upon ChR, the channel opens and allows positive monovalent ions like sodium (Na^+), hydrogen (H^+) and/or potassium (K^+) to traverse the cell membrane down their concentration gradients and affect the ionic milieu in the cytoplasm. Currently, researchers have at their disposal multiple variants of these channelrhodopsins that exhibit different properties. There are those with varying sensitivities to light intensity (Aravanis et al., 2007; Hochbaum et al., 2014) and some that pass negative ions, thereby hyperpolarizing neurons (Zhang et al., 2007). Many labs all across the world are using these unique families of proteins to address important biological / medical questions.

One of the exciting prospects of all of these advances in optical neurobiology is the potential to optically control the activation and inhibition cascades of neural networks. This ability could lead to researchers ultimately being able to understand the cellular basis for memory formation, spinal injuries and even mental and behavior disorders. But unfortunately, we are

currently faced with a serious problem that is limited by our dependence on light itself namely, the crosstalk between the optogenetic actuators and the fluorescence-based sensors. This impasse could provide an opportunity for bioluminescence-based techniques to once again push the boundaries of optical imaging.

The Fluorescence-Optogenetics Disadvantage and the Bioluminescence Advantage

Microscopy and GFP-based imaging techniques are still the most common and efficient ways of assessing cellular states. However, even if you can correct the autofluorescence, photobleaching, and phototoxicity issues outlined previously, there are still other issues that uniquely affect optogenetic studies.

If we are using light to monitor the fluorescent protein/sensor, and then also use light to stimulate a biochemical change within the cells with an optogenetic actuator, we only have roughly a 300-nm range of light to work with (visible wavelengths of light exist between ~400-700 nm). Obviously, scientists have thought of this issue for many years, and have come up with a variety of solutions. I will use channelrhodopsins and cytosolic Ca^{2+}-signaling as an example.

White light is made up of a collection of wavelengths of varying energies. These visible wavelengths of light are a small fraction of what science characterizes as electromagnetic radiation. Of the visible wavelengths, what we describe as the blue wavelengths trigger the opening of channelrhodopsins (ChRs) to elicit ion diffusion and neural activation (Nagel et al., 2003). A Ca^{2+} concentration sensor based on GFP would also absorb light in the blue range and therefore, if both the ChR and the GFP-based Ca^{2+} sensor were expressed in the same cell, whenever the GFP was excited to assay Ca^{2+} concentration, the cell might be stimulated via ChR activation (Miyawaki et al., 1997; Wang et al., 2008; Yang et al., 2016). This problem has been mitigated by

the creation of Ca^{2+}-sensors that are based on red fluorescent proteins (RFPs) and therefore use yellow/orange wavelengths for visualization (Akerboom et al., 2013). There are filters and light sources (sometimes lasers) with sufficient separation between the blue and yellow wavelengths that we can be confident that in the same cell line, we can stimulate ChR with blue light and measure the fluorescence change in the RFP-based Ca^{2+} sensor using yellow light excitation without significant overlap (crosstalk) between the different kinds of light.

The problem becomes more severe when you want to apply additional optical actuators into the system. Channelrhodopsins (ChRs) activate neurons by depolarization while halorhodopsins (NpHRs) inhibit neural activity by hyperpolarizing the neurons, thereby preventing them from firing (Zhang et al., 2007). The good news is that these two types of light-gated channels are opened by different wavelengths of light so neither affects the other's function. The bad news arises when a researcher desires to combine the ChR and NpHR in the same cell while simultaneously trying to use a fluorescence Ca^{2+} sensor to measure the resulting neural activity. NpHR is stimulated by yellow light and ChR is stimulated by blue light and these two combine to virtually cover most of the available visible wavelengths of light that our current fluorescent sensors could use. This particular issue will be explored in depth in Chapter II. Therefore, bioluminescence instead of fluorescence could be a methodology that can take full advantage of all our advances in optical control and image acquisition, without the drawbacks of the optical crosstalk in the visible spectrum.

Bioluminescence reporters continue to shine

Of the known luciferases that exist in nature, firefly luciferase is the most well-studied and the most used in scientific research. Firefly luciferase (Fluc) was first cloned by De Wet and

colleagues (de Wet et al., 1985) and the protein structure was determined by Conti and colleagues in 1996 (Conti et al., 1996). The protein is about 62 kilodaltons (kDa) and uses a substrate called D-luciferin (DeLuca & McElroy, 1974). In the presence of oxygen, ATP, Mg^{2+} and D-luciferin, firefly luciferase catalyzes an oxidation reaction to produce light and CO_2 (DeLuca & McElroy, 1974). The light emitted by firefly luciferase peaks at 560 nm at room temperature and neutral pH (Viviani, 2002). Interestingly, at 37 °C the peak emission becomes red-shifted to around 611 nm (Liang et al., 2012). Scientists have taken advantage of the properties of the firefly luciferase reaction to create a variety of reporters of cellular activity. In particular, firefly luciferase has been used extensively as a reporter for gene expression (Rodriguez et al., 1988; Yamazaki et al., 2000), protein abundance (Yoo et al., 2004), and cell viability (by measuring intracellular ATP concentration (Ludin & Thore, 1975). With the discovery and implementation of differently-colored insect luciferases, which all use the same D-luciferin substrate (Branchini et al., 2005; Niwa et al., 2010), researchers have been able to make numerous scientific advances where a luciferase reporter was optimal. So, although there has not been a Nobel Prize awarded for the discovery and use of bioluminescence as a cellular reporter, there are still numerous applications where luciferases are just as valuable, if not more valuable, than a fluorescence-based reporter.

One field that has taken full advantage of bioluminescence technology is the subdivision of chronobiology which studies circadian rhythms. Researchers studying circadian rhythms are trying to understand the mechanisms governing the apparent 24-hour rhythms that exist in bacteria, fungi, plants and animals. Almost all organisms have an internal, approximately 24-hour rhythm that can function autonomously, can be entrained to environmental cues, and are unexpectedly unperturbed by small temperature changes (reviewed in Bass & Takahashi, 2010 and Johnson, et al., 2017). Firefly luciferase that has been codon optimized for mammalian expression (*luc2*

synthetic gene) (Groskreutz et al., 1995) has been used to report both transcriptional and translational reporters of activity. Under the control of circadian promoters or directly fused to a protein of interest, researchers are able to see what environmental factors, drug treatments, and mutations affect mammalian circadian rhythms (Ono et al., 2013; Tackenberg & McMahon, 2018). Similar techniques have also been used in *Drosophila*, zebrafish and fungi (Brandes et al., 1996; Kaneko & Cahill, 2005; Gooch et al., 2008). Scientists were also able to take the genetically-encoded, luciferase-luciferin pathway (luxABCDE) from the bioluminescent bacteria *Vibrio harveyi* (Belas et al., 1982; Meighen, 1991), transfer it to non-luminescent cyanobacteria, and under the control of rhythmic transcriptional promotors, showed that cyanobacteria have a robust circadian timing mechanism (Kondo et al., 1993; Ishiura et al., 1998; Ouyang et al., 1998). This type of reporter gave researchers insights into how cyanobacteria regulate their entire genomes (Liu et al., 1995), providing a basis for high throughput screening for mutants that impact the core clock mechanism (Kondo et al., 1994). This has no doubt broadened the scope of the kinds of questions future researchers will ask.

As helpful and insightful as all of these luciferase-based techniques have proven to be, one of the biggest drawbacks is that bacterial and insect luciferases are not very bright in transgenic organisms studied in the laboratory setting. Instead of exhibiting the bright yellow glow that we see on warm summers night the light emitted by the transgenic animals is not usually detectable by the human eye (Niwa et al., 2010). In general, terrestrial luciferases produce relatively dim light in the lab, and therefore highly sensitive detection devices are needed to capture the photon output from these reactions, thus limiting the usability of these reporters, especially in contexts where rapid reaction kinetics are of interest. Additionally, scientists have been trying to determine what changes can be made to either the luciferase itself, the luciferin substrate, or the environment to

promote greater brightness for luciferase emission in the lab. As yet, the firefly luciferase and D-luciferin combination has not been amenable to an increase of brightness but the marine luciferases have shown greater promise in this regard.

Improvements in Bioluminescence Imaging

On the other hand, there is a much larger number of marine species exhibiting bioluminescence as compared with creatures from the land and these luciferases have shown greater promise regarding brightness. Of these, the coelenterazine-based luciferases like Renilla luciferase (RLuc) and Gaussia luciferase (GLuc) have been most widely used by researchers (Loening et al., 2007a; Tannous et al., 2005). Renilla luciferase comes from the sea pansy *Renilla reniformis* (Loening et al., 2007a), and has undergone artificial mutagenesis screens to give both a brighter version called RLuc8 (Loening et al., 2006) and a red-shifted version named RLuc8.6 (Loening et al., 2007b). These proteins have been used in many cellular assays including protein-protein interaction experiments using BRET or functional complementation of two halves of a split RLuc. Many of these luciferases (like aequorin) are very bright but coelenterazine, which is the substrate used by most of the commonly used marine luciferases, is rapidly auto-oxidized in media designed for mammalian cells, causing luciferase-mediated light emission to decline sharply after coelenterazine is added to a luciferase system in mammalian cell culture (Zhao et al., 2004). This auto-oxidation also generates an undesirable, dim autoluminescence background. A more stable synthetic substrate was created by Promega called ViviRen™ (Otto-Duessel et al., 2006) which was made by fusing nitrogenous and ester-linked groups onto the key oxidation sites of coelenterazine h, so that the substrate can only emit light after it has been de-esterified by non-specific, intracellular esterases. Therefore, ViviRen™ does not autoluminesce in media, and is still

sufficiently hydrophobic that it permeates into cells where it becomes available to a luciferase after de-esterification. While this new development proved helpful, there were still many more improvements that can been made.

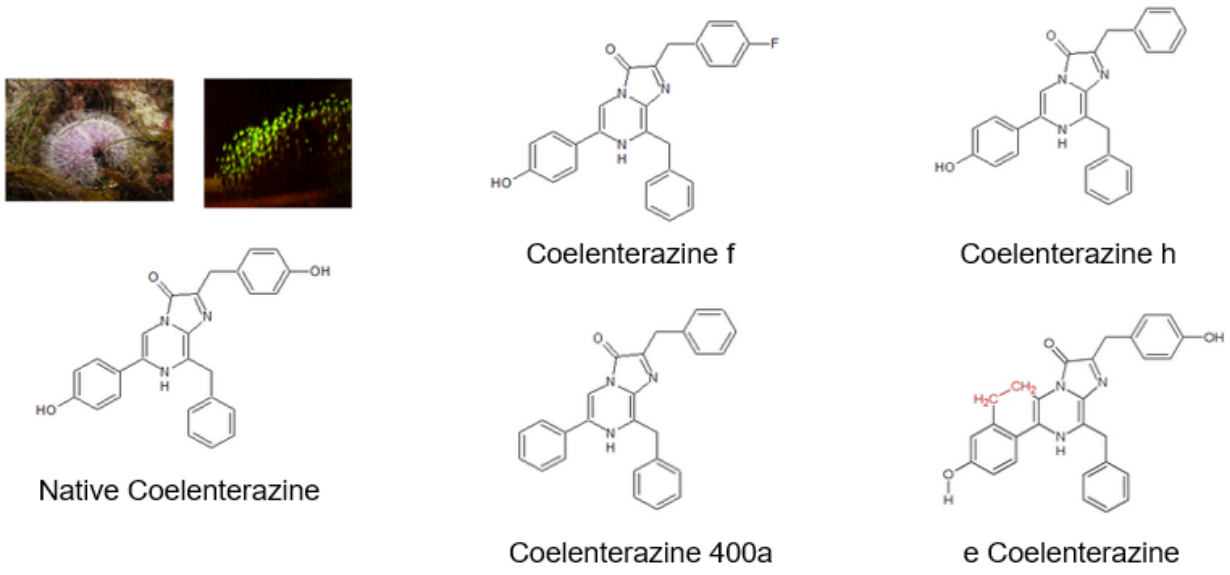

Figure 1.3. *Renilla reniformis* bioluminescence and some of the synthesized coelenterazine analogs. Top left panels show photographs of *Renilla reniformis* in the light and in the dark highlighting the location of the bioluminescent organs. Native coelenterazine describes the naturally-occurring coelenterazine which many marine invertebrates use for bioluminescence. The coelenterazine analogs' chemical structures are shown to demonstrate how changing different atoms can increase emission intensity (coelenterazine f, h, and e) or shift the peak emission wavelength (coelenterazine 400a).

Additional attempts to modify coelenterazine to be a more ideal substrate have yielded even more variants. At its core, coelenterazine is an imidazopyrazinone molecule (Inouye & Sasaki, 2007; Inouye et al., 2000). The atoms that are essential for the luminescence reactions are the central nitrogenous-carboxyl rings (Inouye & Sasaki, 2007). Bioluminescence can be emitted from coelenterazine even when both the central ring as well as some outer groups are modified within certain limits. These coelenterazine analogs each have their own reactivities, half-lives and

display different spectral properties with different luciferases (Fig. 1.3). These different analogs will play a key part throughout this dissertation, especially in chapter III.

In 2012, researchers from the Promega corporation reengineered a small portion of the ~106 kDa, multisubunit, coelenterazine-based luciferase from the shrimp *Oplophorus gracilirostris* to create the brightest luciferase to date (Shimomura et al., 1978; Hall et al., 2012; Tomabechi et al., 2016). They called this new 19 kDa protein NanoLuc (NLuc), and it is 100-times brighter than RLuc and FLuc. This discovery capitalized on the previous work of Japanese scientists who named their secreted luciferase "Nanokaz" (Inouye et al., 2000, Inouye & Sasaki, 2002, Inouye et al., 2013). The team at Promega also co-evolved a new substrate called furimazine which produced brighter light and gave a more sustained signal after its catalysis by NanoLuc (Hall et al., 2012). With the 100x-brighter NanoLuc and furimazine partnership, real-time imaging is greatly enhanced.

The brightness and stability of the NanoLuc-furimazine pair allowed scientists to reapply bioluminescent techniques to previously intractable scientific problems. I will next summarize a variety of cellular reporters available for microscopic use, while explaining some of the principles governing the design and implementation of such reporters.

Disparity of Sensor Abundance Between Fluorescence and Bioluminescence-based Reporters of Cellular Activity

As stated earlier, fluorescence imaging technologies have advanced much more rapidly than luminescence-based techniques and we now have multiple reporters for many cellular applications. At what I define as the most basic side of cellular fluorescence-based imaging are the fluorescence dyes. These are small molecules that produce either spectral changes or intensity

changes in response to some chemical change in the cytoplasm. Currently there are fluorescence dyes that measure Ca^{2+} concentration, like the Fura & Fluo families of dyes (Grynkiewicz et al., 1985; Minta et al., 1989), some that measure cell membrane voltage, like ANEP derivatives and FluoVolt (Fluhler et al., 1985; Bedut et al., 2016) and a variety of other processes. These dyes are usually very bright but have very low signal-to-background ratio (SBR), and it is nearly impossible to control their concentrations in organelles and / or their spatial distribution in cells and tissues. In general, luciferases have excellent SBR.

The next level of fluorescence-based reporters contains those that are proteins and can be genetically targeted to either a population of cells, or to specific subcellular compartments. These reporters can be encoded on a DNA sequence and are introduced to cells by a variety of methods (plasmid transfection, viral transduction, transgenic organism, etc.). Once inside the cells, specific genetic signal sequences can determine roughly how much protein is to be translated, where the protein is targeted, the protein's degradation rate. This method is helpful when trying to observe a protein's spatial dynamics within a cell and allows researchers to visualize what happens when that localization is perturbed.

Finally, by harnessing the properties of Förster Resonance Energy Transfer (FRET) (Piston & Kremers, 2007), one can use the fluorescence energy transfer between two fluorescently-tagged proteins to measure their proximity to one another, and thereby get a sense of whether the proteins are interacting. FRET works because appropriately paired fluorescent proteins can directly transfer energy from one to another. For example, based on its amino acid structure, each fluorescent protein absorbs electromagnetic energy (light) of one specific type (usually based on energy state or wavelength) and then emits a lower energy light as a result. If another fluorescent protein whose absorbance matches well with the emission of another one, energy can be transferred from the

excited protein to the other one as long as they are ~ 5 nm apart. In short, if a researcher genetically fuses the right pair of fluorescence proteins to two proteins of interest, one can decipher if the tagged proteins colocalize inside cells (Piston & Kremers, 2007). This same concept can be used to make a unimolecular FRET-based sensor by fusing a chemically-sensitive linker between the two fluorescent proteins and measuring the change in FRET after the linker's chemically-induced conformational changes modulate the proximity between the two fluorescent proteins (these methods also work with BRET (Y. Xu et al., 1999; X. Xu et al., 2007; Saito et al., 2012, Suzuki et al., 2016)). Today, genetically encoded fluorescence sensors can also report on intracellular Ca^{2+} (Miyawaki et al., 1997), Zn^{2+} (Nolan & Lippard, 2009) and ATP levels (Imamura et al., 2009), membrane voltage (Flytzanis et al., 2014) and even pH (Miesenbock et al., 1998) and outnumber bioluminescence-based reporters.

Return of Bioluminescence Imaging to Circumvent the Drawbacks of Fluorescence Imaging

Over the years, a handful of labs (including our own) have developed bioluminescence imaging for a variety of live-cell applications, and there are a variety of bioluminescent reporters for use on the market, but this field has not experienced the same growth as fluorescence imaging, neither for reporter development nor image acquisition. The recent breakthrough by the Promega corporation in the development of the bright NanoLuc has breathed new life into the possibilities waiting to be unlocked by bioluminescence imaging. NLuc's increased brightness has allowed it to be the ideal luciferase for imaging applications where speed is of upmost importance. As mentioned before, fluorescence intrinsically creates problems such as autofluorescence, photobleaching, and phototoxicity that are not present when bioluminescence is used. With the

advent of brighter luciferases and better substrates a new dawn awaits. It is not far-fetched to suggest that the number and variety of bioluminescent reporters is now poised to increase much like expansion of fluorescence reporters in the late 1990's.

This dissertation covers the development, characterization and application of new bioluminescent reporters from the Johnson Laboratory at Vanderbilt University.

CHAPTER II *

DEVELOPMENT OF CALFLUXVTN, A NOVEL RATIOMETRIC, BIOLUMINESCENCE CALCIUM SENSOR FOR LIVE-CELL IMAGING

Abstract

Optogenetic techniques allow intracellular manipulation of Ca^{2+} by illumination of light-absorbing probe molecules such as channelrhodopsins and melanopsins. The consequences of optogenetic stimulation would optimally be recorded by non-invasive optical methods. However, most current optical methods for monitoring Ca^{2+} levels are based on fluorescence excitation that can cause unwanted stimulation of the optogenetic probe and other undesirable effects such as tissue autofluorescence. Luminescence is an alternate optical technology that avoids the problems associated with fluorescence. Using a new bright luciferase, we here develop a genetically encoded Ca^{2+} sensor that is ratiometric by virtue of bioluminescence resonance energy transfer (BRET). This sensor has a large dynamic range and partners optimally with optogenetic probes. Ca^{2+} fluxes that are elicited by brief pulses of light to cultured cells expressing melanopsin and to neurons-expressing channelrhodopsin are quantified and imaged with the BRET Ca^{2+} sensor in darkness, thereby avoiding undesirable consequences of fluorescence irradiation.

Introduction

New optogenetic methods for stimulating calcium ion (Ca^{2+}) fluxes and neural activity are revolutionizing cellular and neurobiological research (Arenkiel et al., 2007; Boyden et al., 2005;

* Chapter II is derived from the following published article: Yang J, Cumberbatch D, Centanni S., Shi SQ, Winder D, Webb D, Johnson CH (2016) Coupling optogenetic stimulation with NanoLuc-based luminescence (BRET) Ca^{++} sensing. *Nat Commun* 2016 Oct 27;7:13268. doi: 10. 1038/ncomms13268

Miesenböck, 2009). Brief exposure to blue–green light of cells expressing channelrhodopsin or melanopsin can elicit excitatory cation fluxes (channelrhodopsin-2, that is, ChR2) or Ca^{2+} fluxes (melanopsin) (Arenkiel et al., 2007; Boyden et al., 2005; Kumbalasiri et al., 2007; Qiu et al., 2005). In many applications, these optogenetic methods would optimally be partnered with a minimally invasive optical method to directly monitor the impact of the perturbation. For example, optical measurements of neural activity before and after optogenetic stimulation could facilitate recording in freely behaving animals *in vivo* and/or in multiple neurons simultaneously. While there are optical methods for measuring neural activity that use fluorescence sensors for synaptic vesicle pH (Akemann et al., 2012; Akerboom et al., 2012; Chen et al., 2013; Dreosti et al., 2009; Hochbaum et al., 2014; Miesenböck et al., 1998; Murata et al., 2005), genetically encoded Ca^{2+} sensors targeted to the presynaptic terminal and/or dendritic spines that signal the large Ca^{2+} transient in response to an action potential are currently the most promising technique. In particular, the GCaMP family of reporters has undergone considerable optimization by structural design and mutagenesis/screening (Akerboom et al., 2012; Chen et al., 2013; Dreosti et al., 2009).

However, fluorescent sensors for measuring [Ca^{2+}] and/or neural activity are unfavorable for use with optogenetic probes because the continuous excitation that is required to monitor the sensor can (i) trigger tissue autofluorescence and phototoxicity/photoresponses, (ii) only poorly penetrate tissue and (iii) photobleach the probe/sensor. Moreover, optogenetic probes are often directly stimulated by the irradiation used to excite the fluorescent sensor of pH, Ca^{2+} or membrane voltage. Some of the new generation sensors can be excited by longer wavelength light (for example, R-GECO1 (Zhao et al., 2011)) to lessen cross-excitation, but the 'tails' of stimulation by light absorbing pigments render the total exclusion of cross-talk impossible. While two-photon technology in conjunction with fluorescence sensors is under very active development to

circumvent some of these problems (for example, autofluorescence and probe crosstalk) (Akerboom et al., 2012; Chen et al., 2013), this technology is expensive and can photobleach probes with the high-order photon flux (as well as damaging the cells/tissues themselves) (Ustione & Piston, 2011). A totally novel strategy for an optical sensor that is independent of light excitation is worthy of consideration as a partner with optogenetic stimulation.

A completely different approach for an optical sensor of [Ca^{2+}] and/or neural activity would be a luminescence sensor that does not require excitation (Hastings & Johnson, 2003) because the light signal is a result of an enzyme-catalyzed chemical reaction rather than fluorescence. Therefore, the optical measurement of activity is made in darkness, and brief pulses of light would be dedicated specifically to stimulate the optogenetic probe. Because there is no continuous excitation and biological activities are assessed in darkness, there is no autofluorescence, photobleaching, phototoxicity or photoresponse. An optimal luminescence sensor would be ion-specific, sensitive, genetically encodable and ratiometric. The desirability of the first three properties is obvious, but regarding the final optimal property, ratiometric sensors monitor an ionic concentration independently of the intracellular concentration of the sensor (that is, expression level for a genetically encoded sensor) because the measured quantity is the ratio of two wavelengths. Ratiometric recording is less influenced by changes in optical path length, and it also helps to cancel movement and growth artifacts (Thestrup et al., 2014). The currently available genetically encodable luminescent probes for Ca^{2+} (for example, aequorin, obelin, Nano-lantern(Ca^{2+})) have desirable properties in terms of specificity, sensitivity and encodability, but they are not ratiometric (Agulhon et al., 2007; Rogers et al., 2005; Saito et al., 2010) . Moreover, while aequorin has been successfully used as a luminescent reporter of neural activity in zebrafish (Naumann et al., 2010), it has been less successful in mammalian neurons (Agulhon et al., 2007;

Rogers et al., 2005). The studies with aequorin encourage the feasibility of using luminescent reporters of synaptic activity while underscoring that an optimal luminescent probe has not yet been developed for mammalian applications.

Based on ratiometric bioluminescence resonance energy transfer (BRET) technology (X. Xu et al., 2007; Y. Xu et al., 1999; Zhang et al., 2012), we have developed a new Ca^{2+} sensor to use in conjunction with optogenetic probes. BRET avoids the problems of fluorescence excitation (for example, stimulation of an optogenetic probe, autofluorescence, phototoxicity, poor tissue penetration and photobleaching) by monitoring in darkness the luminescence generated by enzymatic catalysis mediated by a luciferase. A newly developed luciferase (NanoLuc) is 100–150x brighter than previous luciferases (Hall et al., 2012), which greatly expands the usefulness of luminescence technology. Our Ca^{2+} sensor is genetically encodable to allow targeting to specific cell types and/or cellular loci, and employs this bright new luciferase to obtain excellent signal strength. We show here that this BRET sensor ratiometrically reports Ca^{2+} fluxes elicited by the optogenetic probes ChR2 and melanopsin in fibroblasts and hippocampal neurons.

Materials and Methods

Construction of plasmids. Each fusion protein was constructed by polymerase chain reaction (PCR) cloning using pVenus-N1 (Addgene ID#: 61854) and pNL1.1 (Promega©) as template DNA for the Venus and Nanoluc (NLuc) moieties respectively, and the Troponin C (TnC) moieties (Thestrup et al., 2014) were created by overlap PCR (primers and sequences in Supplementary Tables 2 and 3). The effect of circular permutations of both NanoLuc (GGGGGSGGGGT linker) and Venus was tested by splitting Venus at amino acid positions 157 and 173 (Nagai et al., 2004), while NanoLuc was split at positions 50, 87, 136 and 148. The TnC

domain was positioned between Venus (N-terminal) and Nluc (C-terminal). TnC conformational changes due to Ca^{2+} binding changed the molecular distance between NanoLuc and Venus, thereby allowing and/or modulating bioluminescence resonance energy transfer (BRET) in response to various Ca^{2+} concentrations [Ca^{2+}]. The CalfluxVTN fusion protein was cloned into plasmids pRSETB (Invitrogen) and pCAG (from VSFP Butterfly 1.2 (Akemann et al., 2012)) {Addgene #: 47978} for bacterial and mammalian expression, respectively. For adeno-associated viral (AAV) transduction, CalfluxVTN and CalfluxVTN-2A-CheRiff were cloned into AAV pCAG-FLEX-tdTomato-WPRE (Addgene #: 51503) and the plasmid was shipped to ViGene Biosciences (Rockville, MD, USA) where they created a mix of serotype 1 + 2 AAV particles. The AAV tdTomato plasmid was first modified to introduce the restriction enzyme sites for EcoR1 and HindIII and then the desired Ca^{2+}-sensor was ligated into the open reading frame.

Protein purification and *in vitro* experiments. Fifteen different combinations of NanoLuc and Venus (including circularly permuted versions) of the BRET Ca^{2+} sensor were constructed and the purified fusion proteins tested *in vitro.* The constructs were inserted into pRSETB, and the BRET ratio (signal at 525 nm divided by signal at 450 nm, see below) of the fusion proteins (isolated via their His6 tags, see below) were measured in high [Ca^{2+}] (50 μM $CaCl_2$) and low [Ca^{2+}] (10 μM EGTA) buffer (100 mM KCl, 30 mM MOPS, pH 7.2). The fusion protein with the largest dynamic range was Venus-TnC-Nluc, and was renamed CalfluxVTN for "CALcium FLUX composed of Venus (V), Troponin (T), and NanoLuc (N)." Using the EcoRI (upstream) and HindIII (downstream) restriction enzyme sites, CalfluxVTN was inserted into pRSETB, then was transfected into BL21 *E. coli* for expression and purification via an N-terminally linked, six-histidine-residue tag (His6). The T7 tag and the enterokinase sites were excised from pRSETB so that the CalfluxVTN sequence is immediately adjacent to the His6

sequence. The His6-tagged fusion protein was purified via TALON® Metal Affinity Co^{2+} Resin and the BRET signal, in response to varying [Ca^{2+}], was measured in Ca^{2+} buffers from Molecular Probes® (Life Technologies™) using a QuantaMaster™ (Photon Technology International Inc.) fluorescence spectrophotometer with the excitation off. BRET ratiometric values were calculated by dividing the light emitted at 525 nm by that emitted at 450 nm after a full scan of the spectrum from 400 to 600 nm. Similarly, the BRET signal of purified CalfluxVTN was also measured microscopically using a hemocytometer to ensure a uniform volume of the protein solution. The BRET ratio was measured using emission filter cube sets of 480/40 nm bandpass (NanoLuc luminescence peak) and 520 LP (Venus fluorescence peak) in the microscopic apparatus described below under "Microscopic Imaging." For all experiments, the NanoLuc substrate, furimazine, was added to a final concentration of 10 μM.

Cellular Expression of Ca^{2+}-Sensors and Recording. The plasmid VSFP Butterfly 1.2 was used as the backbone for the expression of CalfluxVTN in mammalian cells. CalfluxVTN was inserted into the backbone via EcoRI and KpnI sites in order to drive expression by the CAG promoter (Niwa et al., 1991). (A Kozak sequence (Kozak, 1986) was included downstream of the CAG promoter and just upstream of the CalfluxVTN gene). Cell lines were HEK293 (ATCC#CCL-2™) and HeLa (ATCC#CRL-1578™). CalfluxVTN was transfected into HEK293 or HeLa cells via Lipofectamine 2000 (ThermoFisher Scientific Inc.) or GeneCellin (BioCellChallenge) *in vitro* transfection reagents by the manufacturers' instructions. HEK293 and HeLa cells were imaged in the following recording medium (in mM): 1.26 $CaCl_2$, 0.49 $MgCl_2$, 0.41 $MgSO_4$, 5 KCl, 0.44 KH_2PO_4, 4.16 $NaCO_3$, 150 NaCl, 0.34 $NaHPO_4$, 10 HEPES and 0.6 % wt/vol D-glucose. To assay changes in cytosolic Ca^{2+} via CalfluxVTN's BRET signal during live-cell imaging, 1 μM Thapsigargin (TG) or 10 μM ionomycin were added to HEK293 cells. To

initiate cytosolic Ca^{2+} oscillations during live-cell imaging, 10 μM Histamine was added to HeLa cells extracellularly. To compare Ca^{2+}-induced responses of CalfluxVTN vs. GCaMP6s, the Ca^{2+}-sensors (CalfluxVTN and GCaMP6s) were expressed separately in HEK293 cells and the cells were incubated in the recording medium (above) with varying CaCl2 concentrations (1 mM, 5 mM, 10 mM $CaCl_2$). The cells were then imaged on the microscope and their responses to 10 μM ionomycin were recorded using either luminescence microscopy (CalfluxVTN) or epi-fluorescence microscopy (GCaMP6s).

To test CalfluxVTN's responses in neurons, hippocampal neurons were isolated from day 18 rat embryos (Sprague Dawley rats, Charles River Laboratories Inc.), cultured at low density, and transfected via DNA-$Ca_3(PO_4)_2$ precipitation as described previously (Hochbaum et al., 2014; Jiang & Chen, 2006; Kaech & Banker, 2006; Kim et al., 2011; Lin et al., 2010) with 4-8 μg of plasmids encoding CalfluxVTN under the control of the CAG promoter {pCAG (Niwa et al., 1991)}. At DIV 7-8 the neurons were transfected with the relevant DNA constructs. At DIV 10-14, the neurons that were positive for Venus fluorescence were imaged for their responses to the varying experimental perturbations. Neurons from these rats were also transfected via AAV particles (serotype AAV 1 + 2 mix). Pre-made AAV particles (ViGene Biosciences, MD, USA) were diluted in phosphate buffered saline (PBS; GibcoTM) and added to neurons after 1 week in culture. For testing the response of the neurons to varying concentrations of extracellular K^+, the medium surrounding the neurons was exchanged with test buffer (20 mM HEPES pH 7.2, 10 mM D-glucose, 2 mM $CaCl_2$, 1 mM $MgCl_2$, 1 mM Na_2HPO_4, 134 mM NaCl, and 5 mM KCl. This standard test buffer was then exchanged manually within the imaging chamber with test buffers of the same composition except the [KCl] and [NaCl] were reciprocally varied to produce the desired isotonic solutions with different potassium concentrations.

Compatibility with Optogenetic Rhodopsins. Two bi-cistronic expression plasmids were created: CalfluxVTN plus mouse melanopsin (*opn4*) under the control of pCAG (Niwa et al., 1991), and GCaMP6s plus Opn4 under the control of pCAG, each separated by the T2A sequence (Kim et al., 2011). Similarly, another bi-cistronic expression vector was constructed with the channelrhodopsin variant CheRiff (Hochbaum et al., 2014) {Addgene #:51695) replacing *opn4* (Qiu et al., 2005). These were transfected (see Cellular Expression and Characterization) into cells (HEK293 cells or primary hippocampal neurons) and stimulated with ~470 nm (470/30 nm) light for the length of time depicted in each figure. A custom journal was defined in Metamorph Premier® so that illumination and image acquisition could be carefully controlled.

Hippocampal viral injection and brain slice preparation. On the day of surgery, male C57BL/6J mice were anesthetized with isoflurane (3% initial, 1.5% for maintenance) and placed in a stereotaxic apparatus (my NeuroLab, Leica AngleTwo stereotaxic system; Leica Biosystems, BuffaloGrove, IL). Angle Two software was used for setting injection targets in the dorsal hippocampus (coordinates were 2.18 mm posterior to bregma, 2.78 mm lateral to the midline, and 1.73 mm below the skull surface). Other details about the surgical procedure have been described previously (Kash & Winder, 2006). A 33-gauge needle of a 10 µl syringe (Hamilton Company, Reno, NV) was heat sterilized immediately before back filling with AAV-CalfluxVTN virus. 500 nL of the virus was injected bilaterally into the dorsal hippocampus at 50 nL/min using a UltraMicroPump II and Micro4-controller (World Precision Instruments, Sarasota, FL). Five minutes later, the syringe was withdrawn and the scalp wound was sutured. Postsurgical care included immediate subcutaneous saline (1.0 ml per 20 g of body weight) and analgesic (ketoprofen, 5 mg/kg, subcutaneously) followed by additional ketoprofen injections every 24 hours for 3 days. Animals were monitored for health concerns including loss of body weight >20%, signs

of uncontrolled pain, stress or dehydration. No animals displayed these signs and therefore none were removed from further studies. All animal studies were performed under guidelines approved by Vanderbilt University's Institutional Animal Care and Use Committee (IACUC).

Brain slice preparation was performed as previously described (Flavin et al., 2014; Silberman et al., 2015). Mice were removed from the colony and allowed to acclimate for 1 h in a Med Associates sound-attenuating chamber. After the acclimation, mice were anesthetized with isoflurane and then decapitated. Brains were removed quickly and transferred to a 1°C–4°C oxygenated, low sodium sucrose dissecting solution (concentrations in mM: 183 sucrose, 20 NaCl, 0.5 KCl, 2 $CaCl_2$, 1 $MgCl_2$, 1.4 NaH_2PO_4, 10 glucose, 26 $NaHCO_3$). A Leica vibratome was used to prepare coronal brain slices (300 μm) containing the hippocampus. Slices were then transferred to a holding chamber for recordings. The holding chamber contained heated, oxygenated ACSF (119 mM NaCl, 26.2 mM $NaHCO_3$, 2.5 mM KCl, 1 mM NaH_2PO_4, 1.3 mM $MgCl_2$, 10 mM D-glucose, 2.5 mM $CaCl_2$; sterile filtered).

Flow-through microscopic imaging experiments of acute brain slices. The acute brain slices were prepared as described above and then kept in ACSF (119 mM NaCl, 26.2 mM $NaHCO_3$, 2.5 mM KCl, 1 mM NaH_2PO_4, 1.3 mM $MgCl_2$, 10 mM D-glucose, 2.5 mM $CaCl_2$; sterile filtered) at 37 ºC, while bubbled continuously with 95% O2 - 5% CO2. In an open flow chamber (Warner Instruments Inc.: RC-26G), a gravity flow system was set up where the inward flow (2 ml/min) was controlled by gravity but the outward flow was removed by a peristaltic pump (Pharmacia©: LKB-Pump P-1). The ACSF was bubbled with 95% O2 - 5% CO2 before it flowed into the chamber. Because imaging occurred on an inverted microscope, a small nylon mesh was placed between the surface of the acute brain tissue and the glass coverslip that formed the bottom

of the chamber, to allow for good oxygenation of both the top and bottom of the slice. A metal Harp (Warner Instruments Inc.: SHD- 26GH/10) kept the slice in place during imaging.

Microscopic Imaging and Data Analysis. Primary neurons, acute tissue slices, and immortalized cells were imaged on an inverted Olympus IX-71 epifluorescence microscope inside a temperature-controlled, light-tight box. A liquid-cooled EB-CCD (Hamamatsu Photonics K.K., C7190-13W) was used to image the cells at a frame rate of 1-4 Hz. To capture and ratio the BRET images, filters for NanoLuc (EM 480/40 nm bandpass) and Venus (EM 520 longpass) were rotated with a motorized filter turret wheel within the microscope to alternately image the blue vs. yellow/green wavelengths. The speed of rotation of these filters was ~100 ms. For faster imaging (e.g., Fig. 2.9d), an EM-CCD camera (Hamamatsu ImagEM X2) was used with comparable results. This EM-CCD camera was coupled to a light splitter (Hamamatsu W-View Gemini) that used a dichroic filter (495 nm LP) to separate the blue and yellow light and projected them onto distinct regions of the camera's CCD chip. This allowed for simultaneous collection of blue and yellow wavelengths for optimal temporal resolution. During luminescence microscopy, all images were collected in complete darkness. To stimulate the Opn4 or the CheRiff optogenetic probes, ~470 nm (470/30 nm) light was used for the duration stated in the relevant figure legend. Neurons that were cultured on glass coverslips (ThermoFisher™) were inserted into a Chamlide magnetic chamber (Live Cell Instrument, Korea) for imaging.

The images were analyzed with ImageJ software (NIH) using background-subtracted images collected from the blue and yellow channels. After background subtraction, a simple division of the yellow wavelength intensities by the blue wavelengths produced the BRET Ratio values as depicted in all figures. The average light intensity of blue vs. yellow from regions of interest within the cells was compared pixel by pixel to obtain ratiometric BRET estimates of

cytosolic Ca^{2+} over the image. To create the ratiometric photos and movies (e.g., Fig. 2.5b), both blue and yellow channels were background subtracted using the ImageJ function. Then the blue wavelength images were used as a template to create an image that separated the cells completely from the background (cell region was given a value of 255, and background was given 0). The blue and yellow images were then multiplied by this template image where the background was held at 0 and areas within cells were given the full bit value. The resulting images were converted from 16-bit (from camera) to a 32-bit to mitigate losing data after the multiplication step. To finally achieve the ratiometric image, the yellow emission needed to be divided by the blue emission, but to prevent dividing by 0, a gray value of 1 (negligible, since it is out of 4.3 x 109) was added to all the pixels in the blue images, so that dividing the yellow values by the blue values would not result in division by 0 at any pixel. When the final yellow images were divided by the final blue images, the ratio changes that are indicative of $[Ca^{2+}]$ were observed (as indicated by the calibration curve in Fig. 2.1b-c or in Supplementary Fig. 2.8). The ImageJ lookup table (LUT) named "fire" was applied to the images to better highlight the areas were $[Ca^{2+}]$ was changing.

Statistical significance was tested using the Data Analysis Tool Pack from Microsoft Excel (Microsoft©). The Hill coefficient and Kd values (Fig. 2.1c) were determined using OriginLab 6 software (OriginLab©). The emission light spectrophotometric data measured with the QuantaMaster (Figs. 2.1 & 2.2) were collected across the 400-600 nm range in 1-nm intervals. The microscopic data were collected as the average pixel intensity over a user-defined region of interest (ROI). Where t-tests were done, the data fit a normal distribution (Fig. 2.2d, 2.3d, 2.4e-f) and for non-parametric data sets (Fig. 2.5d, 2.7d, 2.9c) ANOVAs were used to determine the significant difference between experimental groups. Except for the negative control neurons in Fig. 2.7d, statistical analyses were performed in cellular experiments that contained a minimum of 10 cells

(in a single experiment) or a minimum of 3 independent experiments, with multiple cells from each group. Unhealthy cells were identified as those cells whose BRET ratio exceeded 3 before any experimental manipulation was done, and were excluded from further analyses.

Note that the BRET ratio scale as a function of [Ca^{2+}] ranges over 1.0-12.1 for the QuantaMaster™ measurements (Fig. 2.1b-c), but the same calibration curve generated with purified CalfluxVTN and Ca^{2+} buffers from Molecular Probes® on the microscopic setup ranges over 1.0-10.5 (Supplementary Fig. 2.8). This difference is due to the BRET ratio from QuantaMaster™ measurements being calculated from peak values of the blue emission (~450 nm) vs. the peak values of the yellow emission (~525 nm, Fig. 2.1b-c), whereas the BRET ratio calculated from the microscopic setup includes all blue emission in the range of 440-520 nm vs. all emission of wavelengths longer than 520 nm (Supplementary Fig. 2.8). Additionally, a higher protein concentration was required for microscopy, due to reduced sensitivity of the EB-CCD camera compared to the QuantaMaster™. These differences cause a substantial difference in the BRET ratio range for any particular [Ca^{2+}]. Because the imaging data illustrated in Figs. 2.9 was generated from microscopic measurements, the BRET ratio calibration curve depicted in Supplementary Fig. 2.8 should be used to evaluate [Ca^{2+}] levels in those experiments. However, much of the literature reporting BRET ratio uses an *in vitro* assay as in Fig. 2.1, and therefore the calibration curve in Fig. 2.1c (= "QuantaMaster" curve in Supplementary Fig. 2.8) is included for making comparisons to other literature (note that the *in vitro* assay is also relevant to Fig. 2.2, Supplementary Figs. 2.1 & 2.2).

Results

***In vitro* characterization of BRET Ca^{2+} sensor**. Our sensor of free calcium ions shares the Ca^{2+} -sensitive troponin-C sequence (from *Opsanus tau*) and linkers with the fluorescent Ca^{2+} indicators Twitch-2 and Twitch-3 (Thestrup et al., 2014). Our BRET sensor interposes this Ca^{2+}-sensitive troponin-C sequence between NanoLuc luciferase (Hall et al., 2012) and a C-terminal truncated version of the fluorescent protein Venus (Kremers et al., 2006; Nagai et al., 2002) with linkers shown in Fig. 2.1a. We call this Ca^{2+} sensor CalfluxVTN for 'CALcium FLUX composed of Venus (V), Troponin (T) and NanoLuc (N)'. The Ca^{2+}-sensitive troponin sequence undergoes a conformational change in response to binding Ca^{2+} that brings NanoLuc closer to Venus so that resonance energy transfer can occur with a concomitant spectral shift (Miyawaki et al., 1997; Thestrup et al., 2014). The spectral shifts of the NanoLuc-catalyzed luminescence as a function of [Ca^{2+}] *in vitro* are shown in Fig. 2.1b, where the 450nm emission of NanoLuc is increasingly resonance-transferred to the 525nm emission of Venus as the [Ca^{2+}] changes from 0.017 mM to 39 mM. Figure 2.1c plots the BRET ratio (525 nm Venus peak : 450 nm NanoLuc peak) as a function of [Ca^{2+}] *in vitro* for two different versions of CalfluxVTN. Because the fluorescent Twitch-3 version of CalfluxVTN exhibited a larger dynamic range within the range of Ca^{2+} concentrations that are likely to be encountered in cells (approximately log -7 to -6 M Ca^{2+}, that is, 0.1–1 mM, Fig. 2.1c), our further experiments used this version to create the luminescent CalfluxVTN. Before this selection, however, we tested 15 combinations of native and circularly permuted Venus and NanoLuc (data not shown); the selected version of CalfluxVTN (Fig. 2.1a)

had the most desirable blend of brightness and dynamic BRET ratio change within the 0.1–1 mM [Ca^{2+}] range.

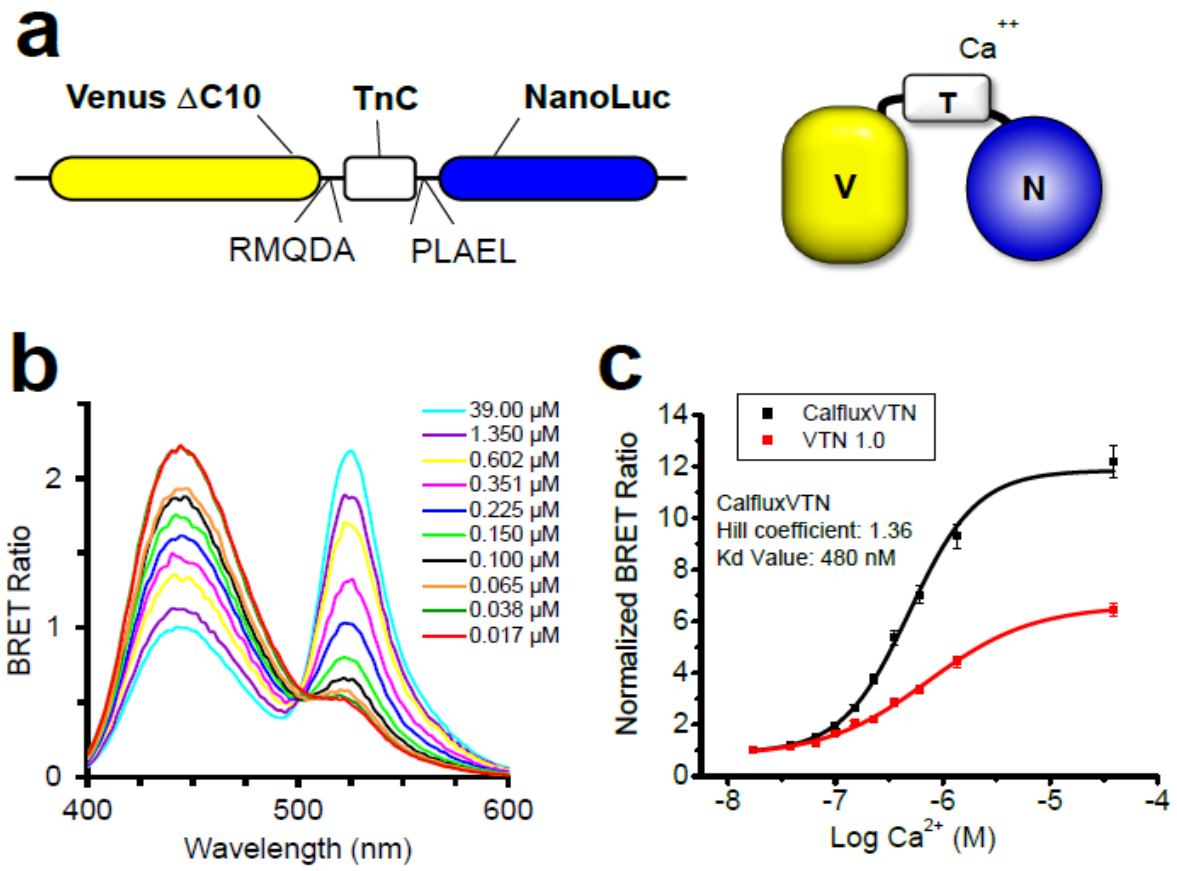

Figure 2.1. Characteristics of CalfluxVTN *in vitro*. (a) The troponin C domain (TnC) was inserted between Venus (with 10 amino acids deleted from the C terminus = CΔ10) and NanoLuc luciferase, using the indicated peptide linkers. **(b)** QuantaMaster spectrophotometer assays of luminescence/BRET spectra from purified CalfluxVTN protein *in vitro*. CalfluxVTN was purified via its 6-His tag and its emission spectrum from 400–600 nm was recorded in buffers with varying concentrations of free Ca^{2+} (range is from 0.017 to 39 mM). Luminescence was initiated by the addition of furimazine substrate. **(c)** Comparison of [Ca^{2+}] dependency *in vitro* for the VTN 1.0 (red trace) versus CalfluxVTN (black trace) versions of the Troponin-C moiety. For these QuantaMaster measurements, BRET ratio values (Venus/NanoLuc) were calculated by dividing the light emitted at the Venus peak (~525 nm) by that emitted at the NanoLuc peak (~450 nm), after a full scan of the light emission spectrum from 400 to 600 nm. Values were normalized by dividing each BRET ratio by the ratio at 0.017 mM Ca^{2+}. Values for the hill coefficient and Kd of CalfluxVTN are shown in c. Mean ± s.d., n = 3.

Before the development of CalfluxVTN, the brightest available luminescent sensor of Ca^{2+} was Nano-lantern(Ca^{2+}) (Saito et al., 2012). By virtue of its much brighter NanoLuc luciferase, CalfluxVTN is at least 30–50x brighter than Nano-lantern(Ca^{2+}) (Fig. 2.2a–c). Moreover, the dynamic range of CalfluxVTN *in vitro* from very low [Ca^{2+}] (~0 mM) to high [Ca^{2+}] (~39 mM) is more than an 11-fold change of BRET ratio (Fig. 2.2d), whereas the dynamic range of Nano-lantern(Ca^{2+}) is ~1.3-fold in terms of its change of intensity in response to free calcium (Fig. 2.2d; the response of Nano-lantern(Ca^{2+}) to [Ca^{2+}] is based on changes of luminescence intensity, whereas the response of CalfluxVTN is based on ratiometric changes in BRET efficiency). Moreover, Calflux not only has a strong signal (bright luminescence, large dynamic range), its response is also specific for Ca^{2+}; in contrast to its exquisite responsiveness to Ca^{2+}, the BRET ratio of CalfluxVTN is not sensitive to changes of Mg^{2+}, pH, K^+ or Na^+ that might be expected to occur within physiological ranges within cells (Supplementary Fig. 2.2).

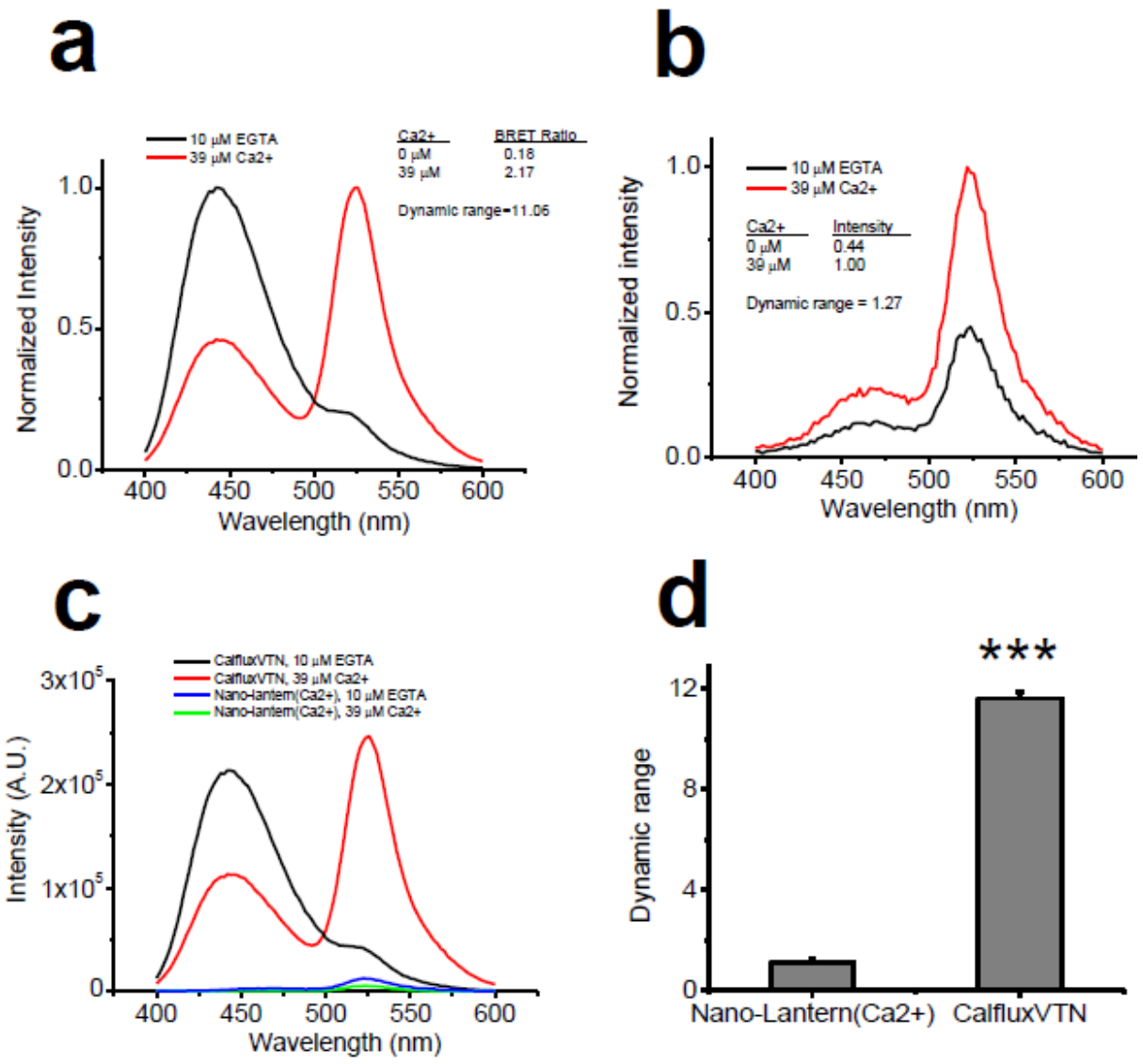

Figure 2.2. Comparison of the intensity and ratio changes of CalfluxVTN and Nano-lantern(Ca^{2+}). **(a)** The normalized emission spectra of equal amounts of purified CalfluxVTN and **(b)** Nano-lantern(Ca^{2+}) proteins. Each protein's effective concentration was estimated by the intensity of its fluorescence signal under the same conditions. Spectra were recorded in 10 mM EGTA or 39 mM Ca^{2+} solutions using a QuantaMaster spectrometer. **(c)** Plots of unnormalized spectra of CalfluxVTN and Nano-lantern(Ca^{2+}) to compare relative intensities of each probe. **(d)** The values obtained in 10 mM EGTA or 39 mM Ca^{2+} solutions were recorded and the maximum dynamic ranges were calculated. Dynamic range was calculated as $[R-R_0]/R_0$ (for CalfluxVTN) or as $[I-I_0]/I_0$ (for Nano-lantern(Ca^{2+})), where R, ratio and I, intensity. (Mean ± s.d., n = 3., ***$P < 0.001$, unpaired t-test). a.u., arbitrary unit.

BRET Ca^{2+} sensor expressed in cell cultures. CalfluxVTN can be expressed in cultured cells under the control of the CAG promoter (Fig. 2.3a,b). In unperturbed, transfected HEK293 cells treated with the furimazine substrate (Hall et al., 2012) the BRET ratio of CalfluxVTN is stable for at least one hour (Supplementary Fig. 2.3). Ca^{2+} levels oscillate in HeLa cells after stimulation with histamine (Miyawaki et al., 1997; Sauvé et al., 1990; Thorn, 1995), and CalfluxVTN faithfully reports this cycle in CalfluxVTN-transfected HeLa cells exposed to 10 mM histamine, as indicated by the oscillation of BRET ratio (Fig. 2.3c,d). The data of Fig. 2.3 were derived from HeLa cells in serum-free medium, but CalfluxVTN and furimazine are equivalently useful in serum-containing medium, for example, when serum (FBS) is included in the medium, many cycles of Ca^{2+} oscillation can also be measured by CalfluxVTN (Supplementary Fig. 2.4). We compared the Ca^{2+}-responsiveness of CalfluxVTN with that of a well characterized fluorescence sensor of Ca^{2+} fluxes, GCaMP6s (Chen et al., 2013). HEK293 cells were exposed to the Ca^{2+} ionophore ionomycin in the presence or absence of various concentrations of extracellular $CaCl_2$ (1, 5 and 10mM $CaCl_2$). The cells were transfected with either the CalfluxVTN expression construct (Fig. 2.4a) or the GCaMP6s expression construct (Fig. 2.4b). As shown in Fig. 2.4c,d, both sensors responded to the ionomycin-stimulated Ca^{2+} flux with large changes in BRET ratio (CalfluxVTN) or fluorescence intensity (GCaMP6), with the magnitude of the response proportionally dependent upon the extracellular $CaCl_2$ concentration. The dynamic range and sensitivity of response was somewhat larger with GCaMP6s than with CalfluxVTN (Fig. 2.4e,f).

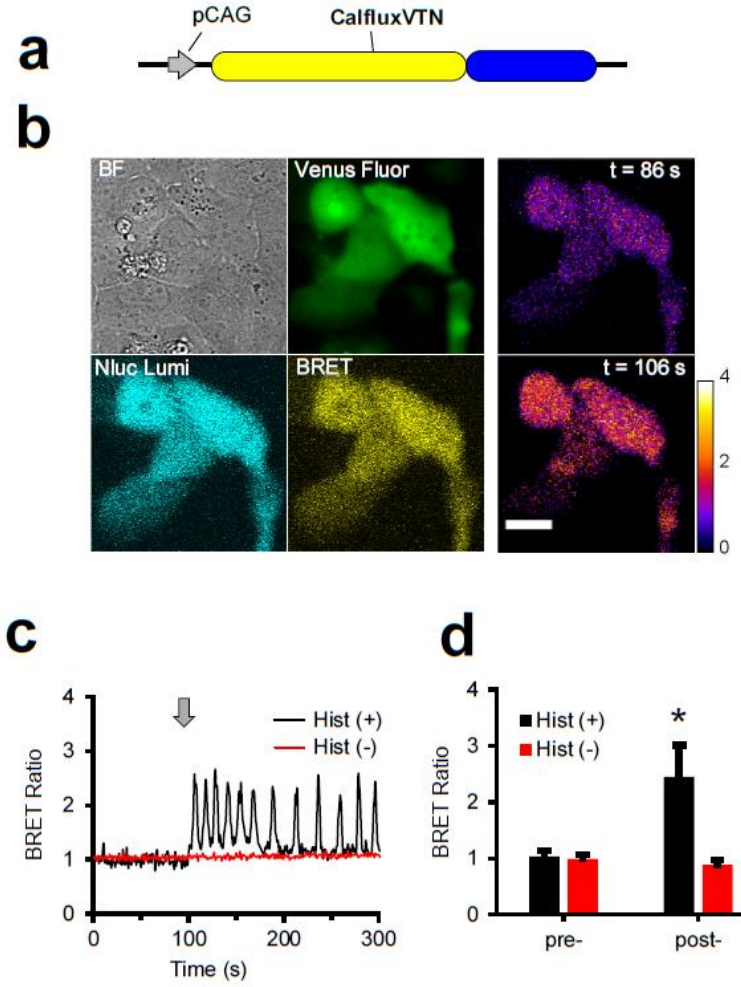

Figure 2.3. CalfluxVTN as an *in vivo* Ca^{2+} sensor in mammalian cells. **(a)** CalfluxVTN construct driven by CAG promoter (pCAG) for mammalian cell expression. **(b)** Photomicrographs of HeLa cells expressing CalfluxVTN. The four leftmost panels are as follows: BF, bright-field image; Venus Fluor, Venus fluorescence image in pseudo-colour green; Nluc Lumi, luminescence emitted at NanoLuc peak wavelength (~450 nm); BRET, luminescence emitted at ~525 nm as a result of BRET. The two rightmost panels are ratiometric BRET images of HeLa cells just before the addition of histamine (t = 86s) and at the first peak of the Ca^{2+} oscillation evoked by histamine (t = 106 s; scale bar, 20 μm); the temporal pattern of the Ca^{2+} oscillation of these cells is depicted in **c**. **(c)** HeLa cells transfected with CalfluxVTN responding to 10 mM histamine (Hist (+), black trace) or vehicle (Hist (-), red trace). Arrow shows when histamine or vehicle was added. The calibration curve generated for microscope analysis Supplementary Fig. 2.8) is relevant to these data. **(d)** Quantification of the data depicted in **c** (For Hist+, n = 15 cells from four separate experiments, for Hist-, n = 14 cells from four separate experiments, mean ± s.e.m., for the Hist+ versus Hist- comparison *P < 0.05, paired t-test).

Therefore, as compared with well-characterized fluorescence Ca^{2+} indicators, CalfluxVTN is also

a stable and specific sensor of Ca^{2+} in unstimulated cells and in cells that have been stimulated by different Ca^{2+}-altering treatments (that is, histamine and ionomycin).

CalfluxVTN is an optimal optogenetic partner with melanopsin. The photopigment melanopsin triggers the release of internal calcium stores in response to blue light (Kumbalasiri et al., 2007; Qiu et al., 2005). We transfected CalfluxVTN in HEK293 cells with (Fig. 2.5a) or without (Figs 2.3a and 2.4a) a co-expressed opn4 sequence that encodes melanopsin (Fig. 2.5b). Active melanopsin depends upon binding of retinal that is present at low levels in mammalian cells (Kumbalasiri et al., 2007; Li et al., 2005; Qiu et al., 2005), but an even greater proportion of active melanopsin can be reconstituted *in vivo* when cell cultures are treated with all-trans-retinal. The BRET signal of HEK293 cells transfected with the CalfluxVTN/opn4 construct (Fig. 2.5a) responded dramatically to optogenetic stimulation by a 10-sec blue light pulse (Fig. 2.5b–d), indicating a significant increase of intracellular Ca^{2+}. Cells treated with retinal (R+) exhibited a slightly stronger response to the light pulse than untreated cells (R-), as expected from the larger pool of active melanopsin in cells treated with retinal. On the other hand, cells transfected with CalfluxVTN but not opn4 (Figs 2.3a and 2.4a) did not respond to the blue light pulse regardless of treatment with retinal (Fig. 2.5c,d). However, all of the cell groups transfected with CalfluxVTN (with or without opn4) responded to pharmacological release of internal Ca^{2+} stores elicited by 1 mM thapsigargin (Fig. 2.5c,d), indicating that in each group the CalfluxVTN sensor was present and responsive to changes of cytosolic Ca^{2+} levels. Note that all the measurements shown in Fig. 2.5b–d were conducted in darkness except for the 10-sec light pulse.

As compared with a fluorescent Ca^{2+} -sensor, a BRET Ca^{2+} sensor can avoid undesirable stimulation of a coupled optogenetic probe because the recording of Ca^{2+}-fluxes by a luminescent sensor is performed in darkness. Figure 2.6 depicts this advantage in a comparison of melanopsin-

stimulated Ca^{2+}-fluxes by CalfluxVTN versus GCaMP6s. As also shown in Fig. 2.5, light pulses to the CalfluxVTN-Opn4-transfected HEK293 cells evoked large changes in BRET ratio, indicative of transient increases of cytosolic Ca^{2+} (Fig. 2.6a). Except for the brief light pulses, the cells in Fig. 2.6a were otherwise in darkness. Moreover, thapsigargin also caused a large sustained

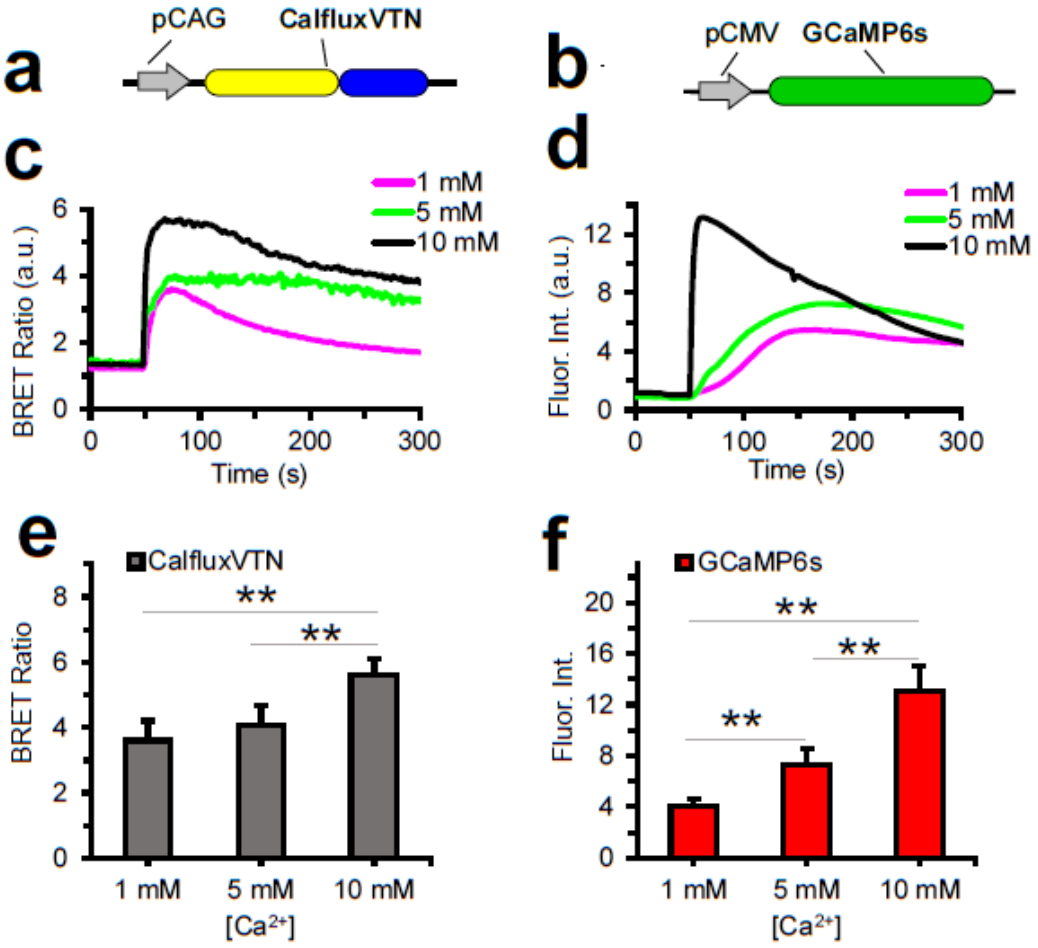

Figure 2.4. Comparison of the Ca^{2+} – induced responses between CalfluxVTN and GCaMP6s. (a) CalfluxVTN driven by pCAG and **(b)** GCaMP6s driven by pCMV in HEK293 cells. **(c,d)** In all, 10 mM ionomycin was added (at ~50 s) to HEK293 cells in 1 mM, 5mM or 10mM $CaCl_2$-containing medium expressing CalfluxVTN **(c)** or GCaMP6s **(d)**. Plots depict the average responses. **(e,f)** Graphs showing the average peaks of the [Ca^{2+}]-dependent responses of CalfluxVTN **(e)** and GCaMP6s **(f)** to ionomycin induced Ca^{2+} – influx. (for each sample group, data come from four separate experiments with a total cell number between 17 and 24; mean ± s.e.m., $^{**}P < 0.01$, paired t-test). The calibration curve generated for microscope analysis (Supplementary Fig. 2.8) is relevant to these data. a.u., arbitrary unit.

change of cytosolic Ca^{2+}. Importantly, there was little variance in the responses among the cells (see error bars in Fig. 2.6a, and also the responses of individual cells in Supplementary Fig. 2.5a–c). In striking contrast, the same protocol performed with the GCaMP6s-Opn4 sensor exhibited significantly more heterogeneous responses, as indicated by the error bars in Fig. 2.6b (and also the responses of individual cells in Supplementary Fig. 2.5e,f). The GCaMP6s-transfected cells were continuously exposed to a dim excitation light to enable recording of the fluorescence of the sensor. The response of some cells transfected with GCaMP6s-Opn4 was very similar to that of the CalfluxVTN-Opn4-transfected cells (compare panel b with panel e in Supplementary Fig. 2.5), but there is considerable variability among the GCaMP6s-Opn4-transfected cells that is not present among the CalfluxVTN-Opn4-transfected cells. Because the variability of the response among the cells transfected with GCaMP6s without Opn4 is low (Fig. 2.6b and Supplementary Fig. 2.5d, first 300 s), our interpretation of this difference is that the dim excitation light quickly sparks some Ca^{2+}-flux in the GCaMP6s-Opn4-transfected cells, as indicated by the recordings in the first 12 s (Supplementary Fig. 2.5f). Therefore, the heterogeneity of these unintended responses is likely due to variability of expression level of melanopsin among the GCaMP6s-Opn4-transfected cells, whereas cells transfected with GCaMP6s (without Opn4) are not light-responsive.

Calflux reports Ca^{2+} flux in hippocampal neurons and slices. Neuronal Ca^{2+} levels increase in response to membrane depolarizations that open voltage-gated Ca^{2+} channels (Church et al., 1994). Channel-opening depolarization conditions include neural activity (for example, action potentials) and high extracellular concentrations of K^+ (Church et al., 1994). To test whether CalfluxVTN could detect depolarization-induced Ca^{2+} fluxes in mammalian neurons, dissociated rat hippocampal neurons at days 5–6 in culture were transfected using a modified calcium

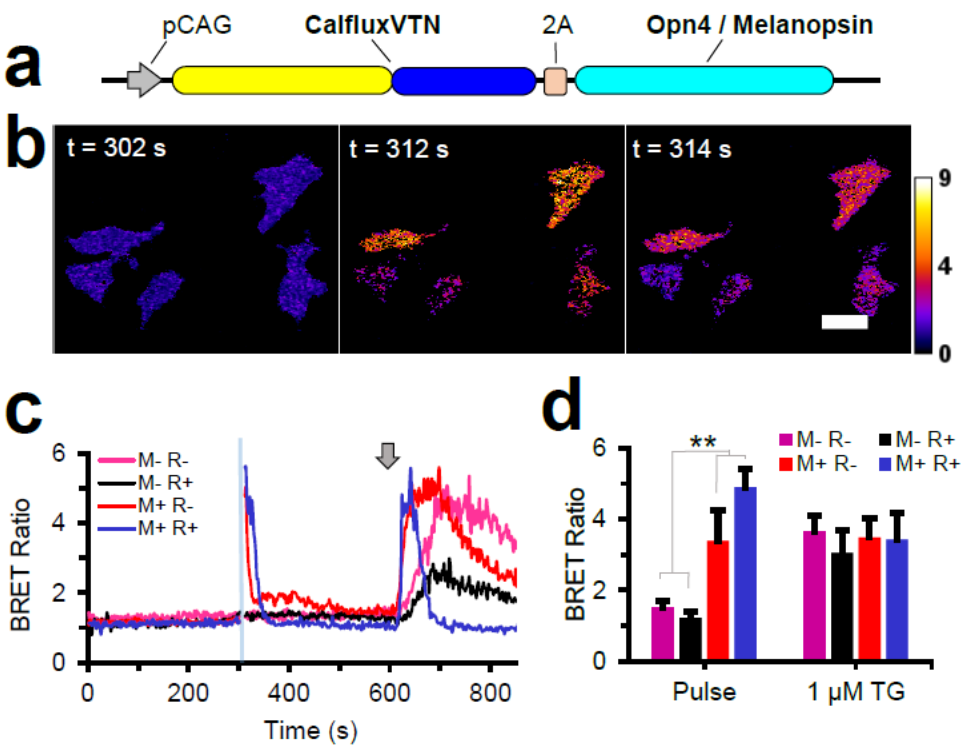

Figure 2.5. Coupling BRET Ca^{2+} sensing with an optogenetics probe that regulates store-operated Ca^{2+} (SOC) release. (a) Bicistronic pCAG-driven construct encoding CalfluxVTN and mouse melanopsin (*opn4*). **(b)** Photomicrographs of the ratiometric image of BRET emitted from HEK293 cells expressing CalfluxVTN and melanopsin (retinal-treated, M+/R+) in **c** over the time course just before (302 s) and for 2 s (times 312–314 s) after stimulation with a 10 s blue light pulse between 302–312 s (scale bar, 20 µm). **(c)** Optogenetically stimulated ratiometric changes in BRET after excitation of melanopsin with 10 s blue light (at blue line, time 302 s; pulse is 470 nm ± 30 nm) in HEK293 cells expressing either the construct in a or CalfluxVTN alone (M = transfected with opn4, R = treated with all-transretinal). HEK293 cells that do not express melanopsin (= M-, construct shown in Figs 2.3a and 2.4a) do not exhibit a BRET ratio change in response to the blue light pulse. Both groups of cells (M+ and M-) show large and persisting changes in BRET ratio in response to stimulation of SOC release by 1 mM thapsigargin (at arrow). Some of the preparations were additionally treated with 100 nM all-trans-retinal (R+) to reconstitute a larger amount of active melanopsin (Kumbalasiri et al., 2007). **(d)** Quantification of the HEK293 cells' responses in **c** of the peak BRET ratio after light stimulus (Pulse); peak ratio after thapsigargin was added (1 µM TG). (For each sample group, data come from three separate experiments with a total cell number between 14 and 16; mean ± s.e.m., $^{**}P < 0.01$, $F = 20.7$, M+ compared with M-, 2-factor analysis of variance (ANOVA)) The calibration curve generated for microscope analysis (Supplementary Fig. 2.8) is relevant to these data. TG, 1 µM thapsigargin.

phosphate method (Kaech & Banker, 2006; Wegner et al., 2008) with the CalfluxVTN-encoding

vector (Fig. 2.7a). Approximately 4–5 days later, CalfluxVTN-expressing neurons (about 10% of the total population) could be detected by the fluorescence of the Venus moiety; these fluorescent cells also expressed robust NanoLuc luminescence in darkness (Fig. 2.7a). The BRET ratio of CalfluxVTN increased as a function of $[K^+]$ in the medium (Fig. 2.7b). These changes were reversible; when the high concentrations of K^+ (for example, 40–60mM KCl) were returned to the standard 5mM KCl concentration, the BRET ratio returned to its original value (Fig. 2.7b,d). These changes in BRET ratio were not the result of physical manipulations or medium changes, because the same protocol of medium replacement using the standard 5mM KCl medium for each change did not alter CalfluxVTN's BRET ratio (Fig. 2.7c). Therefore, depolarizations elicited by extracellular K^+ cause Ca^{2+} fluxes that modulate CalfluxVTN's BRET signal in a $[K^+]$-dependent relationship, and these alterations are reversible.

To determine if the BRET Ca^{2+} sensor could be used with brain slices, we developed an adeno-associated virus construct that expresses CalfluxVTN from the pCAG promoter (AAV-CalfluxVTN, Fig. 2.8a). This AAV vector was stereotactically injected into the dorsal hippocampus of mice. Three weeks later, coronal brain slices containing the hippocampus were prepared and mounted in a flow-through chamber for imaging. The AAV vector transduced hippocampal cells, as confirmed by fluorescence of the Venus moiety of CalfluxVTN (Fig. 2.8b). Furimazine substrate was added to the slowly flowing oxygenated artificial cerebrospinal fluid (ACSF), and NanoLuc luminescence was easily visualized as well as BRET signal emanating from the stratum pyramidale of the CA1 region of the hippocampus (Fig. 2.8c). The ACSF was changed from 5mM KCl to 80mM KCl and back again three times. Each time the slice was exposed to the high K^+ medium, the BRET ratio increased reversibly in the neuron cell body-dense stratum

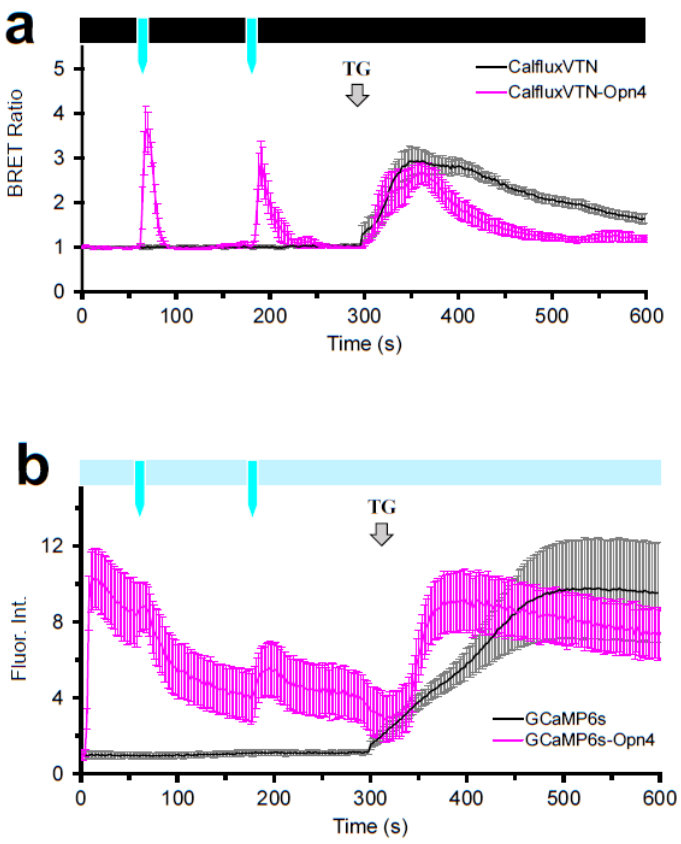

Figure 2.6. Comparison of coupling melanopsin-optogenetic stimulation of Ca^{2+} influx with CalfluxVTN versus GCaMP6s. (a) CalfluxVTN and **(b)** GCaMP6s were expressed in HEK293 cells either alone or in a bicistronic vector that allows simultaneous expression of melanopsin (*opn4*). The average ± s.e.m. responses of all the cells on one plate were plotted in response to blue light stimulation at 60 s and 180 s (indicated by the blue arrows). **(a)** For CalfluxVTN luminescence microscopy, the cells' responses were recorded in darkness (black bar above graph in **a**) and exposed to the two 1-second light pulses (blue arrows), **(b)** For GCamp6s fluorescence microscopy, dim excitation was maintained throughout to record GCamp6s fluorescence (light blue bar above graph in **b**). To stimulate melanopsin (Opn4), two 1-second blue light pulses were presented at 60 s and 180 s by increasing the light intensity of the fluorescence light source to an intensity that was equivalent to that used in a (bright blue arrows that punctuate the dim excitation indicated by the light blue bar). All light pulses exposed the entire field of cells. Grey arrow shows when thapsigargin (TG) was added to increase cytosolic Ca^{2+}. See Supplementary Fig. 2.5 for responses of individual cells. (For the data in this figure n = 11 cells for CalfluxVTN, n = 6 for CalfluxVTN-Opn4, n = 7 cells for GCaMP6s and n = 12 for GCaMP6s-Opn4; mean ± s.e.m.) The calibration curve generated for microscope analysis (Supplementary Fig. 2.8) is relevant to these data.

pyramidale of the CA1 region of the hippocampus (regions of interest (ROIs) 2–5, Fig. 2.8c,d) but

not in other regions (ROI 1, Fig. 2.8c,d). Another example of hippocampal Ca^{2+} responses to K^+-stimulated depolarizations is shown in Supplementary Fig. 2.6.

Neuronal responses to optogenetically induced depolarization. Exposure of neurons-expressing channelrhodopsin to blue light triggers excitatory cation fluxes that depolarize the plasma membrane, eliciting Ca^{2+} fluxes into the neurons (Arenkiel et al., 2007; Boyden et al., 2005). We transfected rat hippocampal neurons with a construct that co-expresses CalfluxVTN and the ChR2 variant CheRiff (Hochbaum et al., 2014) (Fig. 2.9a). As in the case of HeLa and HEK293 cells, CalfluxVTN-transfected hippocampal neurons emit NanoLuc luminescence and BRET (Fig. 2.9a). Exposure to 1 s pulses of blue light to neurons in darkness provoked a dramatic transient increase in BRET ratio of the luminescence measured immediately upon return to darkness (Fig. 2.9b,c, black trace), indicating that light stimulation of CheRiff elicits membrane depolarization and subsequent Ca^{2+} flux that is detected by CalfluxVTN. Neurons transfected with the CalfluxVTN construct without CheRiff but treated with the furimazine substrate did not exhibit any change of BRET ratio in response to blue light pulses (Fig. 2.9b,c, red trace). The light-stimulated responses of CheRiff-expressing neurons can be imaged as shown in Fig. 2.9a where the spatial changes of CalfluxVTN are indicated by pseudocolour encoding of BRET ratio (scale to the right of Fig. 2.9a).

The brightness of NanoLuc enables recording rates that were not possible with the previous generation of dimmer luciferases. These faster recording rates allow higher temporal resolution of cellular events. Figure 2.9d illustrates an experiment in which the recording rate was 40 Hz. The timing of the responses to light pulses and high K^+ medium is well defined. On the other hand, a potential concern about the brightness of NanoLuc is that it might be so bright that it stimulates channelrhodopsin directly. This concern is unfounded, as we determined by varying the

concentration of the substrate furimazine to alter the intensity of luminescence. If the luminescence intensity was sufficient to stimulate channelrhodopsin directly and thereby elicit Ca^{2+} fluxes, the

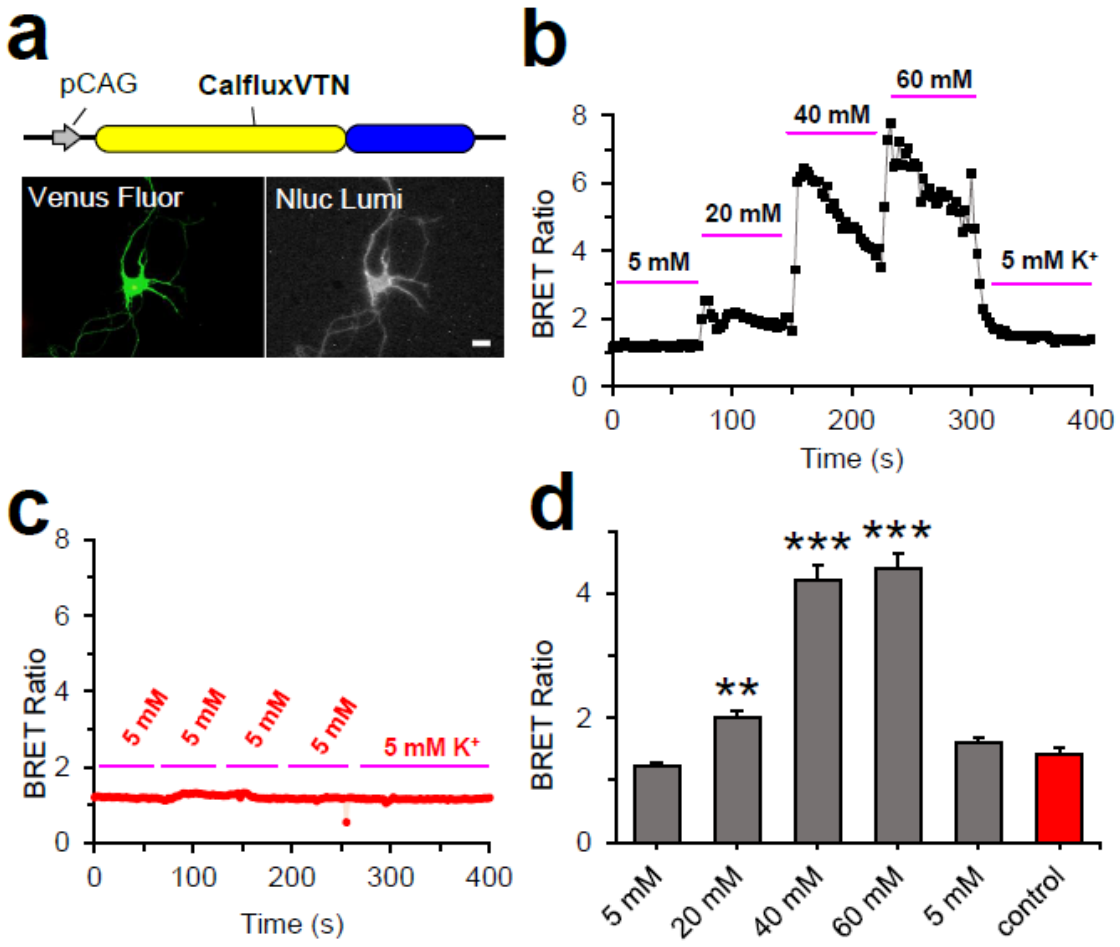

Figure 2.7. CalfluxVTN reports depolarization-evoked Ca^{2+} fluxes in rat hippocampal neurons. (a) CalfluxVTN construct driven by CAG promoter (pCAG) for mammalian cell expression (upper panel), and photomicrograph of a single hippocampal neuron expressing the construct. Fluorescence of the Venus moiety (lower left panel) and luminescence of NanoLuc (lower right panel) are shown (scale bar, 10 μm). **(b)** BRET ratio increased (indicating increase of intracellular [Ca^{2+}]) in hippocampal neurons as the medium was exchanged with increasing concentrations of K^+ (from 5 to 60 mM KCl; n = 6 independent cells). **(c)** When medium was exchanged repeatedly with control medium (5 mM KCl; n = 3 independent cells), there was no change in BRET ratio, indicating that the changes observed in **b** were not due to physical manipulations. **(d)** Quantification of the neurons' responses to varying [K^+] illustrated in **b** and **c** (mean ± s.e.m. $^{**}P < 0.01$, $^{***}P < 0.001$, 1-factor analysis of variance (ANOVA)). The calibration curve generated for microscope analysis (Supplementary Fig. 2.8) is relevant to these data.

BRET ratio would be expected to increase as furimazine concentrations are raised in ChR2-expressing neurons, but not in neurons that are not expressing ChR2. Our measurements show that the BRET ratio is essentially constant in hippocampal neurons within a range of furimazine concentrations above and below our standard experimental condition that vary the intensity of luminescence emission (Supplementary Fig. 2.7). A constant BRET ratio was observed whether or not channelrhodopsin (the CheRiff variant) was expressed in the neurons (Supplementary Fig. 2.7).

Discussion

As we proposed in 2012 (Zhang et al., 2012), the characteristics of BRET provide an untapped opportunity to develop genetically encodable and ratiometric optical sensors that could be ideal for optogenetic applications, especially to prevent the cross-excitation that can occur between a fluorescent sensor and the optogenetic probe (for example, ChR2 or melanopsin). A sensor that requires continuous photonic excitation will likely stimulate the optogenetic probe to some extent, thereby perturbing the very process that the sensor is supposed to be non-invasively measuring. Simultaneously, a luminescence BRET sensor avoids other problems associated with fluorescence irradiation such as tissue autofluorescence, poor tissue penetration, intrinsic tissue photoresponsiveness (for example, retina or plant tissue) and excitation-induced tissue photodamage (Hastings & Johnson, 2003; X. Xu et al., 2007; Y. Xu et al., 1999; Zhang et al., 2012). Moreover, while two-photon technology may reduce some of these problems (for example, autofluorescence and probe crosstalk), the high-order photon flux required for two-photon excitation can photobleach the probe and/or photodamage the tissue (Ustione & Piston, 2011). As

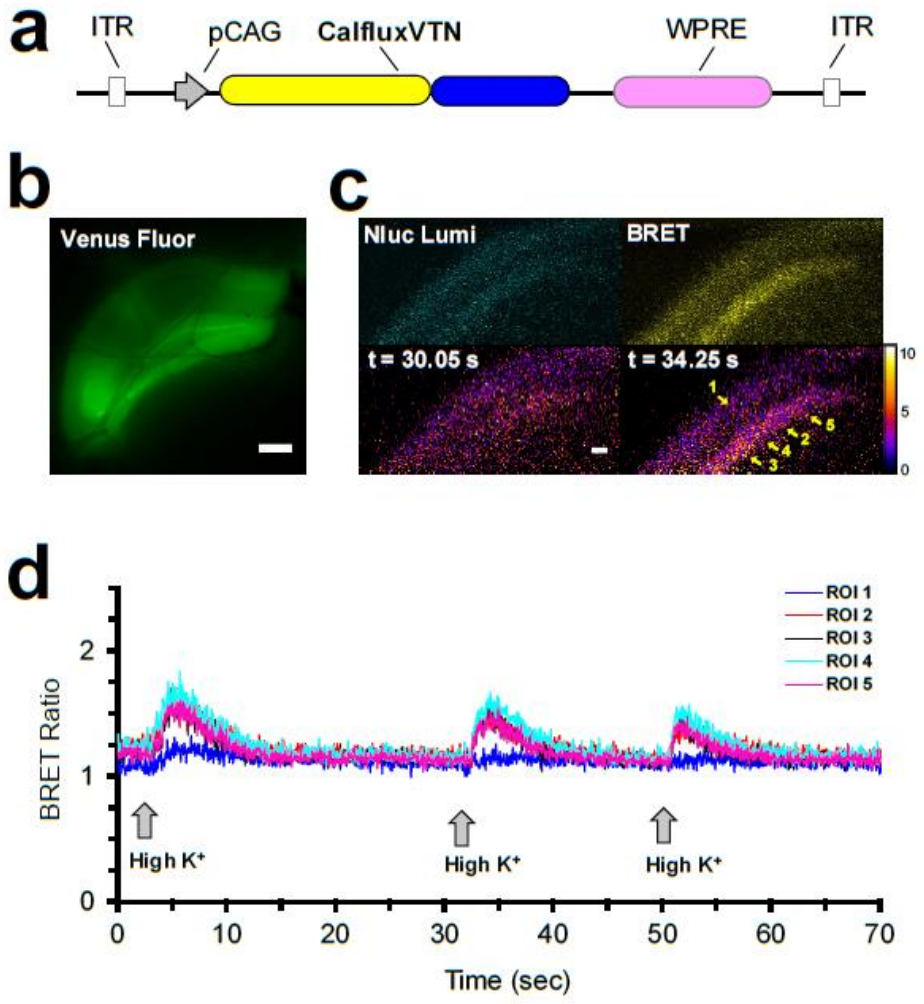

Figure 2.8. CalfluxVTN reports high K^+ induced Ca^{2+} -flux in acute hippocampal brain slices. (a) Adeno-associated virus (AAV) vector expressing CalfluxVTN, ITR, inverted terminal repeat of AAV, WPRE, regulatory element that stimulates expression of the insert. **(b)** Venus fluorescence signal of CalfluxVTN from acute brain slices containing dorsal hippocampus from mice injected with AAV-CalfluxVTN (scale bar, 300 μm). **(c)** Top-left panel: image of NanoLuc emission signal ('Nluc Lumi') from hippocampal CA1/pyramidal layer slice, top-right panel: BRET signal of identical region in 'Nluc Lumi' panel ('BRET'), lower panels: ratiometric image of same region, before (lower-left panel) and after (lower-right panel) high K^+ stimulation (scale bar, 50 μm). **(d)** Results of a flow-through experiment where high K^+ (80 mM) was applied three times sequentially to an acute hippocampal slice while recording the CalfluxVTN BRET ratio (indicating Ca^{2+} influx). ROI's represent the numbered regions of interest in **c** (lower right panel). See Supplementary Fig. 2.6 for another example of hippocampal slice responses to high K^+ stimulated depolarization. The calibration curve generated for microscope analysis (Supplementary Fig. 2.8) is relevant to these data.

we show in Figs 2.5 and 2.9, a BRET-based sensor can monitor a cellular parameter (for example,

Ca^{2+}) in darkness, then a brief flash of light can be applied to stimulate the optogenetic probe, after which time the BRET sensor is consulted in darkness to assess the cellular response.

No technique is perfect, but the traditional liabilities of BRET/luminescence sensors have been greatly ameliorated by the newly developed luciferase NanoLuc (Hall et al., 2012). In the past, BRET/luminescence assays have been hampered by the dimness of the luminescence level and the instability of the substrate needed for the luciferase-catalyzed reaction (esp. coelenterazine). In both of these respects, however, NanoLuc is revolutionary (Hall et al., 2012). NanoLuc is 100–150x brighter than Renilla luciferase (RLuc) or firefly luciferase (FLuc) (Hall et al., 2012). Even though it has been possible to enhance the brightness of RLuc by imaginative BRET partners (Saito et al., 2012), RLuc remains much dimmer than NanoLuc, and consequently CalfluxVTN is 30–50x brighter than the brightest RLuc-based Ca^{2+} sensor, Nano-lantern(Ca^{2+}) (Saito et al., 2010, Saito et al., 2012). An ongoing advantage of luminescence over fluorescence techniques is its superior signal to noise ratio (SNR), and with NanoLuc's brightness, SNR is even better than with previously available luciferases. Moreover, the development of NanoLuc concomitantly entailed the evolution of a new substrate, furimazine, which produces less autoluminescence as well as being more stable in cell culture media that includes serum (as in Supplementary Fig. 2.4) than its ancestral substrate coelenterazine (Hall et al., 2012). We confirmed that the luminescence level of NanoLuc expressed within cell cultures was strong and the BRET ratio stable for over one hour (Supplementary Fig. 2.3). Therefore, furimazine-based NanoLuc Ca^{2+} sensors (such as CalfluxVTN) will be more manageable and stable than Ca^{2+} BRET sensors such as BRAC or Nano-lantern(Ca^{2+}) that use coelenterazine (Saito et al., 2010, Saito et

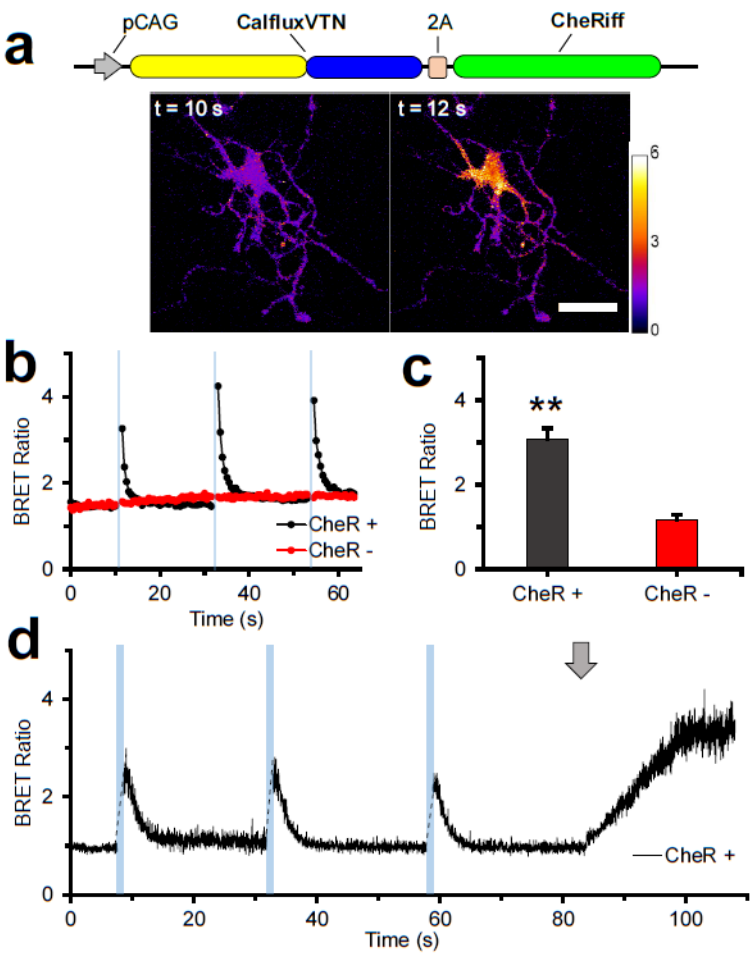

Figure 2.9. CalfluxVTN detects Ca^{2+} fluxes elicited by optogenetically stimulated depolarization. (a) CheRiff is a ChR2 variant that evokes a peak photocurrent when excited by blue (460 nm) light. CheRiff was co-expressed with CalfluxVTN in rat hippocampal neurons and emission wavelengths detected by light microscopy. Micrographs show BRET ratiometric images before (10 s) and after (12 s) blue light stimulation (scale bar, 20 μm). BRET ratio pseudocolour scale is shown next to the right micrograph. **(b)** One-second blue light (470 nm ± 30 nm) pulses to cells expressing CalfluxVTN with (CheR+) and without (CheR-) CheRiff; these populations of cells were imaged at 1 Hz recording rate. **(c)** Quantification of the changes in BRET ratios seen in **b** after stimulation with blue light (with CheRiff, n = 11 independent cells; without CheRiff, n = 8 independent cells, mean ± s.e.m. $^{**}P < 0.01$, F = 34.6, 1-factor analysis of variance (ANOVA)). **(d)** Responses of another hippocampal neuron transfected with CheRiff imaged at a higher recording speed (40 Hz). Blue bars indicate the time of 1-second blue light pulses, while the grey arrow indicates the addition of 80 mM high K^+ medium. The calibration curve generated for microscope analysis (Supplementary Fig. 2.8) is relevant to these data. The neurons in **a** – **c** were transfected with DNA-$Ca_3(PO_4)_2$ precipitation whereas the neurons in the experiment of **d** were transduced with the AAV-CalfluxVTN vector.

al., 2012). Nevertheless, furimazine is not as stable as some other bioluminescence substrates such

as beetle luciferin, and consequently for long-term experiments (for example, circadian rhythm experiments), further optimization of substrate stability would be invaluable.

CalfluxVTN effectively tracks Ca^{2+} transients resulting from Ca^{2+} oscillations (Fig. 2.3c,d, Supplementary Fig. 2.4), high K^{+}-induced depolarization (Figs 2.7 and 2.8), and optogenetic stimulation of melanopsin (Figs 2.5c,d and 2.6a) or ChR2 (Fig. 2.9), however, further testing will be required to ascertain the kinetic limits of this version of the sensor in tracking very rapid events, such as the Ca^{2+} transients that accompany action potentials. The dynamic range of CalfluxVTN is large (~10–12, Figs 2.1c and 2.2, Supplementary Fig. 2.8) and not only dramatically surpasses the dynamic range of previous BRET reporters based on RLuc (Fig. 2.2, (Saito et al., 2010, Saito et al., 2012)), but surprisingly eclipses the dynamic range of its fluorescent parent Twitch-3 (dynamic range ~7, (Thestrup et al., 2014)). However, the dynamic range and sensitivity of response is larger with the sixth-generation fluorescence sensor GCaMP6s than with this first-generation BRET sensor CalfluxVTN (Fig. 2.4). Undoubtedly further optimization of CalfluxVTN or similar sensors is warranted. Nonetheless, even in its current form, the large dynamic range and brightness of CalfluxVTN is responsible for the excellent SNR that is obvious in the responses to optogenetic stimulation (Figs 2.5, 2.6 and 2.9). The desirable properties of CalfluxVTN indicate its readiness to be applied to other biological questions that involve Ca^{2+} fluxes. These may include *in vivo* applications. For example, FLuc-based reporters have successfully monitored the expression of gene expression continuously from the brain of freely moving mice for up to 3 weeks in constant darkness with a fiber-optic (Ono et al., 2015). NanoLuc-based sensors are substantially brighter than FLuc-based sensors and therefore the successful development of this new generation of BRET sensors heralds a surge of novel applications of luminescence technology that circumvents the technical problems of fluorescence.

Supplementary Data Figures

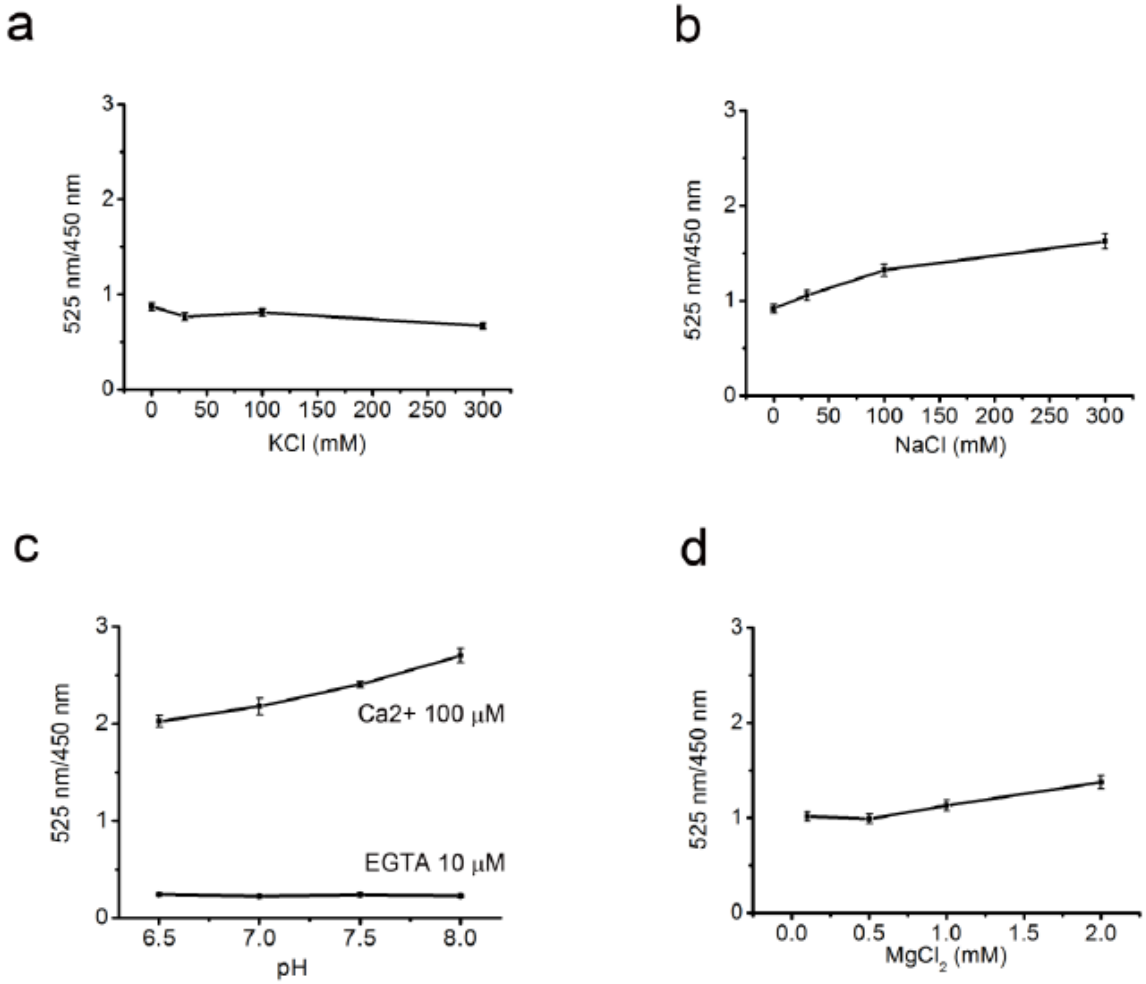

Supplementary Figure 2.2. Insensitivity of CalfluxVTN to other ions *in vitro*. CalfluxVTN was purified via a His-6 tag and the BRET ratio was recorded in solutions with increasing concentrations of ions as shown. The BRET ratio in response to increasing [K^+] (panel a); [Na^+] (panel b); pH (panel c); [Mg^{2+}] (panel d). Data points represent mean ± S.D.

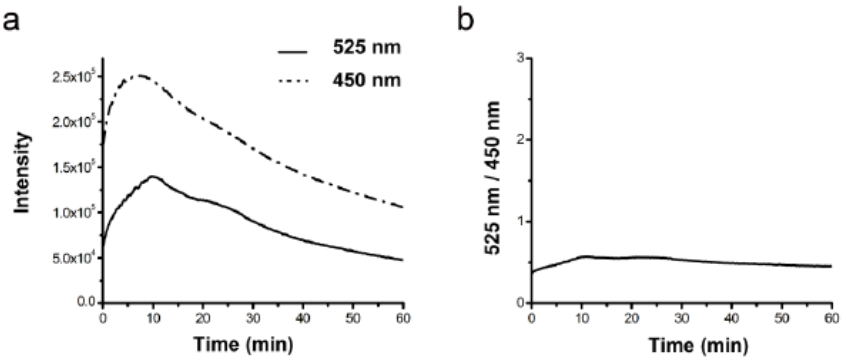

Supplementary Figure 2.3. Stability of BRET signal for CalfluxVTN expressed in HEK293 cells. (a) HEK293 cells expressing CalfluxVTN were suspended in imaging media and the intensity of NanoLuc luminescence (NLuc) and the intensity of the resonance transfer to Venus (BRET) were monitored over time. (b) Stability of the BRET ratio over the course of 1 hour.

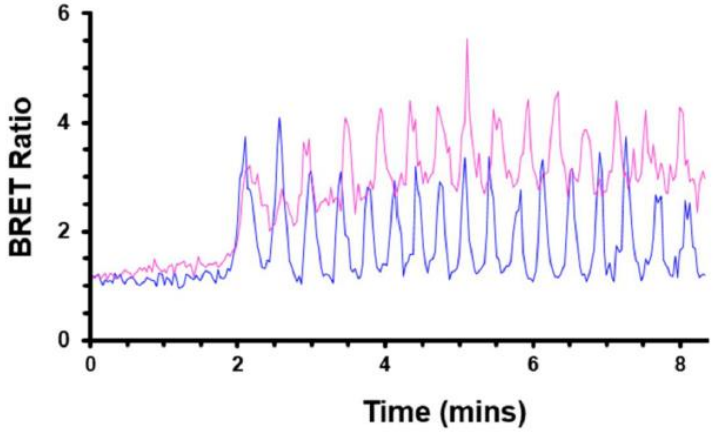

Supplementary Figure 2.4. BRET ratio values collected in two different HeLa cells after 10 µM histamine was added to the medium at ~1.7 minutes. The medium consisted of FluoroBriteTM DMEM, 10 % fetal Bovine serum (FBS), and the experiment was carried out at 37ºC. Each trace (blue vs. pink) represents one HeLa cell's Ca^{2+} response to histamine stimulation.

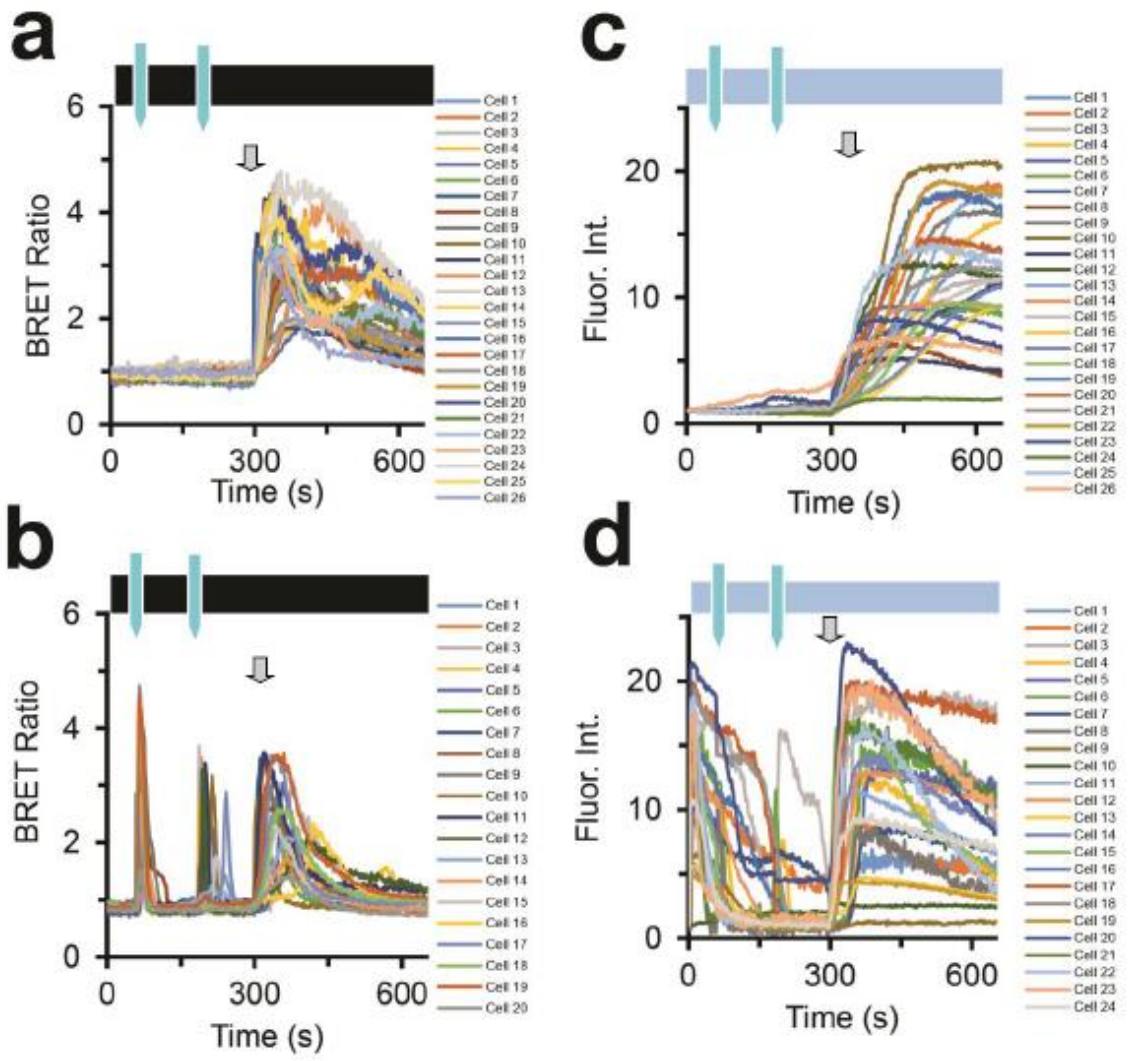

Supplementary Figure 2.5. Comparison of individual HEK293 cells used to test CalfluxVTN versus GCaMP6s as optimal optogenetic partners with melanopsin (Opn4). The CalfluxVTN alone (a), and the CalfluxVTN-2A-Opn4 (b) were imaged in darkness with two, whole-field, blue light flashes at 60 s and 180 s (black bar with blue tick marks) while the blue light flashes in the GCaMP6s alone (c) and the GCaMP6s-2A-Opn4 (d) were generated by increasing the intensity of the excitation light from dim continuous background (to excite the fluorescence of GCaMP6s) to bright 1 sec pulses at 60 and 180 sec to stimulate melanopsin (same light intensity as the pulses given to the CalfluxVTN samples). Gray arrows with black outlines depict where 1 μM Thapsigargin was added to the cells.

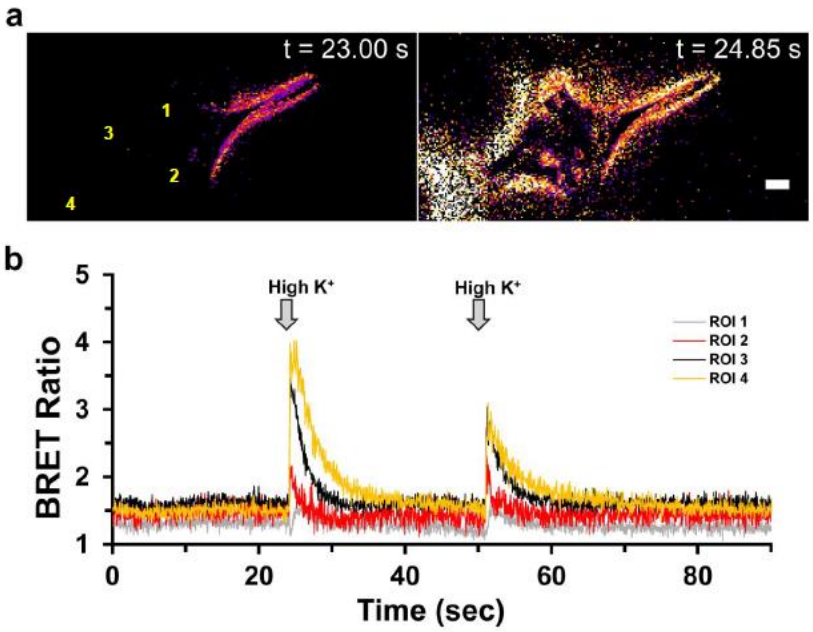

Supplementary Figure 2.6. Acute, coronal brain slice containing the dorsal hippocampus shows Ca^{2+} transients resulting from high K^+ (80 mM) stimulation. (a) BRET ratio images just before (left) and just after (right) high K^+ addition to the flow apparatus. Numbers correspond to regions of interest (ROI) in panel b. (b) BRET ratio values come from multiple ROIs within the acute dorsal hippocampal slice responding to high K^+ (80 mM) stimulation with Ca^{2+} transients. Image acquisition speed was 20 Hz. (scale bar = 50 um)

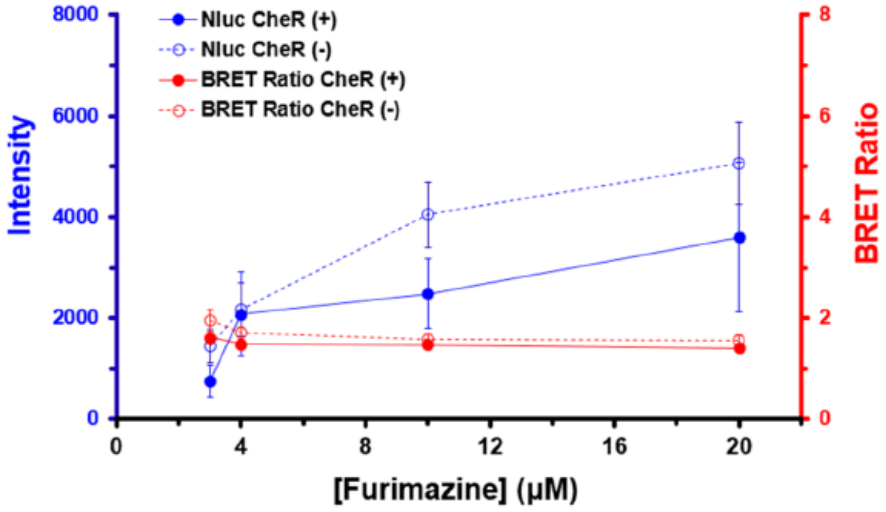

Supplementary Figure 2.7. Comparison of the relationship between Nanoluc (Nluc) intensity and the corresponding BRET ratio in hippocampal neurons expressing CalfluxVTN and CheRiff (CheR) simultaneously. Furimazine concentration was increased in the same neurons (CalfluxVTN with and without CheRiff) and both the intensity of the Nluc signal and the BRET ratio were immediately measured. Luminescence intensity increased with increases of furimazine concentration, but the BRET ratio remained stable (mean ± S.E.M.). Ten micromolar furimazine is the standard concentration used in the experiments reported in this study.

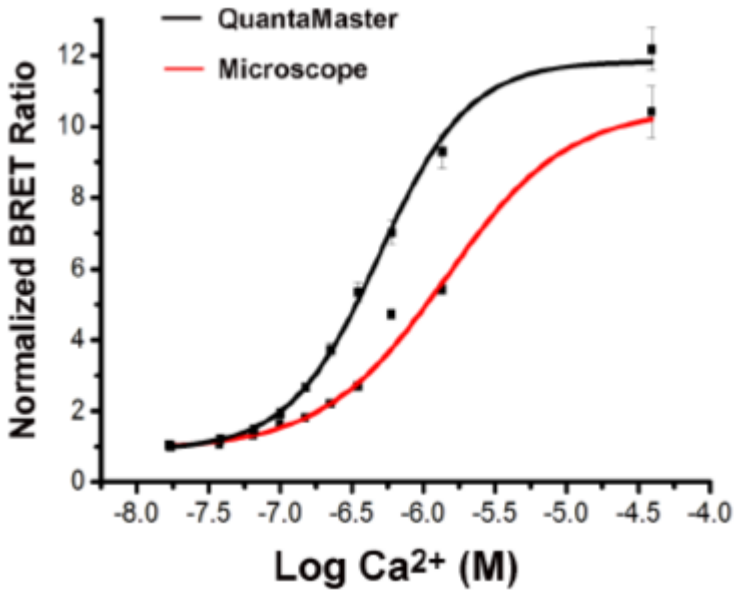

Supplementary Figure 2.8. BRET ratio calibration curve generated as in Fig. 1c with purified CalfluxVTN and Ca^{2+} buffers from Molecular Probes® except that these Ca^{2+}-buffered solutions were placed on a microscope slide (red trace) and imaged on the microscopic setup. In this case, the "Venus" signal is all the light emitted from 520 nm and longer, whereas the "NanoLuc" signal is all the light emitted in the range of 440-520 nm. The BRET ratio is calculated from those signals as "Venus"/"NanoLuc". For comparison, the calibration curve from Fig. 1c was included (black trace). Data points represent the mean ± S.E.M.

CHAPTER III

NOVEL BIOLUMINESCENT CALCIUM ION REPORTERS ALLOW FOR GREATER UTILIZATION OF SMALL MOLECULE LIBRARIES IN HIGH THROUGHPUT SCREENS

Abstract

High throughput screens (HTSs) are a beneficial early component of bringing a drug to market. However, based on assay fluorescence conditions, some small molecules are being discarded because of emission properties which directly overlap with the fluorescence assay probe. Here, we describe the Ca^{2+}-sensitive ratiometric, luminescence-based probe CalfluxCTN which reliably reports intracellular [Ca^{2+}] changes in the presence of a fluorescent compound with a very high quantum yield and efficiency (fluorescein). Initial characterizations illustrate the usefulness of CalfluxCTN with whole-plate imagers, include successful Z`-factor measurements (> 0.5) and applicability for assays that may need to be run over the course of several hours.

Introduction

Fluorescence sensors have become standard tools for studying cellular and molecular processes (Zhang & Xie, 2012; Rodriguez et al., 2017). Some of the commonly used sensors are relatively small molecule probes such as Fura2, Fluo-4, and Fluo-8 (sensors of cytosolic Ca^{2+} levels (Tsien et al., 1985; Gee et al., 2000; Vetter, 2012)), while others are genetically encodable such as GCaMP6 and Cameleon (also [Ca^{2+}] sensors, (Miyawaki et al., 1997; Miyawaki et al., 1999; Chen et al., 2013). Genetic engineering by structure-based mutagenesis and directed evolution has optimized the fundamental properties of fluorescent proteins to adapt them to myriad

applications. However, all these sensors inextricably depend upon fluorescent excitation that can trigger background fluorescence (e.g., tissue autofluorescence), phototoxicity, photoresponses (in photosensitive tissues), and photobleaching of the sensor. Autofluorescence in particular can be problematic because all tissues have background autofluorescence due to NADPH, flavins, lysosomes, etc., and many tissues have especially high autofluorescence due to characteristic pigments (e.g., chlorophyll, hemoglobin), extracellular matrices (e.g., collagen, elastin, etc.), or after fixation for histology.

While background fluorescence is sometimes merely an annoyance that can be circumvented by using a fluorescent sensor with different properties (e.g., excitation/emission wavelengths), in some applications the background fluorescence creates uncorrectable problems that have deleterious biomedical implications. One such application is the discovery of new drug candidates by High-Throughput Screening (HTS) of cell cultures. HTS often relies upon fluorescence sensors of a physiological response within cells in which compounds from a chemical library are tested one by one for their ability to act as agonists or antagonists. But when the compounds being tested (e.g., agonist, antagonist, and/or allosteric modulator) are themselves fluorescent, this background fluorescence interferes with the signal from the sensor (Zhang & Xie, 2012). Many compounds within small molecule libraries that are used for HTS (especially xanthines (Shukla & Mishra, 1994), curcumins (Chignell et al., 1994) and coumarins (Reddy et al., 1986)) exhibit intrinsic fluorescence emission. These very same molecules may have beneficial biomedical properties: for example, xanthine derivatives are well-characterized neural stimulants while both curcuminoids and coumarin-like molecules have been effective in treating a variety of cancers (Musa et al., 2008; Chearwae et al., 2005; Changenet-Barret et al., 2016; Monteiro et al., 2016). As shown below, potentially effective compounds in HT screens that are intrinsically

fluorescent will cause a background that might cause many efficacious compounds to be ignored, or at best, necessitate retesting by a non-fluorescent assay (in some very high throughput screening situations, an entire plate of compounds might be thrown out because of the global interference by one highly fluorescent compound in the plate). Our spectral measurements of ~100,000 randomly chosen compounds from the Vanderbilt (VICB) Discovery Collection found that ~7000 compounds are intrinsically fluorescent. That is a large percentage of small molecule HTS libraries to ignore simply because the sensor assay is inadequate.

An optimal HTS sensor would be impervious to fluorescence interference and enable an assay of every compound in the HTS library in the initial screen. Luciferase-based sensors are an option that avoids the problems associated with fluorescence excitation and have been previously used in HTS contexts ranging from cell viability screens to gene expression changes (Zhang & Xie, 2012; Siebring-van Olst & van Beusechem, 2018). However, those previous luminescence HTS experiments used old-generation luciferases that were dim (therefore noisy read-outs), and there has been no attempt to demonstrate the advantages of luminescent sensors when screening libraries that include fluorescent compounds. A luminescence sensor does not require excitation because the light signal is a result of an enzyme-catalyzed chemical reaction rather than fluorescence. Therefore, the optical measurement of response is made in darkness so that the intrinsic fluorescence of any compound in the chemical library is not stimulated.

We have demonstrated the usefulness of BRET (Bioluminescence Resonance Energy Transfer (Y. Xu et al., 1999; X. Xu et al., 2007)) luminescence sensors in another context where overlapping fluorescence spectra is deleterious, namely in optimal coupling of BRET sensors with optogenetic actuators (Yang et al., 2016). BRET luminescence sensors are ratiometric, so they monitor a targeted activity independently of the intracellular concentration of the sensor (e.g.,

expression level for a genetically encoded sensor) because the measured quantity is the ratio of intensities at two wavelengths, and not a single intensity alone. Moreover, ratiometric recording is less sensitive than intensity recording to the presence of fluorescent or light-absorbing compounds in the library because the change that is monitored is not the signal intensity of one wavelength but the ratio of two separate wavelengths.

We here apply our new BRET Ca^{2+} sensor called Calflux to circumvent fluorescence background problems for HTS. BRET avoids the problems of fluorescence background that hampers HTS by monitoring luminescence signals in darkness without any exogenous excitation. Our BRET Ca^{2+} sensor is genetically encodable to allow targeting to specific cell types and/or cellular loci, and it employs a newly developed luciferase (NanoLuc™) that is 100-150X brighter than previous luciferases (Hall et al., 2012) with excellent signal-to-noise ratio (SNR). We show here that background fluorescence does not interfere with agonist or antagonist screens when using BRET sensors. Finally, we introduce a luciferase substrate (not previously used for HT screens) that sustains the lifetime of the BRET/luminescence signal for hours so that stable & reliable HTS results can be obtained that are directly comparable among replicate plates.

Materials and Methods

DNA plasmid construction. The CalfluxCTN DNA was assembled from 5` to 3`: Clover (with a 9-amino acid deletion in the C terminal – CΔ9), Troponin C (TnC) from *Opsanus tau*, then NanoLuc (NLuc). The CalfluxCTN fusion protein was made via polymerase chain reaction (PCR). The Ca^{2+}-sensitive TnC domain for CalfluxCTN was synthesized using Twitch-2B fluorescent Ca^{2+} indicator as a template (Thestrup et al., 2014), while the plasmids pcDNA3.1 Clover (ThermoFisher) and pNL1.1 (Promega ID#: N1001) were used as DNA templates for the Clover

and NLuc respectively. To create *E. coli* expression plasmids, DNA was inserted into the pRSETB plasmid using the restriction enzyme sites EcoRI and HindIII to create a N-terminal six-histidine-tagged (His6) protein. For mammalian expression, pcDNA3.1/Puro-CAG-VSFP-CR (Addgene ID#: 40257) was used as the backbone, where the VSFP portions were removed and CalfluxCTN inserted via the NheI and BamHI restriction enzyme sites.

***In vitro* Ca^{2+} assays.** BL21 *E. coli* was used for expression of CalfluxCTN under the control of the pRSETB plasmid. Bacteria were grown in shaking culture for 48 hours at 37 °C and cells were lysed via sonication. Using the His6 tag fused to the construct, the protein was purified via TALON Co^{2+} metal affinity resin (Clontech Laboratories Inc.). To assess the emission spectrum of the purified proteins in response to changing Ca^{2+} concentration ($[Ca^{2+}]$), a QuantaMaster fluorescence spectrophotometer was used. Furimazine (Promega ID#: N1110) solution (10 μM final concentration for these experiments) was added to each tube containing purified protein combined with a variety of Ca^{2+} buffers (Invitrogen) and the light emitted from 400 nm and 600 nm was collected.

Mammalian cell expression and selection of stably-expressing cell lines. CalfluxCTN was expressed in CHO cells which already stably expressed human muscarinic receptor 1 (hM_1) (gift from Coleen Niswender, Vanderbilt Medical Center). The CHO cells were grown in Gibco DMEM/F-12 (Ham) + GlutaMAX™ supplemented with 10% FBS, 10 mM HEPES and 1 % antibiotic-antimycotic (Gibco) in a humidified 37 °C incubator. Cells were transfected with mammalian expression plasmids using the transfection reagent GeneCellIn (Bulldog Bio). Since CHO cells previously stably-expressed hM_1 under G418 selection, after a 72-hour wait period,

both 10 μg/ml puromycin and 800 μg/ml G418 sulfate (RPI Corp) were added to the selection media. Cells that survived the selection process were counted in a hemocytometer, diluted (0.8 cells per 200 μl) and plated in clear-bottomed, tissue culture treated, 96-well plates (Costar, Corning Inc) for clonal selection. Afterwards, cells were again grown in growth media free of selection agents for the remainder of experiments.

Optical data acquisition for *in vivo* experiments. Cells were imaged in either OptiMEM media (Gibco) or in a simple HEPES-buffered salt solution: in mM – 1.26 $CaCl_2$, 0.49 $MgCl_2$, 0.41 $MgSO_4$, 5 KCl, 0.44 KH_2PO_4, 4.16 $NaHCO_3$, 150 NaCl, 0.34 Na_2HPO_4, 10 HEPES pH 7.2, and D-glucose was added fresh at 0.6% wt/vol. For the PMT-based plate reader experiments, a PolarStar Optima plate reader (BMG Labtech Inc.) was used to collect the light emitted from mammalian cell lines with 470/10 EM, and either 530/10 EM or 520 LP emission filters. For some plate reader experiments, luciferin substrate was added by hand immediately before imaging and then the plate was inserted into reader, while in other experiments the luciferin substrate was mixed with the stimulation molecule so that a non-luminescent pre-substrate-addition state was recorded. Cells were either imaged in the previously mentioned HEPES-buffered solution or in OptiMEM media without phenol red. For the 384-well plate experiments where entire plates were imaged, a custom PanOptic II plate imager (WaveFront Biosciences) and a Hamamatsu FDSS 7000 were used. The PanOptic II captured images using an EM-CCD (Andor iXon). For BRET recordings, the filters used were custom, 50 mm diameter, 460/70 nm EM and 520 nm LP (SemRock) and each filter was passed in front of the emission path using a filter turret to capture the desired light output. The images were binned 4 x 4, with a pre-amp gain of 2, an exposure time of 100 – 500 ms depending on the initial brightness for the plate. For fluorescence recordings, a GFP filter set

with 482/35 nm EX and 536/40 nm EM filters were used. The FDSS 7000 also used GFP filters and an Orca-ER CCD imager (Hamamatsu).

Coelenterazine analogs. Most of the coelenterazine analogs were purchased from Nanolight™ Technology. Furimazine was procured from Promega while coelenterazine 400a/1-bisdeoxycoelenterazine (C400a) and proprionated coelenterazine 400a/acetoxymethyl bisdeoxycoelenterazine (BC400a) was synthesized by the Vanderbilt Chemical Core (Nashville, TN) (Levi et al., 2007). The other coelenterazine analogs were purchased from Nanolight Technology (Prolume Ltd). The analogs were dissolved in 200 proof ethanol and the exact concentrations used in each experiment are stated in each figure legend. For long term storage, each analog was stored under argon gas at -80 °C.

Carbachol checkerboard. A 30 μM carbachol (saturating, final concentration) vs. vehicle (media) checkerboard was used to determine the effectiveness of CalfluxVTN as a high throughput screening reporter. Using the robotic arm and 384-well head of the PanOptic II, a 2-fold concentration of ingredients were added to a black, clear bottomed 384-well plated from a another 384-well plate where either 60 μM (2x) of carbachol or vehicle were in distributed like a checkerboard pattern. For experiments with C400a, ~ 10 μM final concentration was used and was added right before imaging of the plate. However, when BC400a was used as the luciferin, cells were incubated with a 60 μM concentration for 35 minutes before imaging. Excess BC400a was not rinsed prior to imaging. When testing how well the Ca^{2+} sensors performed with a highly fluorescent background 10 μM fluorescein (final concentration) was added to half a plate in the case of CalfluxCTN, or just in one well for Fluo8-AM (Abcam plc, CAS#: 1345980-40-6)

experiments. Fluo8-AM was used at ~ 5 μM and was incubated with the cells for 50 mins – 1 hour before rinsing with PBS (Gibco) and then imaging. Because CHO cells actively pump molecules like Fluo8 back outside of the cytoplasm (Yin & Wang, 2016), 1 mM of the organic anion transporter (OAT) inhibitor Probenecid (Sigma) was used to inhibit those pumps and maintain a stable concentration of cytosolic de-esterified Fluo8 for imaging.

BRET ratio measurements under the influence of fluorescein. Determining how fluorescein affected the BRET ratio in unstimulated cells was achieved via fluorescein concentration response curves (CRCs) with a range of 0 to 100 μM fluorescein using a 3-fold, serial dilution between each concentration. Cells with these fluorescein-contaminated BRET ratio measurements were compared with cells exposed to no fluorescein at all.

Carbachol concentration response curves (CRCs). To measure the sensitivity of the Ca^{2+} response of CalfluxCTN to carbachol stimulation in $CHOhM_1$ cells, a 384-well plate was used which contained serial dilutions of carbachol (Sigma). The maximum, final concentration of carbachol per well was 20 μM and then it was diluted 3-fold until 12 concentrations were made. The concentrations ranged from 0.17 nM to 20 μM. For Fluo8-AM carbachol CRCs, an identical protocol with the same concentrations were used and the effective half-maximal concentration (EC50) was determined by curve-fitting in R.

Scopolamine concentration response curves (CRCs). To determine the effective working concentration of scopolamine that would antagonize a 30 μM stimulation, CHO cells incubated in 5 μM Fluo8-AM were plated in 96-well plates in OptiMEM with a serial, 10-fold dilution of

scopolamine (50 μM to 0.05 nM, and 0 nM). Once inserted into the plate reader (PolarStar Optima) 30 μM carbachol was injected into each well and the fluorescence change was recorded.

Impact of fluorescein on recordings of antagonist activity. CHO cells were plated in 96-wells plates and 30 μM carbachol was injected into each well using the PolarStar Optima plate reader. Half of the wells contained 10 μM scopolamine (muscarinic receptor antagonist) and the difference between the responses after carbachol addition +/- 10 μM scopolamine were calculated. The 10 μM scopolamine concentration was used after it was determined by CRC calculations that it was close to the minimum concentration that could produce significant antagonism of the 30 μM carbachol stimulation. Additionally, 10 μM is also the standard concentration of HTS assay test compounds. While half of wells contained 10 μM scopolamine (on the horizontal axis: 1 through 12), all wells A through H also contained serial dilutions of fluorescein (in μM: 10, 2.5, 0.625, 0.156, 0.039, 0.010, 0.002, 0). This multi-factor paradigm would allow for comparison of fluorescein's impact on inhibited and non-inhibited cells. Identical plate structures were used for both the fluorescent Fluo8-AM measurements and the BRET CalfluxCTN recordings.

Data analysis. Data from the PolarStar Optima and the WaveFront Panoptic II were output as text files. The software program RStudio IDE, based on the language R (including the packages tidyverse, stringr, scales, RColorBrewer), was used to load, extract, and visualize all the data. Examples of code used in the data analysis are included. For time series experiments, emission counts were normalized by dividing all data points by the baseline emissions prior to stimulation when the signals collected from the "blue" and "green" channels were stable. For checker board experiments, the time-point of peak data was defined as mean of the 5 seconds when the highest

BRET ratio was reached in carbachol stimulated wells. The Z`-factor calculations (Zhang et al., 1999) were performed using the average peak ratio after high carbachol stimulation compared with the same time-point in the vehicle-treated wells in a checkerboard-formatted 384-well plate. The Z`-factor for each plate was calculated as follows:

$Z` = 1 - \frac{3(SDpos + SDneg)}{|MEANpos - MEANneg|}$, where SDpos represents the standard deviation of the carbachol stimulated wells, SDneg the standard deviation of the vehicle treated wells, and MEANpos and MEANneg are the means of the carbachol and vehicle treated wells respectively. A non-linear least squares (nls) function in R using the sigmoid formula:

$y = a + \frac{b}{c^x + d}$, (where a = y intercept, and b, c, & d are adjustable parameters that collectively contribute to the slope angle, direction and maximal value) was used to fit the BRET ratio vs. Ca^{2+} response in purified CalfluxCTN as well as the carbachol CRCs. Starting parameters for each model were set by visual inspection of the data and then allowed to converge on the most accurate coefficients.

Results

***In vitro* characterization of CalfluxCTN.** Our BRET sensors of free calcium ions share the Ca^{2+}-sensitive troponin-C sequence (from *Opsanus tau*) and linkers with the fluorescent Ca^{2+} indicator Twitch-2B (Threstrup et al., 2014). Our CalfluxCTN sensor interposes this Ca^{2+}-sensitive troponin-C sequence between NanoLuc luciferase (Hall et al., 2012) and a C-terminal truncated version of the fluorescent protein Clover (Lam et al., 2012) with linkers shown in Fig. 3.1A. We call this Ca^{2+} sensor CalfluxCTN for "CALcium FLUX composed of Clover (C), Troponin (T), and NanoLuc (N)." The Ca^{2+}-sensitive troponin sequence undergoes a conformational change in

response to binding Ca^{2+} that brings NanoLuc closer to Clover so that resonance energy transfer can occur with a concomitant spectral shift (Threstrup et al., 2014; Mank et al., 2006).

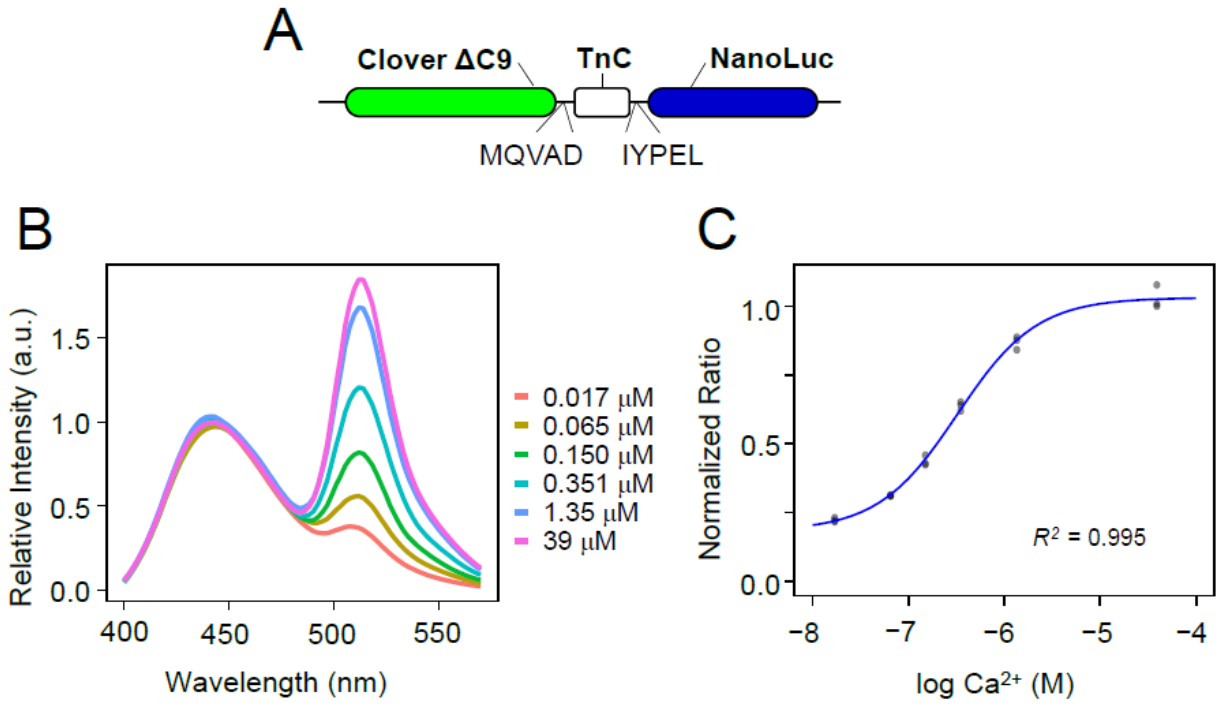

Figure 3.1. Characterization of purified CalfluxCTN *in vitro*. (**A**) Schematic of the amino acid sequence and general structure of CalfluxCTN. Clover with a C-terminal deletion of the last 9 amino acids fused to Troponin C (TnC) and NanoLuc (Nluc). Amino acid symbols of the linkers are included. (**B**) *In vitro* spectrum measurements of CalfluxCTN in response to buffers of different [Ca^{2+}] using furimazine as substrate. Spectra were normalized to the emission intensity at 444 nm. Spectra were normalized to the emission intensity at 444 nm. (**C**) BRET ratio (515 nm Clover peak : 450 nm NanoLuc peak) changes of CalfluxCTN plotted against log_{10} molar [Ca^{2+}]. Measurements were taken with a PTI QuantaMaster Fluorescence Spectrophotometer. (Representative data from three separate experiments.)

The spectral shifts of the NanoLuc-catalyzed luminescence as a function of [Ca^{2+}] *in vitro* are shown in Fig. 3.1B, where the 450 nm emission of NanoLuc is increasingly resonance-transferred to the 515 nm emission peak of Clover as the [Ca^{2+}] is ramped from 0.017 μM to 39 μM. Fig. 3.1C plots the BRET ratio (515 nm Clover peak : 450 nm NanoLuc peak) as a function of [Ca^{2+}] *in vitro* for CalfluxCTN, showing an excellent BRET response within the range of Ca^{2+} levels that spans basal cytosolic [Ca^{2+}] to typical Ca^{2+} activation concentrations. We tested several different

versions of CalfluxCTN to identify an optimal response to [Ca^{2+}] (Supplementary Fig. S3.1). As compared with our previously reported CalfluxVTN (where Venus served as the fluorescent moiety (Yang et al., 2016)), CalfluxCTN is more responsive to very low [Ca^{2+}] levels than is CalfluxVTN, but CalfluxVTN exhibits a larger dynamic range to changes in [Ca^{2+}] (Supplementary Fig. S3.2A & B).

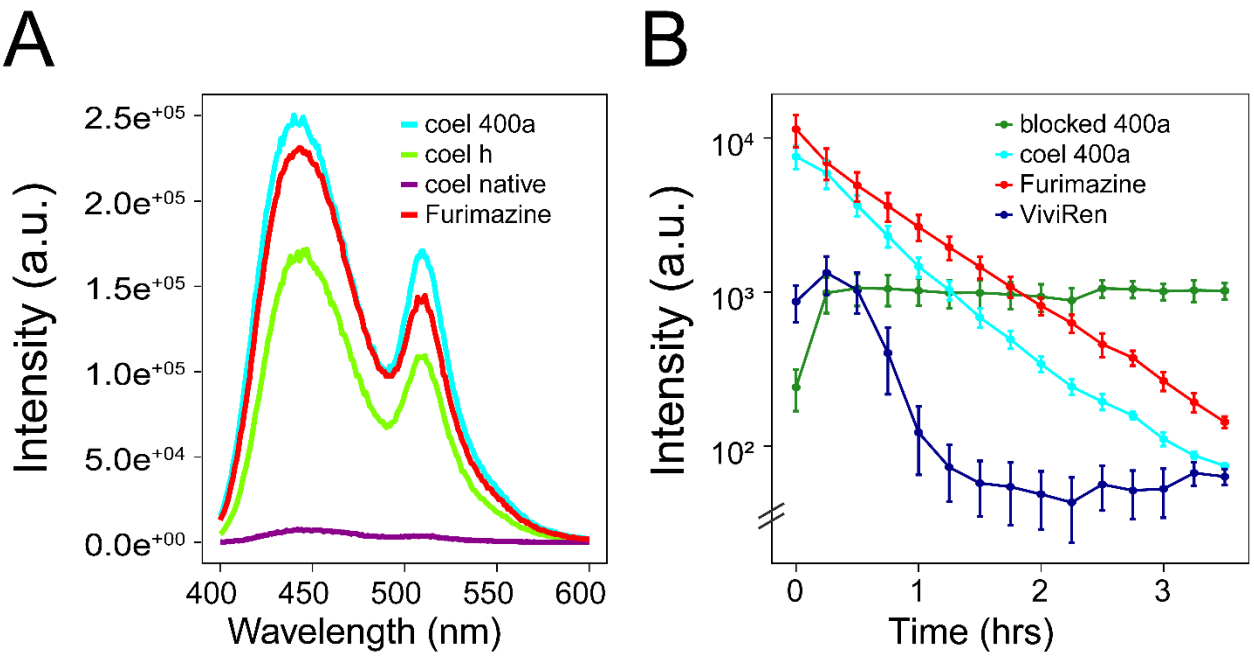

Figure 3.2. Properties of CalfluxCTN emission with different coelenterazine analogs. (**A**) CHO hM_1 cells expressing CalfluxCTN were tested with different coelenterazine analogs as substrates for Calflux and the emission spectra measured. (**B**) The total brightness of CalfluxVTN light emission over the course of 3 hours was measured. Included are "chemically blocked" (extracellularly inert) coelenterazine analogs ViviRen™ and blocked coelenterazine 400a ("blocked 400a" = acetoxymethyl bisdeoxycoelenterazine). All cells are unstimulated. Data points represent mean ± S.E.M. of three independent experiments (n = 3). Structures of these substrates are shown in Supplementary Fig. 3.4.

We chose to use the more sensitive CalfluxCTN in HTS applications rather than CalfluxVTN because its emission peak (515 nm) most closely matches that of fluorescein (Supplementary Fig. S3.2C), which we use herein to model the effect of endogenously fluorescent compounds in a screening library. This matching of emission wavelengths therefore constitutes the "worst-case

scenario" for fluorescence interference and therefore provides the best proof-of-principle that a luminescence sensor is superior for high-throughput screening of libraries that include a significant number of fluorescent compounds.

Effects of different luciferase substrates in cells. The substrate designed by Promega to optimally work with NanoLuc is furimazine (Hall et al., 2012), but other analogs of coelenterazine are effective substrates for NanoLuc and Calflux. We tested different coelenterazine analogs with Calflux to determine the optimal compromise between brightness and sustained signal intensity for HTS applications. As shown in Fig. 3.2A, the bimodal spectrum of CalflluxCTN is essentially identical with all substrates we tested. The luminescence of Calflux is brightest with furimazine, but coelenterazine 400a (1-bisdeoxycoelenterazine (Pfleger et al., 2006)) is equivalent. The luminescence signal with coelenterazine h (2-deoxycoelenterazine) (Pfleger et al., 2006) is approximately 1/2 that of furimazine or coelenterazine 400a, and the signal with native coelenterazine (Shimomura et al., 1962) is ~30X lower than with the brighter substrates. Although furimazine & coelenterazine 400a allow the brightest signal with Calflux, the signal is short-lived, peaking about 10 min after addition to cells transfected with Calflux and decaying over the next several hours (Fig. 3.2B and Supplementary Fig. S3.3A & B). Because Calflux is a ratiometric reporter (Fig. 3.1B & C), the signal decay is not a problem for accurate estimation of $[Ca^{2+}]$ levels as shown by the fact that the BRET ratio is stable for at least three hours (Supplementary Fig. S3.3C). However, as the signal intensity declines towards background, the signal-to-noise ratio (SNR) also decays. We therefore tested two versions of protected substrates that are inactive extracellularly but permeate into cells and are activated by intracellular enzymes (esp. esterases) that remove the chemical blocking groups. One is ViviRen^{TM}, a commercially available protected version of coelenterazine h.

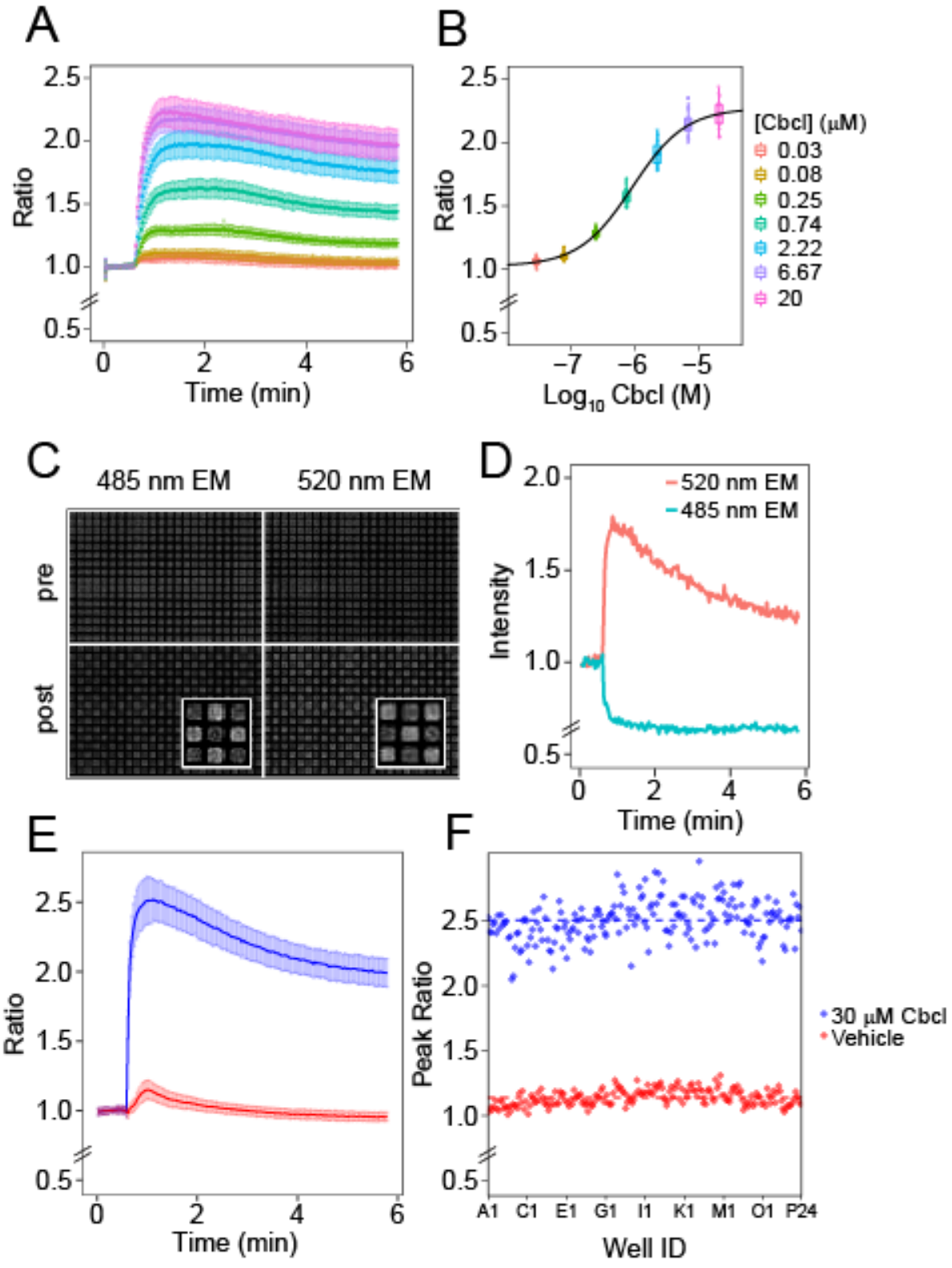
A
Ratio
Time (min)
B
Ratio
Log10 Cbcl (M)
[Cbcl] (μM)
0.03
0.08
0.25
0.74
2.22
6.67
20
C
485 nm EM
520 nm EM
pre
post
D
Intensity
520 nm EM
485 nm EM
Time (min)
E
Ratio
Time (min)
F
Peak Ratio
Well ID
A1
C1
E1
G1
I1
K1
M1
O1
P24
30 μM Cbcl
Vehicle

Figure 3.3. Response of CalfluxCTN to muscarinic receptor stimulation. CHO cells stably expressing CalfluxCTN were imaged using the WaveFront Panoptic II system in a 384-well plate. (**A**) Time course of CHO hM_1 cells stably expressing CalfluxCTN responding to different concentrations of the cholinergic agonist carbachol (concentrations identified to the right of panel B). Error bars at each time point are mean +/- S.D. for 16 wells. (**B**) Distribution of concentration response curve ratios of five independent experiments shown in A (mean +/- SEM, n = 5). (**C**) Luminescence intensity photograph of entire plate showing each well from which luminescence (at 485 nm and at 520 nm) was measured before ("pre") and after ("post") carbachol stimulation. Insets show magnified image of nine wells after carbachol addition. (**D**) Intensity measurements taken from the 485 nm and 520 nm channels from well A1 in the plate illustrating the reciprocal 485/520 intensity changes after carbachol (Cbcl) stimulation from which the BRET ratios were calculated. (**E**) Time courses for the wells shown in panel C, where the line represents the mean response and the error bars are +/- S.D. (**F**) Scatter plot showing the distribution of the peak responses to either 30 μM Carbachol or Vehicle measured at time = 1 min. Dotted lines indicate the means of each group. The Z`- factor for this representative plate was 0.52.

As shown in Fig. 3.2B, the luminescence from Calflux-transfected cells with ViviRen^{TM} began at a 10-fold lower level than furimazine/ coelenterazine 400a and declined further but stabilized at a low luminescence value after 1 h. We also tested a protected version of coelenterazine 400a ("blocked 400a"), namely acetoxymethyl bisdeoxycoelenterazine (Levi et al., 2007). The luminescence of Calflux-transfected cells treated with this blocked 400a started at a 10-fold lower level than furimazine or coelenterazine 400a, but the luminescence signal from cells was remarkably stable for at least 3 h thereafter (Fig. 3.2B). Because Calflux is so much brighter than previously available luminescent sensors (i.e., not based on NanoLuc), the 10-fold lower initial intensity is not a problem for SNR, and the stable signal allows more time flexibility for HTS assays and for assays that continue for an extended time. Therefore, we consider that blocked 400a allows an optimal trade-off between signal intensity vs. longevity.

Application of Calflux for HTS. G-protein coupled receptors (GPCRs) are a frequent target of HTS discovery of pharmacological agents. To determine the applicability of Calflux sensors for identifying compounds that agonize or antagonize GPCRs, we co-transfected CHO cells with CalfluxCTN and the human muscarinic acetylcholine receptor M_1 (hM_1R). Stimulation of this receptor with acetylcholine or its agonist carbachol elicits a Ca^{2+} release from intracellular stores, thereby increasing cytosolic [Ca^{2+}] (Inoue et al., 1995; Tong et al., 1999). As shown in Fig. 3.3A & B, the BRET response to carbachol treatment of CHO cells that are stably transfected with CalfluxCTN and hM_1R is dose-dependent and reproducible.

In a typical HTS 384-well plate format using a WaveFront Panoptic II that permits imaging of every well simultaneously, we monitored the response of the CalfluxCTN-transfected hM_1R cells in real time with an image capture rate of 100-250 ms per image. As shown in Fig. 3.3C (upper panels), the pre-stimulation signal in both the green (520 nm EM) and blue (485 nm EM) channels was consistent among the wells, yielding a reproducible BRET ratio before carbachol treatment of approximately 1.0. At time 0.6 min, 30 μM carbachol vs. vehicle control was added in a "checkerboard" pattern that is obvious in the post-stimulation images shown in Fig. 3.3C (lower panels). The carbachol-treated cells increased their [Ca^{2+}] level, which was reported by Calflux as an increase of green luminescence simultaneously with a decrease in blue luminescence (Fig. 3.3D), as expected from the *in vitro* characterization of Calflux response to Ca^{2+} (Fig. 3.1B). Wells that received carbachol clearly showed a decreased blue luminescence and an increased green luminescence (see insets in lower panels of Fig. 3.3D). These data were quantified as BRET ratios and reorganized into time-courses of the control vs. carbachol-treated groups as shown in Fig. 3.3E. There is excellent separation between the two groups and precise quantification of the Ca^{2+} fluxes elicited by hM_1R stimulation with low well-to-well variability. The peak response (at

time = 1 min) of each well is plotted in Fig. 3.3F, and the resulting Z' factor was calculated to be 0.52, which is well within the commonly accepted range for excellent separation of response vs. no-response for HTS (0.4-1.0) (Zhang et al., 1999).

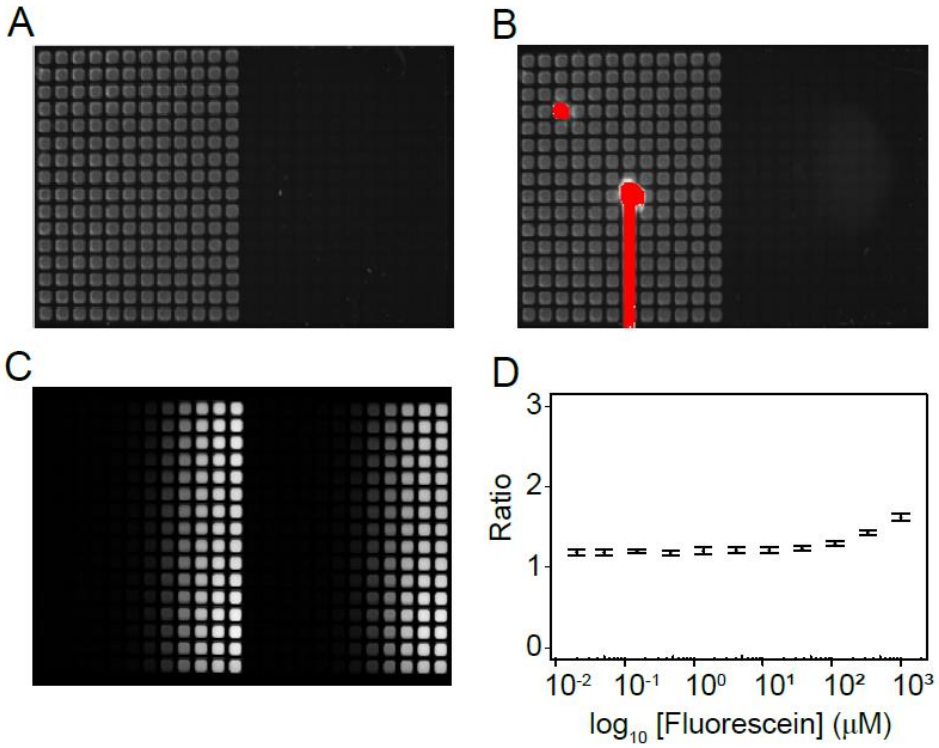

Figure 3.4. Visual demonstration of fluorescence crosstalk during fluorescence-based cell assays. (**A**) Fluorescence image taken of a 384 -well plate using the Hamamatsu FDSS 7000 where the left half of the plate was loaded with cells containing 5 μM Fluo8-AM, while the rest of the plate is free of cells. The acquisition settings were set for a typical fluorescence screen. (**B**) Fluorescein was added to two wells and the fluorescence scan of the plate was re-acquired. 1 μM fluorescein was added to well D3 (near top left) and 10 μM fluorescein was added to well I7 (middle of the left half of the plate). (**C**) In a separate experiment, CHO cells stably expressing CalfluxCTN were plated across an entire 384-well plate and a range of concentrations of fluorescein was added to the wells. Panel C depicts the fluorescence of the plate as captured by the WaveFront Panoptic II to show the gradient of fluorescence intensities generated by fluorescein. (**D**) Luminescent BRET ratios of unstimulated CHO cells stably expressing CalfluxCTN in the fluorescein-gradient plate of panel C. Calflux BRET ratio is not affected by background fluorescence except for a slight increase at the very highest concentrations of fluorescein.

Fidelity of BRET signals in highly fluorescent backgrounds. As described in the Introduction, small molecule libraries for HTS typically include 5-10% of compounds that are intrinsically fluorescent. Fluorescent compounds are typically ignored during initial screens with fluorescent

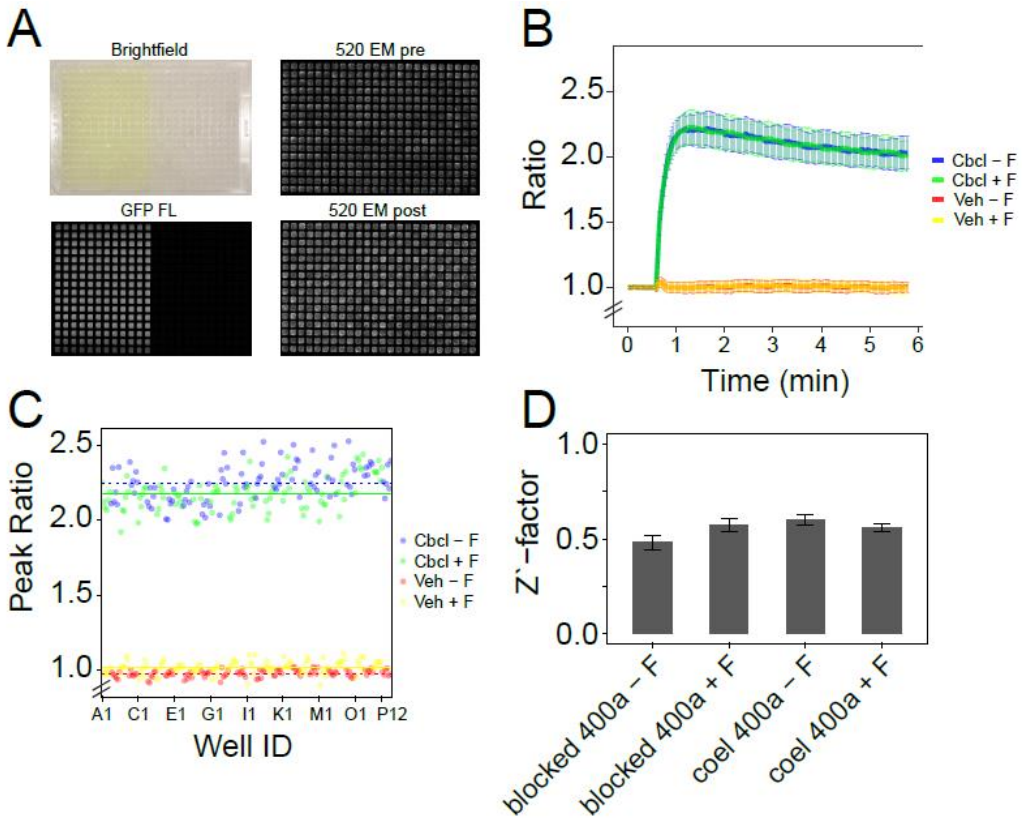

Figure 3.5. Fidelity of CalfluxCTN BRET signal changes elicited by agonists in highly fluorescent backgrounds. (**A**) Images of 384-well plates with half of the wells containing 10 µM fluorescein (columns 1-12 contain fluorescein, while columns 13-24 do not). Upper left, brightfield image of white plate showing yellow color of fluorescein-containing wells on left side. Lower left, black HTS plate showing fluorescence of fluorescein-containing wells on left side. Right images show the luminescence (at 520 nm) of the same black HTS plate emanating from CHO cell stably expressing CalfluxCTN before ("pre") and after ("post") treatment with carbachol. (**B**) Time course of BRET ratio changes in response to 30 µM carbachol (Cbcl) checkboard pattern (Veh – vehicle) showing the mean +/- SD of each treatment of the black plate in panel A. The response is essentially identical in the presence (+ F) or absence (- F) of 10 µM fluorescein (+/- F). (**C**) Peak response of BRET ratio to the checkerboard stimulation shown in panel B. The dotted line depicts the mean of the peak response of fluorescein-treated wells (+ F) while the flat line shows wells without fluorescein (- F). (**D**) Summary of Z` factors of CalfluxCTN with blocked and non-blocked coelenterazine 400a substrates in the presence (+ F) or absence (- F) of fluorescein (mean +/- SEM, n = 6).

sensors because their fluorescence washes out the sensor's signal. An example is shown in well D3 of Fig. 3.4B, where the background of 1 μM fluorescein obscures the Fluo8 fluorescence signal of that well. Moreover, the fluorescence of some compounds is so bright that its emission overwhelms the sensor signal emanating from adjacent wells, thereby necessitating rescreening the compounds of the adjacent wells even though they are not intrinsically fluorescent. An example of this "flare-out" phenomenon is also shown in Fig. 3.4B, where 10 μM fluorescein in well I7 causes fluorescence "bleed" for half of the entire column #7. Note that 10 μM is the standard concentration of compounds tested in initial HT screens, so a fluorescent compound in a test might easily be as bright as 1-10 μM fluorescein. The images in Fig. 3.4A & B were taken with a Hamamatsu FDSS 7000 system, which is a standard HTS system. With the WaveFront Panoptic II system, the camera can respond even more dramatically to the flare-out problem so that half of the entire plate is spoiled (Supplementary Fig. 3.5).

Therefore, a luminescence-based HTS method that avoids excitation could be advantageous. Fig. 3.4C & D illustrates the imperturbability of the luminescence BRET signals in cells over a wide range of fluorescence background. We used fluorescein with CalfluxCTN because their emission peaks coincide (Supplementary Fig. S3.2C) and therefore this combination constitutes the worst-case scenario for potential interference. The BRET ratio of CalfluxCTN in unstimulated CHO cells is essentially unaffected by the presence of fluorescein at concentrations up to ~10 μM, which is a standard initial concentration of compounds tested in HTS. The same imperturbability is obvious during the dynamic stimulation of Ca^{2+} fluxes by carbachol acting on hM_1R (Fig. 3.5). The response to the agonist carbachol is essentially identical in the presence or absence of fluorescein. Therefore, a strong fluorescence background of compounds in a HTS

library will have no significant effect on the kinetics, well-to-well variability, or Z' factors of a BRET sensor such as Calflux (Fig. 3.5D).

BRET sensor reveals antagonist action undetected by fluorescent sensors. As a further demonstration of the value of a luminescence sensor, we assessed the detectability of an antagonist in a mock HTS screen based on Calflux vs. a fluorescence Ca^{2+} sensor (Fluo8). Scopolamine is a well-characterized antagonist of the carbachol stimulation of the M_1-GPCR (Klinkenberg & Blokland, 2010). We asked the question of whether an intrinsically fluorescent antagonist with the properties of scopolamine (here represented by scopolamine + fluorescein) could be most efficiently detected by a sensor with an intrinsic fluorescence emission profile similar to the antagonist (here represented by Fluo8) as compared with the luminescence BRET sensor Calflux. Fig. 3.6A & C shows that the Calflux signal for neither the carbachol-induced stimulation of M_1-R nor the antagonism of this response by scopolamine is significantly affected by even a strong fluorescence background. Conversely, the Fluo8 signal is dramatically repressed by modest concentrations of fluorescein to the extent that the difference between the presence vs. the absence of scopolamine becomes invisible (Fig. 3.6B & D). In an unbiased HT screen, this means that a modest fluorescence background will completely wash out the ability to detect a potentially valuable antagonist when using a fluorescent sensor whereas a luminescent BRET sensor will have no trouble discovering the antagonist.

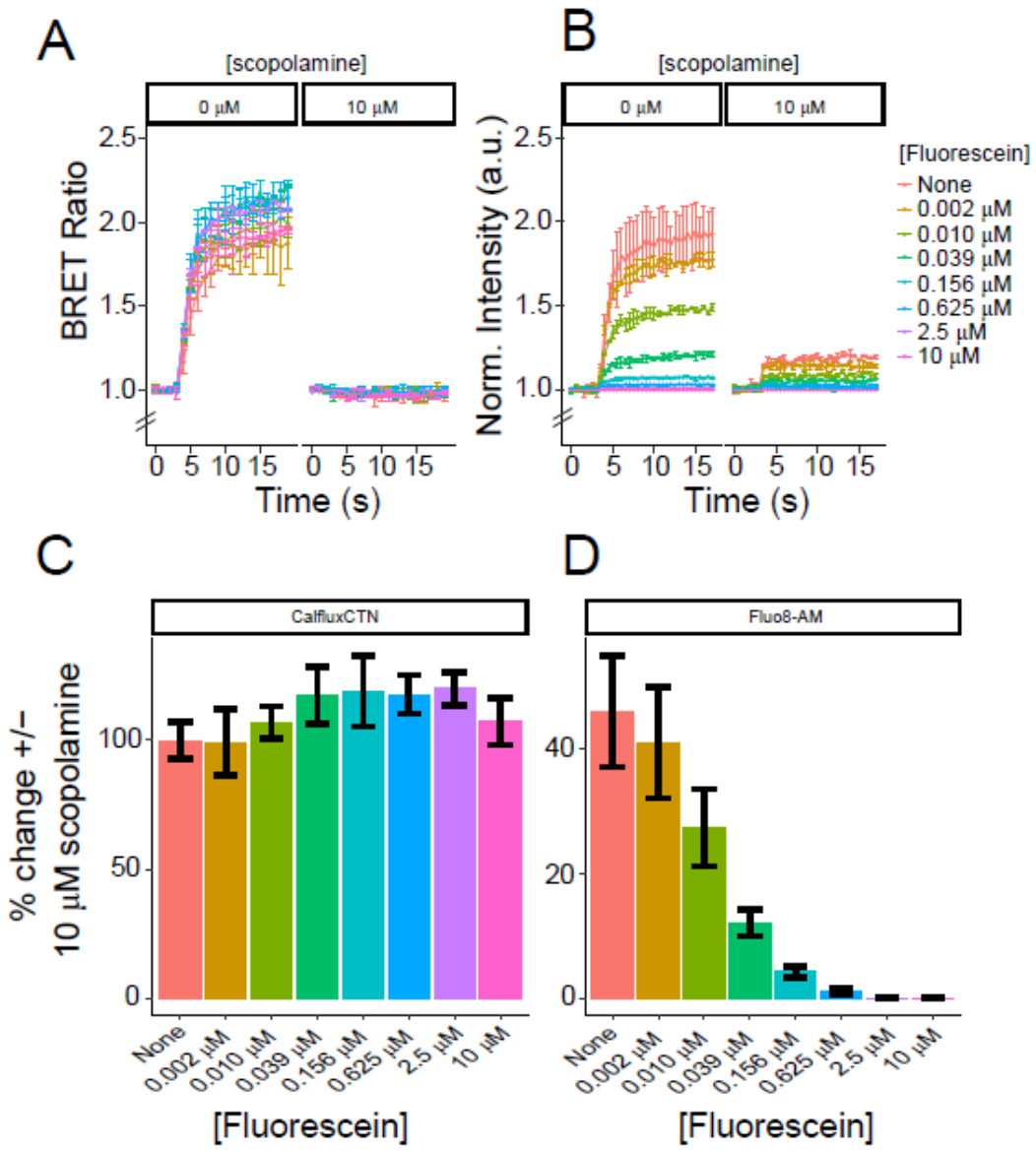

Figure 3.6. BRET sensor reveals antagonist action undetected by fluorescent sensors. CHO cells responding to stimulation of 30 µM carbachol with or without 10 µM scopolamine. (**A**) CalfluxCTN: left, BRET ratio response to carbachol shows large changes despite the presence of fluorescein in the reaction mixture; right, BRET ratio clearly shows the antagonism of 10 µM scopolamine +/- background fluorescence (key to concentrations of fluorescein shown to the right of panel B). (**B**) Fluo8: left, as the concentration of fluorescein increases, the Fluo8 intensity change in response to Ca^{2+} decreases; right, scopolamine represses the Fluo8 response, but above a modest fluorescence background (0.156 µM fluorescein and above, there is no differential between + scopolamine and - scopolamine due to the high baseline caused by fluorescence background (Supplementary Fig. S3.6). Data for panels **A** and **B** are mean +/- SD of 16 wells from representative 96-well plates. (**C**) CalfluxCTN: fluorescein has no significant effect on the BRET ratio percent difference between carbachol stimulation +/- scopolamine. (**D**) Fluo8: background fluorescence (fluorescein) lowers the detectable repression by the antagonist scopolamine. Data in **C** and **D** are mean +/- SEM of 48 wells from 3 different plates.

Discussion and Conclusions

In this study, we have characterized the drawbacks of using fluorescence-based methods for HTS when some druggable molecules (Lipinski et al., 2001) are also optically excitable. Moreover, we have demonstrated that test compounds with sufficiently high quantum yields and extinction coefficients can not only obscure measurements within the confines of their own wells, but can also perturb measurements of entire plates in some cases (Zhang & Xie, 2012). As a solution to these issues, we proposed and developed the Ca^{2+} sensor CalfluxCTN to show that background autofluorescence has no impact on luminescence signal fidelity. The CalfluxCTN signal was tested in the presence of fluorescein to show that even in the most likely case of optical interference (fluorescence, luminescence and/or absorbance), cytosolic [Ca^{2+}] can still be reliably monitored with our luminescence reporter (Fig. 3.3). Additionally, we demonstrated how a fluorescent molecule can increase the false negative and false positive detection rate of both agonist and antagonist HT screens (Fig. 3.5, 3.6).

In our estimation, the value of our BRET-based Ca^{2+} reporter as a replacement for fluorescence sensors in HTS is undeniable. Routinely, when researchers find a fluorescent molecule in their libraries that perturbs the assay, depending on the extent of the perturbation, either that molecule or the entire plate is disregarded. This approach makes sense since it is costly to screen the hundreds of thousands of compounds in a given library, and the average library size continues to increase each year (Macarron et al., 2011). Although there is a low probability that the discarded molecules are all cures for major illnesses, at this rate (~5-10 % fluorescent compounds per library), there really is no way to estimate how many good lead compounds are being overlooked due to assay limitations. Another element of complexity that reiterates the need for sensors like Calflux, is the fact that the number of older Americans taking multiple, daily

prescription drugs continues to increase (Zhong et al., 2013). Therefore, it is necessary to not only investigate the actions of one drug, but also how it interacts with other drugs since allosteric modulators of receptor function can have a positive or negative impact on drug efficacy (Han et al., 2015). Having one or multiple fluorescent allosteric modulators in HTS assays could increase the difficulty by an order of magnitude.

Obvious drawbacks to using our BRET-based Ca^{2+} sensor would depend on whether test compounds have any influence on the luciferase – luciferin catalysis or if coelenterazine substrates impact the target of the screen. So far, coelenterazine and its analogs have been used for many years in different scientific contexts and the working concentrations have yet to show adverse effects in mammalian systems. Additionally, a fluorescence-based Ca^{2+} sensor could still be used as long as the excitation and emission wavelengths do not overlap with fluorescence compounds similar to fluorescein within the library (e.g. Fura-Red (Kurebayashi et al., 1993), Calcium Crimson (Eberhard & Erne, 1991), or RCaMP (Akerboom et al., 2013)). However, without prior knowledge of the properties of constituent compounds in the library, researchers would have to run multiple assays using several different Ca^{2+} sensors which would increase costs and time. Furthermore, no matter where on the EM spectrum a fluorescence molecule's emission peaks, there will always be some lower intensity emission at other wavelengths that may interfere with any given fluorescence sensor, whereas a luminescence-based sensor will not be perturbed by any fluorescence background.

This report highlights the properties that make the CalfluxCTN Ca^{2+} sensor ideal for HTS applications. Bright BRET-based sensors can circumvent the artefacts common to fluorescence-based assays when test compounds share similar fluorescence properties with the sensor. Bioluminescence reporters can also be modified to sense a variety of ions and can have other

BRET partners (Suzuki et al., 2016; Chu et al., 2016) which expands the capabilities of HTS while introducing the possibility of multiplex assays.

Supplementary Data Figures

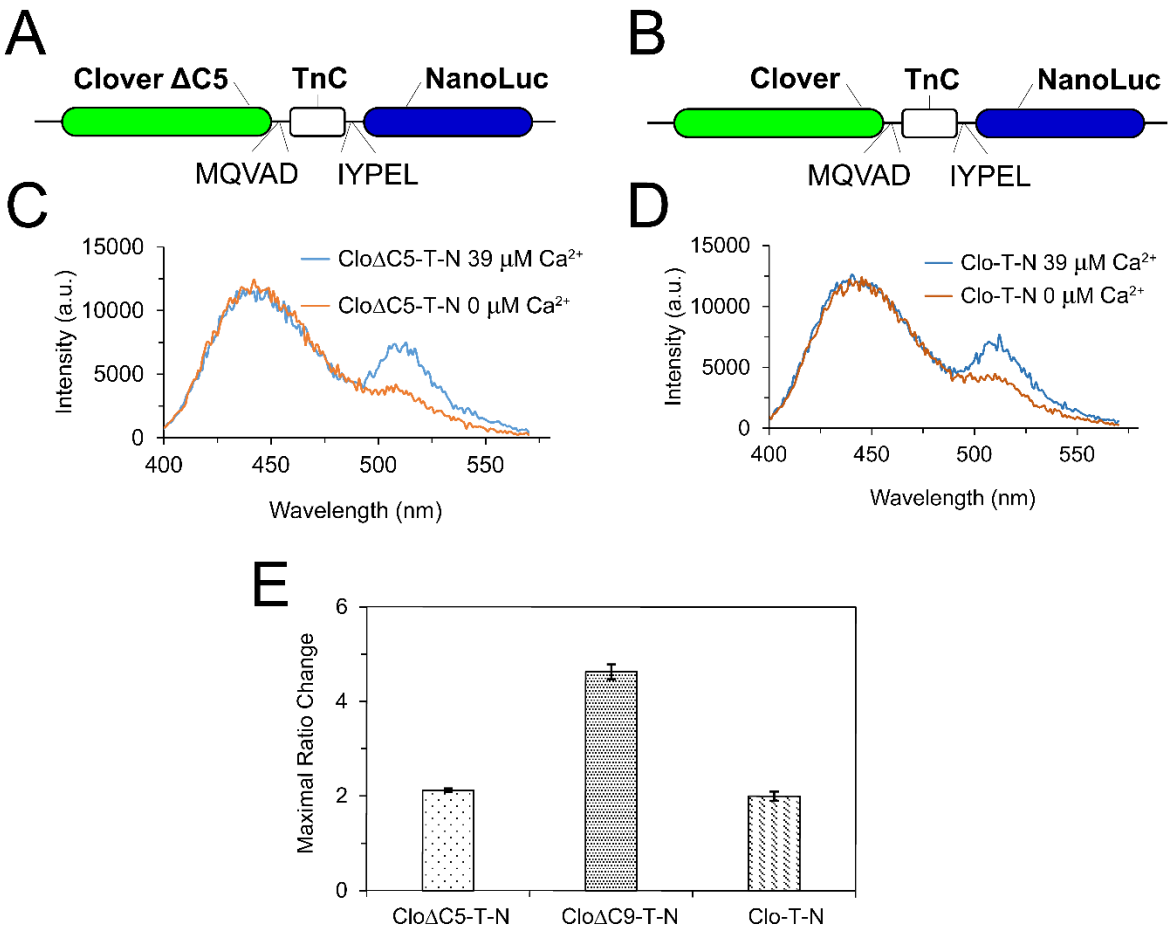

Supplementary Figure S3.1. Preliminary configurations of Ca^{2+} sensors based on Nluc BRET with Clover. (**A**) Clover with a 5-amino acid C-terminal deletion fused to TnC and Nluc. (**B**) Diagram of a different version where full-length Clover is C-terminally-tagged to Nluc and TnC. (**C**) Emission spectra probe with the 5-amino acid Clover deletion showing maximal ratio change from 0 to 39 μM Ca^{2+}. (**D**) Emission spectra of maximal response to Ca^{2+} changes using the version illustrated in panel B. (**E**) Comparison of maximal BRET ratio changes among CalfluxCTN and the two preliminary configurations. Maximum delta-BRET ratio change was defined as the BRET ratio difference between free Ca^{2+} (0 μM) and saturated Ca^{2+} (39 μM). Bars depict mean and error bars (+/- S.D.) of replicates (n = 3).

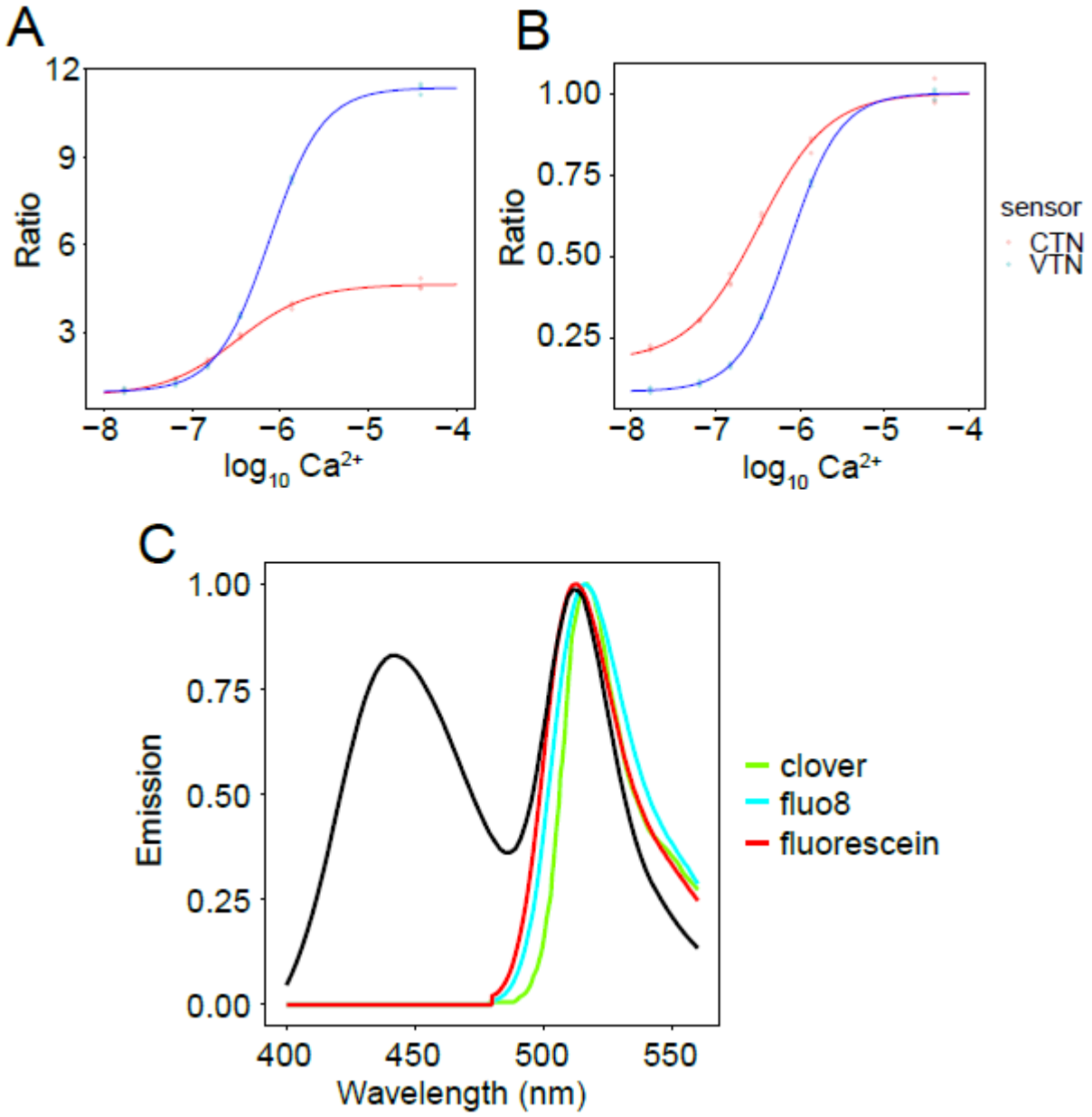
A
12
9
6
3
Ratio
−8
−7
−6
−5
−4
log10 Ca2+
B
1.00
0.75
0.50
0.25
Ratio
−8
−7
−6
−5
−4
log10 Ca2+
sensor
CTN
VTN
C
1.00
0.75
0.50
0.25
0.00
Emission
400
450
500
550
Wavelength (nm)
clover
fluo8
fluorescein

Supplementary Figure S3.2. Comparison of CalfluxCTN vs. CalfluxVTN sensitivity and overlap of emission spectra of fluorescence and luminescence. (**A & B**) Ratio measurements of purified samples of CalfluxCTN and CalfluxVTN in different Ca^{2+} concentration buffers. The same data are normalized differently to give a sense of both dynamic range as well as sensitivity to Ca^{2+}; panel A is normalized to low [Ca^{2+}], while panel B is normalized to saturating [Ca^{2+}]. (**C**) Spectral data showing the emission properties of fluorescein (red), Fluo8 (cyan), and Clover fluorescent protein (green) as compared with the CalfluxCTN luminescence emission spectrum (black).

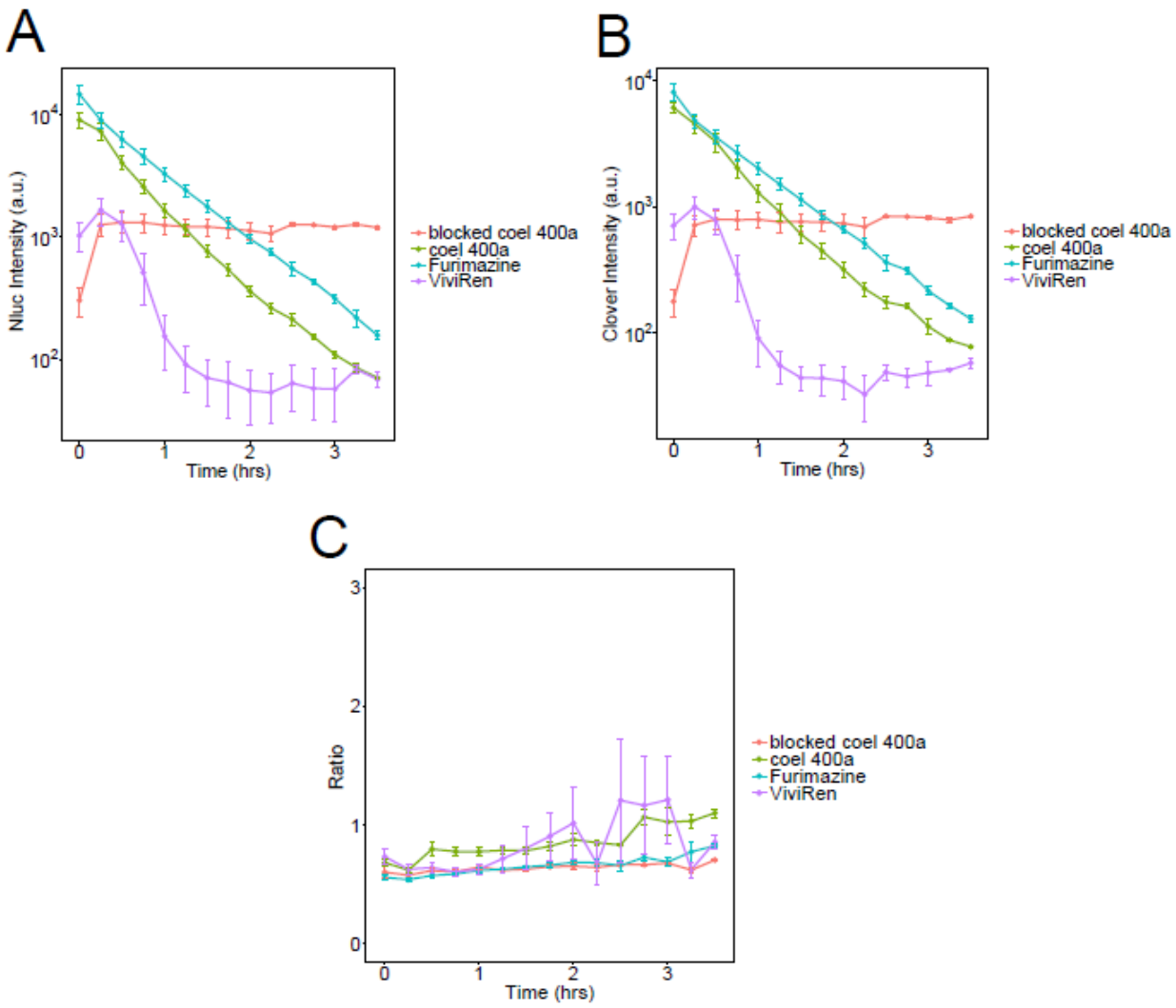

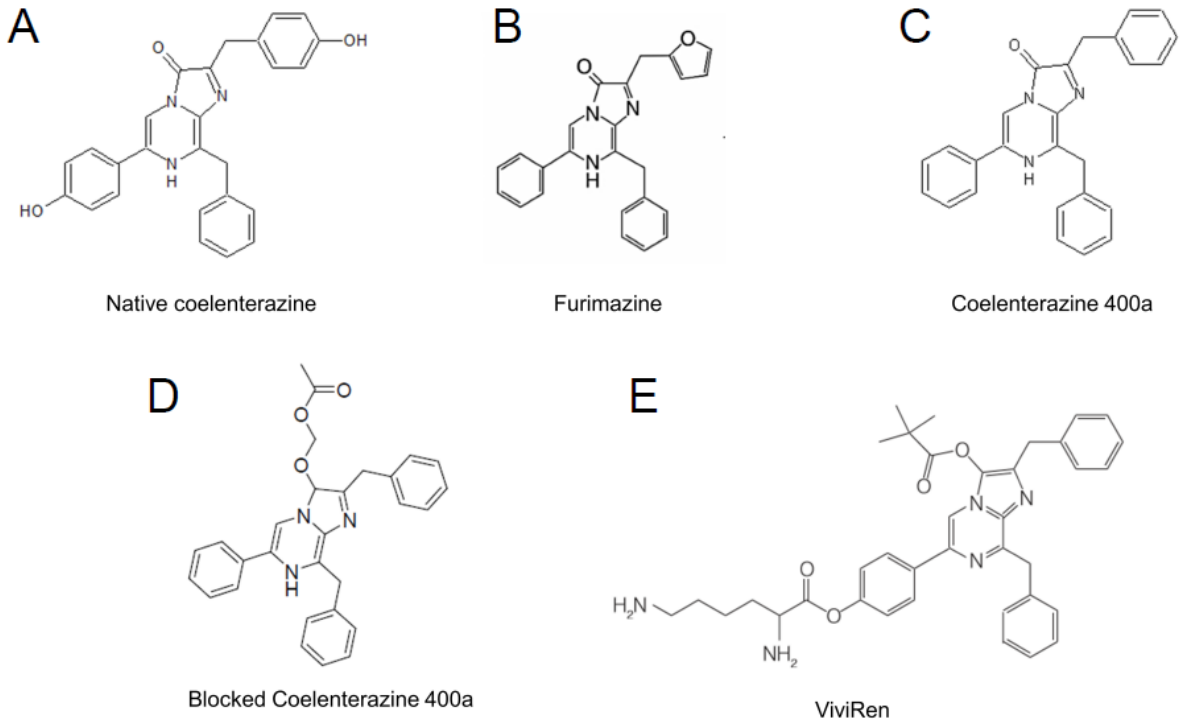

Supplementary Figure S3.4. Structures of the different coelenterazine analogs used in Figure 3.2. Each substrate is labeled under the structure.

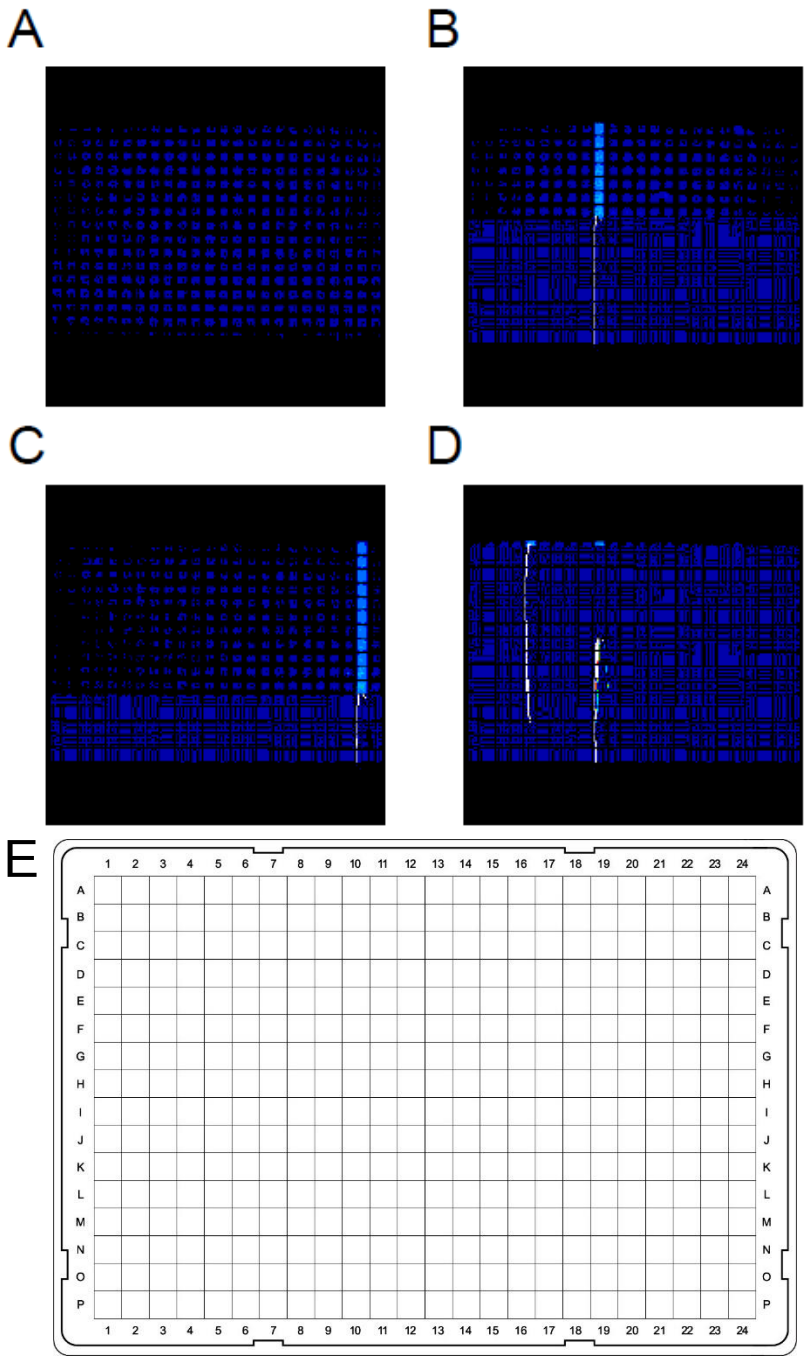

Supplementary Figure S3.5. Visual illustration of fluorescence bleed-through affecting the highly sensitive EM-CCD detector in the WaveFront Panoptic II HTS system. Signals from plates were pseudo-colored for clarity, and images were taken under conditions that are standard for Fluo8 assays. (**A**) Image of an empty 384-well plate. (**B**) The same plate as in panel A was imaged after 20 µl of 10 µM fluorescein was added to well K10 and the rest of the plate's wells remained empty. (**C**) Another plate tested after 20 µl of 10 µM fluorescein was added to well O23 only. (**D**) Image of a third plate in which 20 µl of 10 µM fluorescein was added to two wells (D5 and K10), while all other wells remained empty. (**E**) Typical 384-plate layout.

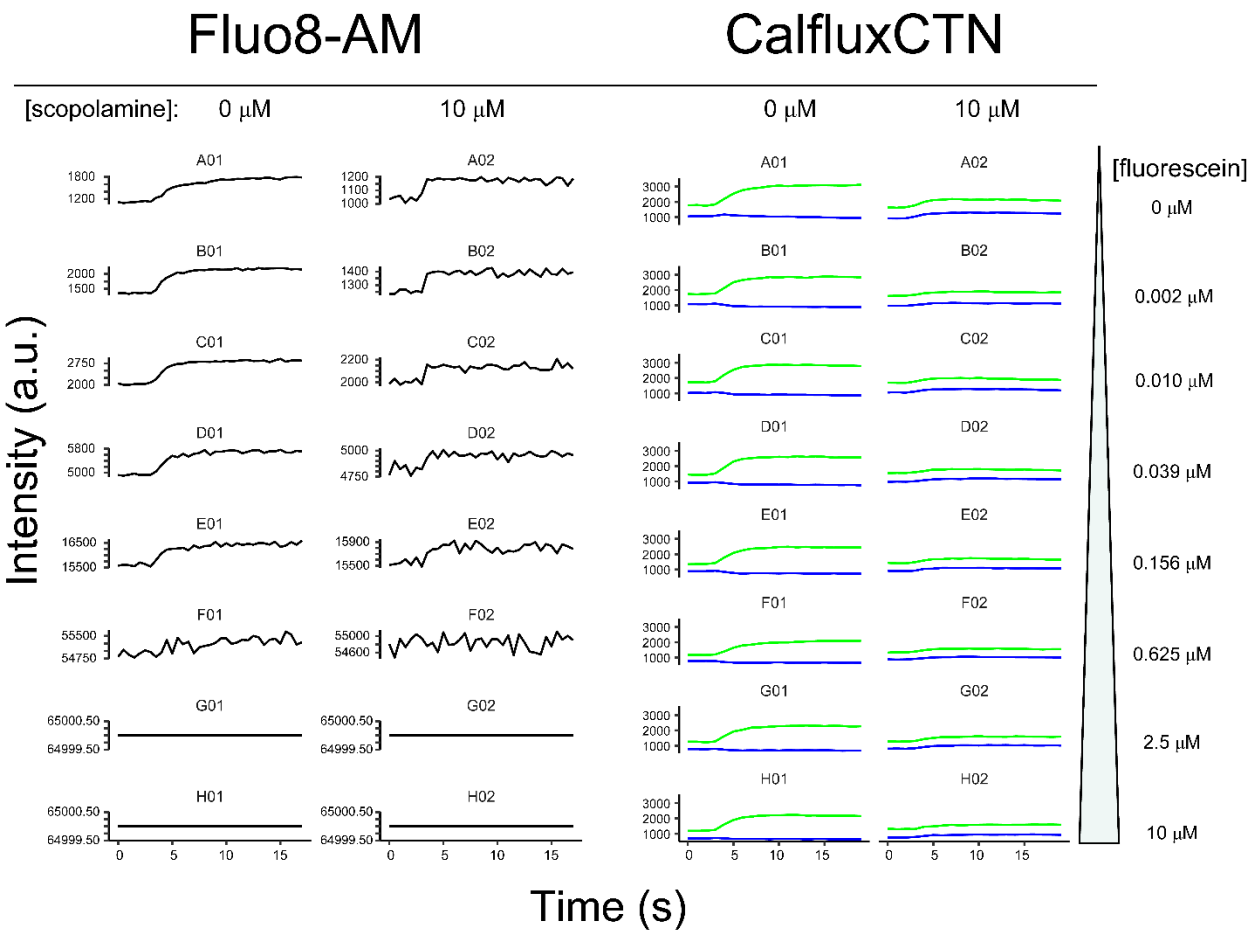

Supplementary Figure S3.6. Investigating the limits of detection when a fluorescence background interferes with fluorescence-based vs. luminescence-based optical recording; the case of antagonist detection. CHO cells in 96-well plates were transfected with CalfluxCTN or treated with Fluo8-AM and signals recorded with a PolarStar Optima PMT plate reader (BMG). The time courses of the signals are plotted from individual representative wells (as labeled). The left half of the figure depicts recordings from CHO cells incubated with 5 μM Fluo8-AM dye, while the right half shows bioluminescent recordings of CHO cells stably expressing CalfluxCTN. The adjacent panels for each type of Ca^{2+} sensor illustrate the signal changes recorded after the addition of 30 μM carbachol (agonist) without (left panels) or with (right panels) the antagonist 10 μM scopolamine. Note that the ordinal scales and dynamic ranges in the Fluo8 data change dramatically from 0-10 μM fluorescein (from 1200-1800 at 0 μM fluorescein to 64999-65000 at 10 μM fluorescein) as a result of the large fluorescence background caused by the fluorescein. Each axial range is independent of the other axes and the last 2 rows (2.5 & 10 μM fluorescein) have essentially a flat line recording of 65000 units with no difference between +scopolamine vs. -scopolamine. On the other hand, all the CalfluxCTN luminescence data are plotted on the same ordinal scales independently of the fluorescein concentration (blue lines are signal at 470/10 nm and green lines are the signal at 520 nm long pass).

CHAPTER IV

PROMISING PROJECTS FOR FURTHER EXPLORATION

Abstract

In addition to the projects described in chapters two and three, I have been involved in several other endeavors linked to expanding the usefulness of bioluminescence-based cellular probes. For most of these projects, I did not have enough time to generate a robust set of publication quality data. In this chapter, I will outline a few of the projects that looked very promising in the initial stages, but which would need extensive follow-up to bring them ultimately to completion. The following sections within this chapter will focus on further uses of the cellular Ca^{2+}-sensors. The last section will describe a methodological consideration when using our microscope setup, since a slight tweak of the software used to acquire images can result in false imaging data.

As stated in the general introduction and elsewhere in this thesis, increasing the number of optical tools for visualization of cellular phenomena is expected to allow researchers to ask more detailed scientific questions, and ultimately reveal the inner workings of the physiological processes of organisms. Model systems (either whole organisms, or portions of an organism) give scientists a simpler set of parameters to understand multifaceted biology therefore allowing them to make assertions about more complex phenomena and test more detailed hypotheses. I chose three well-studied model systems to test the efficacy of using our Ca^{2+} sensor in different contexts: the nematode *Caenorhabditis elegans*, mouse pancreatic islets, and human induced pluripotent stem cell cardiomyocytes (hIPSCs).

Imaging Intracellular Ca^{2+} Oscillations in *Caenorhabditis elegans*

Introduction

Since CalfluxVTN can track cytosolic Ca^{2+} changes reliably in cell culture, we tried to find other model systems amenable to our probe. *Caenorhabditis elegans* (*C. elegans*) was deemed to be a good model system because it would allow us to detect bioluminescence in an intact, translucent organism. In addition, *C. elegans* have a very complicated spatiotemporal autofluorescence pattern (Yin & Brunk, 1991; Pincus et al., 2016; Teuscher & Ewald, 2018) which can impair fluorescence imaging. Therefore, a bioluminescence-based sensor like CalfluxVTN might be ideal in this context.

The brightest autofluorescent signals in the *C. elegans'* body come from the intestine and the uterus (Pincus et al., 2016). Although the identity of the type of molecules which cause this fluorescence is controversial (Yin & Brunk, 1991), these chemicals are excited by a broad range of wavelengths of light. This autofluorescence also increases with respect to the age and health of the organism (Pincus et al., 2016). Although there have been many studies that use fluorescence technologies to study phenomena in *C. elegans* (Iwasaki et al., 1997; Dal Santo et al., 1999; Nguyen et al., 2016), the autofluorescence is still bright enough to obscure fluorescent tags that exhibit low expression levels (Teuscher et al., 2018).

Aside from autofluorescence issues, fluorescence Ca^{2+} imaging has been used extensively to study *C. elegans.* In the early days, fluorescence dyes were used to observe large, non-neuronal Ca^{2+} oscillations in the body wall that correlate with excretion (Dal Santo et al., 1999) and more recently, genetically encoded calcium indicators (GECIs) allowed researchers to image individual neurons in the brain in freely moving animals (Nguyen et al., 2016). There are also unique transcriptional activators which can drive expression in each cell in the entire *C. elegans* body,

allowing researchers to study single neuron and network properties quite easily. With the large number of *C. elegans* mutants already available and the tractability of *C. elegans* as a good genetic screening model, CalfluxVTN could be additionally leveraged to probe new scientific questions. Therefore, I investigated how well *C. elegans* would work with a bioluminescence probe like CalfluxVTN which is based on light emission from NanoLuc luciferase and furimazine.

Materials and Methods:

These experiments were performed in collaboration with Siwei Hei, Ph.D. (lab of David Miller, Ph.D., Vanderbilt University). Wildtype N2 Bristol strain worms were grown on Nematode Growth Media (NGM) (Brenner, 1974) with an *E. coli* OP50 bacteria lawn as their feeding source. Worms were allowed to grow at room temperature inside a humidified plastic container.

To achieve CalfluxVTN expression in *C. elegans*, the DNA for CalfluxVTN was inserted into a pMyo2-expression plasmid by overlap PCR. This plasmid would drive expression in the muscles of the mouth. The new DNA plasmid was injected into the gonads of young hermaphrodites. The eggs that were laid were transferred to fresh plates to develop and the matured worms were checked for YFP expression (Venus moiety on CalfluxVTN). Successfully transformed worms were selected and plated separately from those that did not show YFP fluorescence. YFP filters were Chroma 480/20 EX, 520 LP EM with a 500 LP dichroic. After a few generations, worms expressing YFP were removed when they achieved a density that would lead to starvation and added to new bacteria-coated plates.

For imaging, larger worms were gently removed from their maintenance plates using a small metal pick and placed on 2 % low melting point agarose pad on a glass cover slide with 10 μL of imaging solution (in mM: 1.26 $CaCl_2$, 0.49 $MgCl_2$, 0.41 $MgSO_4$, 5 KCl, 0.44 KH_2PO_4, 4.16

$NaCO_3$, 150 NaCl, 0.34 $NaHPO_4$, 10 HEPES and 0.6 % wt/vol D-glucose, or M9 solution (in mM: 22 KH_2PO_4, 42.3 Na_2HPO_4, 8.6 NaCl, 18.7 NH_4Cl). A small square coverslip was added on top while wax was melted and used to seal most of the edges of the coverslip to limit liquid evaporation. The seal made between the agar pad, the two pieces of glass and the 10 μL of media prevented the worms from moving during imaging. Furimazine (1 μL) was then added to the imaging solution via a small access hole left in the wax seal. Worms were immediately imaged after the addition of furimazine.

Results

To determine whether CalfluxVTN could emit light in the *C. elegans* we first expressed CalfluxVTN under the control of the Myo2 promoter. This promoter should limit expression to the muscles of the larynx/pharynx at the anterior portion of the body (Okkema et al., 1993). After the animals were secured under a coverslip, furimazine was added (final concentration 10 μM) and within 3-4 seconds luminescence was observed (Fig. 4.1A). *C. elegans* are surrounded by a pressurized, tough cuticle (Gilpin et al., 2015) so it was encouraging and gratifying that furimazine was able to permeate intracellularly through the cuticle to be catalyzed by the NanoLuc luciferase.

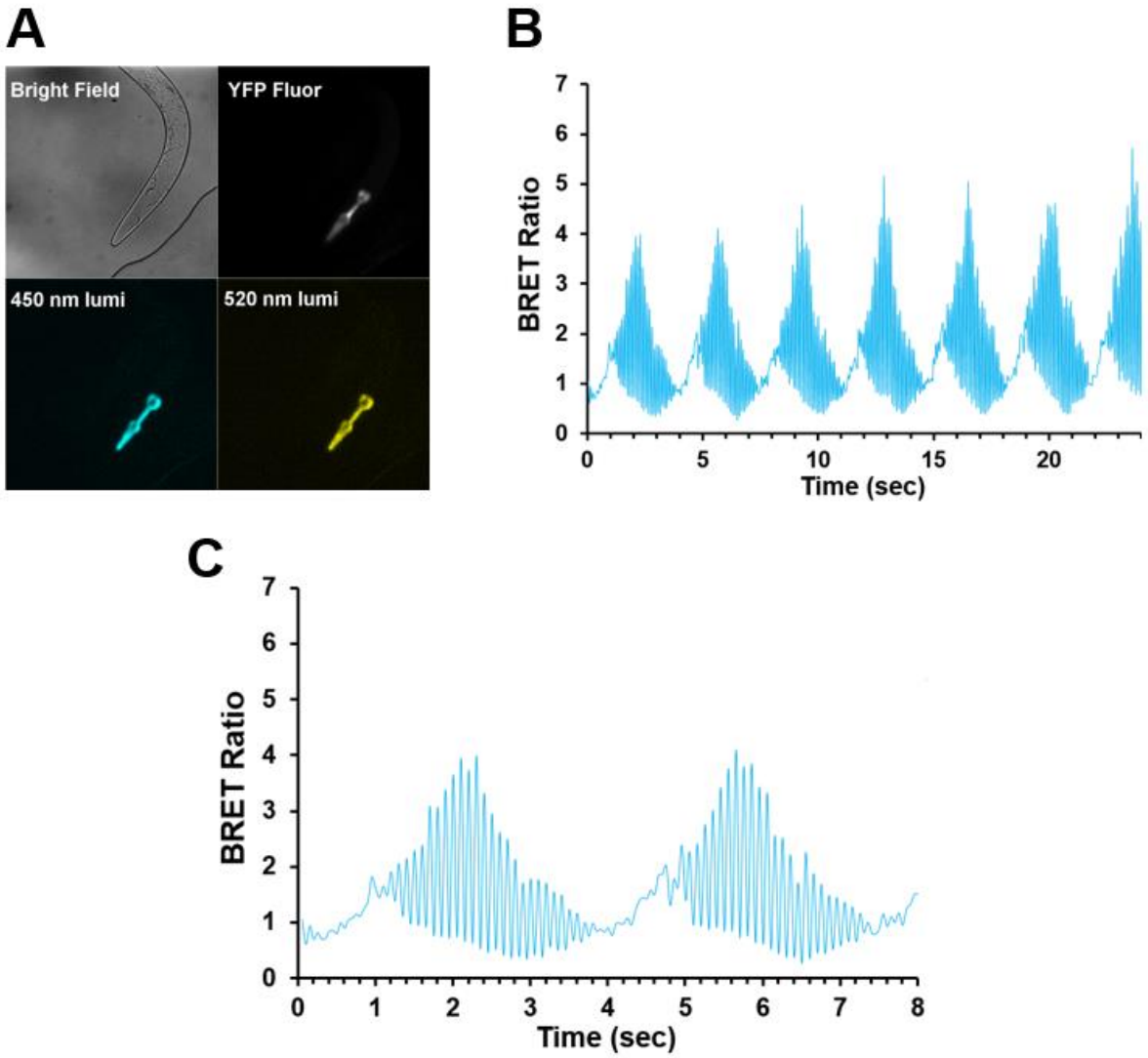

Figure 4.1. Expression of CalfluxVTN under the Myo2 promoter in *C. elegans*. (**A**) Depiction of microscope images of a single *C. elegans*, first a bright field image, then YFP fluorescence (YFP Fluor) and bioluminescence images (lumi) detailing the wavelengths of light being collected. (**B**) The ratiometric signal (BRET Ratio) recorded over time of emission from the anterior portion of the pharynx/larynx of the organism. (**C**) Zoomed-in version of panel B illustrating the periods of both the slow and fast BRET ratio oscillations.

The detection of bright luminescence in the expected regions of the pharynx was exciting. In an effort to measure the rate of decay of the luminescence signal and the stability of the BRET ratio while the worm was secured, an image was taken every 250 ms for about 30 seconds. A

BRET ratio oscillation was observed in the unperturbed worm and persisted for the entire recording which was reminiscent of the well-known Ca^{2+} oscillations reported during larynx pumping (Kerr et al., 2000).

At first glance the Ca^{2+} oscillations have a very interesting waveform characterized by what seems to be an interaction between two waveforms. There is a low-frequency oscillation with a roughly 4-sec period, and larger-amplitude oscillation with a 10 Hz frequency and that is more prominent in the falling phase of the 4-sec rhythm. However, after further investigation we decided that the high frequency rhythm was probably caused by an artifact due to timing discrepancies between the filter switching apparatus and the image collection software controlling the camera (this will be discussed later in this chapter). Interestingly, this lack of filter-switching coordination still does not explain why the high-frequency pattern was less prominent in the rising phase than in the descending phase of the 4-sec Ca^{2+} oscillation. Regardless, the 4-sec rhythm matches well the previously reported larynx-pumping rhythm (Kerr et al., 2000).

However, subsequent attempts to repeat this experiment were frustrated because all worms recorded after initial testing, appeared to no longer produce NanoLuc luminescence. We could see expression of Venus protein in the expected regions (Okkema et al., 1993; Kerr et al., 2000) but no luminescence was observed after the furimazine substrate was added. I hypothesized that the lack of light emission was due to the furimazine precipitating out of solution (unbeknownst to me, Promega may have changed key ingredients in their proprietary formulation of furimazine), but multiple attempts, with multiple different imaging solutions suggested that the issue might have something to do with the worms themselves.

Discussion and Conclusions:

Since Ca^{2+} signaling can give an indication of the state of a neural network, it made sense for us to observe whether our probe is useful in a functionally more complex neural system compared with the single neurons or brain slices described in Chapter II. We decided to try a whole organism, in this case *C. elegans* that is easily reared and has a translucent body that is amenable for optical recording.

We were able to achieve tissue-specific expression of our DNA construct and there were no overt signs of modifications to physiology. Expression of CalfluxVTN in the muscle tissue of the larynx/pharynx did not seem to affect regular locomotion or feeding behaviors. In addition, in the initial tests there were clear luminescence signals in both the blue and green wavelengths indicating that the furimazine is able to penetrate the *C. elegans* cuticle and that expressing NanoLuc in this organism produced a functional protein. Encouragingly, the Ca^{2+} sensor was able to track the low-amplitude, low-frequency 0.1 – 0.3 Hz Ca^{2+} oscillations that are characteristic of those seen in the *C. elegans* larynx/pharynx tissue (Kerr et al., 2000) even though the high-frequency artifact was overlaid on top of them.

Inexplicably, all subsequent attempts to repeat the results of the first test were unsuccessful. When I was finally able to confirm that the high-frequency pattern may not be representative of the cytosolic Ca^{2+} within the muscle cells, none of the remaining *C. elegans* worms showed any luminescence signal. Fluorescence microscopy imaging revealed there was still a Venus signal in the larynx, but addition of furimazine (NanoLuc substrate) did not yield any bioluminescence.

We speculate that there might be a variety of reasons for this absence of luminescence, from decreases in furimazine tissue penetration to erroneous selection of non-luminescent (but fluorescent) parent worms to create subsequent generations of worms, while trying to maintain a

well-fed stock. Hopefully, if we re-transform our construct into fresh wild-type worms, we will circumvent this inability to repeat our initial results. The bottom line is that the preliminary characterization of CalfluxVTN's efficacy in measuring Ca^{2+} transients in a whole organism like *C. elegans* appears to be very encouraging.

Imaging Ca^{2+} in Mouse Pancreatic Islets

Introduction

Type II diabetes is a disease that affects an estimated 20 million people in the US, and millions more worldwide. Severe complications from this illness is the third-leading cause of death of North Americans each year (DiMenna & Arad, 2018). Usually, Type II diabetes occurs as a result of chronic hyperglycemia, insulin resistance, and pancreatic islet malfunction (DiMenna & Arad, 2018; Kahn, 2003). Gaining a better understanding of how this sequence of events leads to such a debilitating illness could potentially lead to new therapies. Pancreatic islet malfunction refers to improper secretion of metabolism hormones by the alpha (α) and beta (β) cells and persons suffering from type II diabetes have reductions both in β-cell number and insulin secretion (Virostko et al., 2006). Although the exact mechanisms have not been completely deciphered, it is clear that Ca^{2+}-signaling plays a role in proper insulin secretion.

Beta cells are electrically active and coupled to each other via gap junctions. Proper secretion of insulin depends on coordinated activities of ATP-sensitive potassium channels as well as voltage-gated calcium channels (Benninger et al., 2014; Rutter et al., 2017). The visualization of Ca^{2+} dynamics in islet cells has been accomplished by both fluorescent (Chen et al., 2016) and bioluminescent techniques (Kennedy et al., 1996) but Ca^{2+}'s exact role in insulin secretion and β-

cell metabolism still remains controversial. Additionally, since whole islets are more functionally intact than dispersed islet cells, techniques to visualize Ca^{2+} changes in whole islets could enlighten our understanding of islet secretion dynamics.

Most recently, researches have been studying islet metabolism by transplanting whole islets into the eyes of animals. Then, using the fluorescence signal from NADPH, they are able to observe energy balance changes in a virtually unperturbed islet (Li et al., 2016; Kim & Jun, 2018). Even though it is possible to use GCaMPs to image Ca^{2+} directly using this method, there is still a significant autofluorescence signal that needs to be overcome (Chen et al., 2016). It is precisely because of autofluorescence signals like these that we decided to investigate how well our bioluminescent Ca^{2+}-sensor CalfluxVTN could track Ca^{2+} dynamics in whole islets in culture.

Materials and Methods

C57Bl6 mice were around 6-8 weeks old before being euthanized under isoflurane anesthesia. Pancreatic islets were separated from the pancreases of mice via digestion with collagenase and Ficoll-gradients centrifugation (Philipson et al., 1994; Dadi et al., 2014). The islets were plated in RPMI 1640 medium supplemented with 10% fetal bovine serum with penicillin and streptomycin and placed in a 37°C CO_2 incubator. After 24 hours in culture, the islets were transfected with AAV-pCAG-CalfluxVTN (serotype 1+2) and allowed to incubate for 2-3 days. When YFP expression could be detected by eye under a fluorescence microscope, the islets were deemed ready for bioluminescence imaging. Whole islets were kept intact throughout the experiment. Islets were depolarized by exposure to 40 mM K^+. In brief, the islets were incubated in 5 mM K^+ media (in mM: 1.26 $CaCl_2$, 0.49 $MgCl_2$, 0.41 $MgSO_4$, 5 KCl, 0.44 KH_2PO_4, 4.16 $NaCO_3$, 150 NaCl, 0.34 $NaHPO_4$, 10 HEPES and 0.6 % wt/vol D-glucose) and pre-stimulus images

were collected. Then, while imaging continued, medium with 40 mM K^+ was added and the resulting changes in bioluminescence ratios were measured (total Na^+ was reciprocally decreased to allow for identical osmolarity between the 5 mM and 40 mM K^+ media).

Results

To test whether our Ca^{2+} sensor could reliably track Ca^{2+} changes in pancreatic islet cells, I transfected the islets with serotype 1+2 AAV particles where CalfluxVTN would be expressed under the control of the non-specific CAG promoter (Fig 4.2A). Subsequent microscope images of the islets revealed the expression pattern of the CalfluxVTN DNA (Fig 4.2B). The islets did not seem to show detectable morphological abnormalities and expression appeared to be asymmetrically limited to the outermost layer of cells. We did not check to see the exact internal distribution of expression via confocal microscopy, but this topology of expression is consistent with AAV-based expression in islets (Craig et al., 2009). Luminescence BRET ratio measurements showed that Ca^{2+} levels in the transfected cells could be increased by high K^+ stimulation and persisted for many seconds (Fig. 4.2C) (Kenty & Melton, 2015). Presumably, this Ca^{2+} response is due to membrane depolarization by the high K^+. These observations show that CalfluxVTN is a good candidate for future experiments when the Ca^{2+} response of islet cells is being investigated.

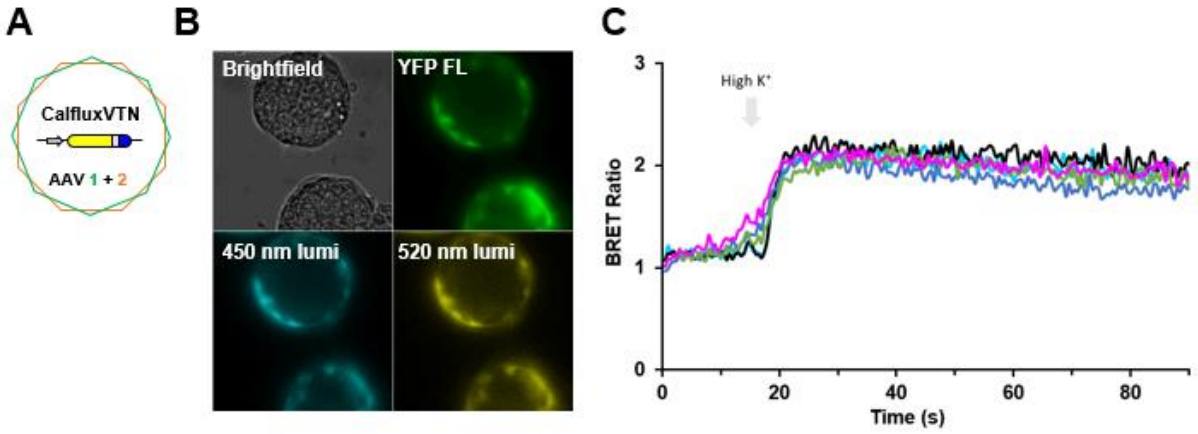

Figure 4.2. Expression of CalfluxVTN in whole, primary mouse pancreatic islets. (**A**) Expression was achieved via AAV particle transfection using a mixed of serotypes 1 and 2. (**B**) Microscope images of whole islets revealed the pattern and efficiency of AAV transfection of CalfluxVTN. (**C**) Depolarization and subsequent Ca^{2+} increase in individual islets that were stimulated with 40 mM K^{+}.

Discussion and Conclusions

Once again, it is clear that CalfluxVTN is useful for tracking cytosolic Ca^{2+} changes in another model system – namely, whole pancreatic islets. The AAV transduction of CalfluxVTN showed the hallmarks of AAV expression vectors, with protein only expressed in cells on the periphery of the islets (Craig et al., 2009). In addition to expression in the islets, potassium depolarization elicited a large increase in intracellular Ca^{2+} that was captured by the change in BRET ratio of all cells in which CalfluxVTN was expressed.

Since this test was first conducted using healthy islets, future experiments compare Ca^{2+} dynamics between healthy islets and those where beta- or alpha-cells are malfunctioning. In

addition, we should consider ways to have successful expression of CalfluxVTN within the interior of the islets, to get a sense of the Ca^{2+} dynamics within the tightly packed cells inside the islets. Furthermore, in future experiments CalfluxVTN might even be useful for studying Ca^{2+} dynamics in a fully intact animal. CalfluxVTN shows great promise in reporting depolarization-dependent Ca^{2+} changes in mouse islets and more opportunities to push the usefulness of CalfluxVTN await.

Human Induced Pluripotent Stem Cell Ca^{2+} Imaging

Introduction

The ability to create stem cells from fully differentiated cells allows researchers to understand how the final fate of cells is determined after they divide from their progenitor/embryonic cells. Somatic cells can simply be reprogrammed by the expression of 4 transcription factors (c-Myc, Oct4, Sox2, Klf4) to become induced pluripotent stem cells (IPSCs) (Takahashi & Yamanaka, 2006). In addition, learning how cells develop and form new tissues and organs could shed light on the kinds of mechanisms that can go wrong in diseased states.

Scientists who study the heart have been extensively researching the uses of IPSCs for a variety of applications. Since IPSCs can be divided and passaged for much longer than primary cells (Takahashi & Yamanaka, 2006) they provide a better model for repeatable research studies. Additionally, grafting of IPSC cardiomyocytes (IPSC-CMs) into the heart might prove to be a useful remedy for myocardial infarction where apoptosis has occurred and dead cells would need to be replaced (Ebert et al., 2015). Furthermore, because IPSC-CMs can be derived from a patient directly, the variability in efficacy of therapeutic drugs can be tested while taking individual genetic variation into account (Ebert et al., 2013). Ideally, this approach should minimize drug

side-effects and potentially determine why some patients do not respond like the majority in clinical trials.

The IPSC field is still in its infancy and there are a lot of hurdles to overcome before using IPSCs becomes commonplace in both clinical and research settings. For instance, IPSC-CMs are not identical to primary CMs extracted from patients and sometimes need to be "matured" because they most resemble embryonic CMs in their protein expression and channel properties (Patterson et al., 2012). Also, IPSC-CMs usually exhibit a mixture of characteristics of CMs from different regions of the heart and are therefore heterogenous in their morphology and responses to stimuli. Furthermore, IPSCs continue to "evolve" *in vitro* based on their culture conditions, since cell density, 3D-surface architecture and mechanical disturbance can all have an effect on the IPSC phenotype (Ebert et al., 2013).

Cardiomyocytes are electrically active cells that exhibit Ca^{2+} fluxes and this makes them another ideal model for testing how efficacious CalfluxVTN can be as a Ca^{2+} sensor. This section describes using CalfluxVTN transfected into human IPSCs to measure Ca^{2+} oscillations under the microscope.

Materials and Methods

In collaboration with Lili Wang, Ph.D. (lab of Bjorn Knöllman, Vanderbilt University), human-derived IPSCs (hIPSCs) were differentiated from fibroblasts collected from consenting adults via dermal punch biopsies. After the fibroblasts were transfected with the relevant transcription factors cocktail (Epi5™ episomal oriP/EBNA1 plasmids from ThermoScientific) the cells were plated on glass-bottomed 35-mm dishes in RPMI media supplemented with B27 without insulin (Life Technologies) and allowed to adhere for 2-3 days at low density (Parikh et al., 2017).

After the cells were allowed to attach, they were transfected with pCAG-CalfluxVTN AAV viral particles (serotype 2 and 8), and the fluorescence intensity of the Venus moiety was measured as

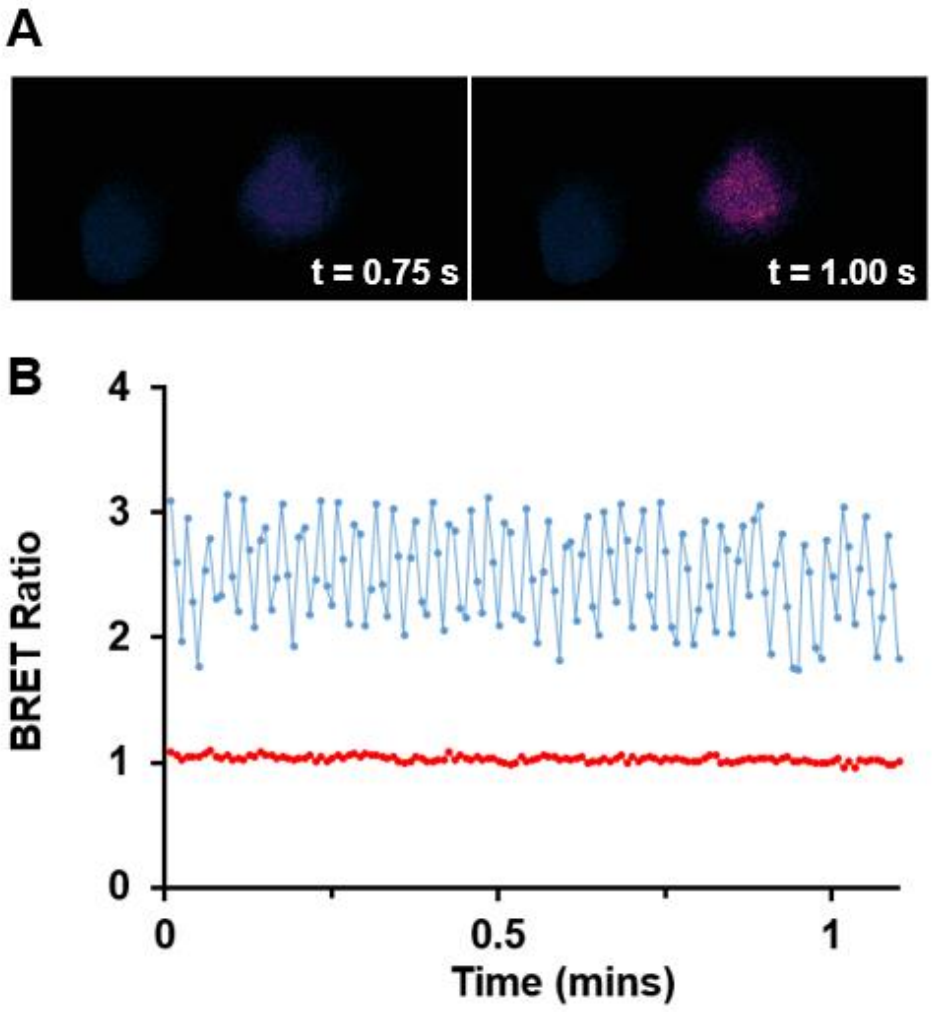

Figure 4.3. Expression of CalfluxVTN under the CAG promoter in hIPSC cardiomyocytes (CM). (**A**) Microscope images show single hIPSC-CM's after transfection. Images have been pseudo-colored to illustrate ratio changes. One cell is oscillating (right cell), the other not (left cell). The first panel shows the BRET ratio at the nadir of the oscillation, while the second panel shows the zenith of the oscillation. (**B**) Blue line depicts BRET ratio changes in the cell that is oscillating (right cell), and red line shows no BRET change in the cell that has not oscillating (left cell).

a proxy for the cellular expression of the Ca^{2+}-sensor. For imaging experiments, media was replaced with phenol red-free RPMI with B27, and spontaneous Ca^{2+} oscillations were measured.

Results

A mix of serotype 1 and 2 Adeno-associated virus (AAV) particles were used to transfect the induced pluripotent stem cells with CalfluxVTN. Expression of CalfluxVTN was observed in 60-70% of cells (data not shown) and cell morphology appeared to be unaffected by CalfluxVTN proteins being evenly distributed in the cytosol (Fig. 4.3A). Although a high proportion of cells were transfected, <1% of CalfluxVTN-expressing cells showed spontaneous BRET ratio oscillations (Fig. 4.3B). Those that did show BRET ratio oscillations, indicating oscillating cytosolic Ca^{2+} concentration, were able to sustain a 0.5-1 Hz oscillation for the duration of recording. These cells had not been stimulated by any external factors. The BRET ratio at the nadir of the oscillation is consistently higher than the ratio of non-oscillatory cells suggesting that the oscillating cells have a higher basal Ca^{2+} level than those that are quiescent. This experiment, like those before, displays the versatility and reliability of CalfluxVTN in a variety of model systems.

Discussion and Conclusions

With the goal of showing that CalfluxVTN is useful in many contexts in cell biology, I have been successful in showing the CalfluxVTN AAV particles are able to transfect human-derived induced pluripotent stem cells from healthy volunteers. Only a small proportion of transfected hIPSC cardiomyocytes showed spontaneous Ca^{2+} fluxes. Additionally, after inspection using brightfield microscopy, some of the cells showed rhythmic contractility movements which were also unstimulated. These contractions are reminiscent of primary cardiomyocytes in culture

(Ferreira-Martins et al., 2009; Viatchenko et al., 1999). It was not entirely clear in my experiments if there was a correlation between the cells that showed contractions and those that exhibited Ca^{2+} oscillations. Previous work has shown that IPSCs exist as heterogenous populations of different heart cell subtypes in addition to being at different stages of maturity (Ebert et al., 2013). Future studies on this project should standardize cell densities, time-in-culture, and other external factors to ensure that the hIPSCs are more uniform.

Limitations in Coordination of Imaging Software and Mechanical Components of Our Microscope Setup

Performing repeatable experiments is the goal of science; fully understanding the limitations of the tools of measurement can facilitate this objective. Specifically, when analyzing images of time series, the method by which images are acquired plays a significant role in determining what conclusions can be drawn from the data. A previous section described how a high frequency oscillation was observed when measuring Ca^{2+} transients in *C. elegans* worms (Chapter IV, section 1). However, after further analysis, we concluded that this rhythm was due to miscommunication between the computer acquisition system and the microscope filter-switcher, not to actual Ca^{2+} measurements.

The fluorescence microscope in the Johnson lab can acquire the light emission from two wavelengths of a sample by two distinct methods. First, two filters are switched back and forth so that the emission images are collected from one wavelength range, and then the other. The second method is to use a Hamamatsu Gemini W-View (dual-view) that collects the light from the separate wavelengths simultaneously and partitions the two images onto either half of the camera's CCD chip. Filter-switching provides a larger field of view because the entire CCD chip is used for both wavelengths, but the dual-view allows superior temporal resolution of any ratiometric changes

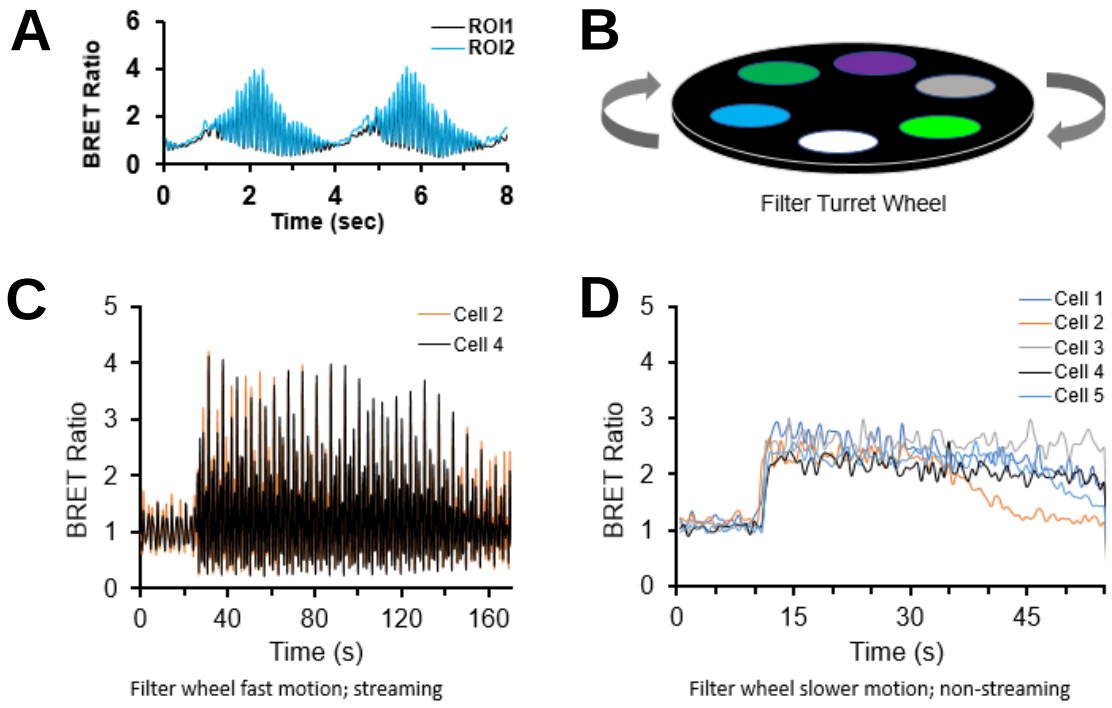

Figure 4.4. Characterization of the signal recorded while the filter turret is given non-ideal image acquisition parameters. (**A**) Previous data from *C. elegans* depicting saw-toothed BRET ratio oscillation in pharynx muscle. (**B**) Cartoon schematic of our automated emission filter-switcher inside our microscope. (**C**) Saw tooth pattern in BRET ratio recorded using filter-switcher in non-oscillatory CHO hM_1 cells expressing CalfluxCTN when image acquisition is too fast for filter switching. (**D**) Similar experiment on the microscope with filter switcher showing the cells exhibiting expected changes in Ca^{2+} and subsequent BRET ratio when the filter wheel settings are optimal. Both bottom panels were treated with 30 μM Carbachol.

because the blue and yellow images are collected at the same time rather than alternating. When BRET ratio measurements were recorded from non-oscillatory cells, it was possible to produce an oscillation effect by causing the filter switcher to take images faster than it takes the filter turret wheel on the microscope to place the filter in the right orientation (Fig. 4.4C). Interestingly, appears to be a high-frequency oscillation in the noise. When those same cells were imaged under a more optimal acquisition protocol the high frequency oscillation was no longer observed (Fig. 4.4D). Since the *C. elegans* experiment was done using the filter switcher, it is possible that the timing was non-ideal and that was the reason for the high-frequency BRET oscillation. Of note, the high-frequency artifact was only observed during filter-switching experiments. Therefore, it is important to ensure that the image acquisition times for BRET imaging are never below 100 milliseconds per wavelength when using the filter-switcher.

CHAPTER V

GENERAL SUMMARY & CONCLUSION

Harnessing naturally occurring luminescent enzymes for use as reporters of cellular activity has a long history. Multiple innovations in molecular biology, ecology, optics, and computer processing together have played significant roles in creating the long list of probes available to scientists. Each new probe has been optimized to fit specific technical niches and over time, new optical sensors will continue to push the boundaries of what is measurable in living cells. This dissertation chronicles the creation of luminescence-based, ratiometric, genetically-encoded Ca^{2+} indicators and describes their applicability to a variety of biological problems while also highlighting their strengths and weaknesses.

I have shown that the bright luciferase NanoLuc can transfer energy to yellow and green fluorescence proteins via Förster energy transfer and that this phenomenon can be used to create Ca^{2+} sensors that have their greatest Ca^{2+}-sensitivities in the physiologically-relevant range of nM – μM cytosolic Ca^{2+} (Chapters II and III). I have shown that while these luminescent Ca^{2+} sensors are bright enough to be imaged at very high speed, their brightness does not cause optical crosstalk with optogenetic actuators, making them ideal for cell-culture optogenetic experiments (Chapter II). Additionally, in some contexts, AAV versions of our sensors can potentially track neural activity.

I have also demonstrated that these kinds of luminescent sensors can be used in a high throughput screening context where they outperform well-established fluorescence-based reporters when there are fluorescent compounds in the screening library (Chapter III). Our HTS application is merely one of many possible situations in which an autofluorescent background can

complicate measurements while using a fluorescent sensor, but have no impact upon a luminescence / BRET sensor. Furthermore, since bioluminescence is an enzymatic reaction and the emitted light intensity decays over time as the amount of available substrate is used up, we have devised ways to create stable light emission via chemically-modifying key atoms of the luciferin substrate (Chapter III).

With the promise that our probes have shown in varying model systems (Chapter IV) the future of bioluminescence-based reporters of cellular activity will continue to grow and find more specialized uses as detection devices become more sensitive and microprocessor times continue to speed up. I am grateful that I can add my input via this dissertation to that ever-moving, onward-marching, scientific discourse.

REFERENCES

1. Agulhon C, Platel JC, Kolomiets B, Forster V, Picaud S, Brocard J, Faure P, Brulet P (2007) Bioluminescent imaging of Ca^{2+} activity reveals spatiotemporal dynamics in glial networks of dark-adapted mouse retina. *J Physiol*. 2007 Sep 15; 583(Pt 3):945-58.
2. Akemann W, Mutoh H, Perron A, Park YK, Iwamoto Y, Knöpfel T (2012) Imaging neural circuit dynamics with a voltage-sensitive fluorescent protein. *J Neurophysiol*. 2012 Oct;108(8):2323-37.
3. Akerboom J, Chen TW, Wardill TJ, Tian L, Marvin JS, Mutlu S, Calderón NC, Esposti F, Borghuis BG, Sun XR, Gordus A, Orger MB, Portugues R, Engert F, Macklin JJ, Filosa A, Aggarwal A, Kerr RA, Takagi R, Kracun S, Shigetomi E, Khakh BS, Baier H, Lagnado L, Wang SS, Bargmann CI, Kimmel BE, Jayaraman V, Svoboda K, Kim DS, Schreiter ER, Looger LL (2012) Optimization of a GCaMP calcium indicator for neural activity imaging. *J Neurosci*. 2012 Oct 3;32(40):13819-40.
4. Akerboom J, Carreras Calderón N, Tian L, Wabnig S, Prigge M, Tolö J, Gordus A, Orger MB, Severi KE, Macklin JJ, Patel R, Pulver SR, Wardill TJ, Fischer E, Schüler C, Chen TW, Sarkisyan KS, Marvin JS, Bargmann CI, Kim DS, Kügler S, Lagnado L, Hegemann P, Gottschalk A, Schreiter ER, Looger LL (2013) Genetically encoded calcium indicators for multi-color neural activity imaging and combination with optogenetics. *Front Mol Neurosci*. 2013 Mar 4; 6:2.
5. Amos B (2000) Lessons from the history of light microscopy. *Nat Cell Biol.* 2000 Aug; 2(8):E151-2.

6. Ando R, Hama H, Yamamoto-Hino M, Mizuno H, Miyawaki A (2002) An optical marker based on the UV-induced green-to-red photoconversion of a fluorescent protein. *Proc Natl Acad Sci USA*. 2002 Oct 1; 99(20):12651-6.

7. Aravanis AM, Wang LP, Zhang F, Meltzer LA, Mogri MZ, Schneider MB, Deisseroth K (2007) An optical neural interface: in vivo control of rodent motor cortex with integrated fiberoptic and optogenetic technology. *J Neural Eng*. 2007 Sep; 4(3):S143-56.

8. Ardevol A, Hummer G (2018) Retinal isomerization and water-pore formation in channelrhodopsin-2. *Proc Natl Acad Sci USA*. 2018 Apr 3; 115(14):3557-3562.

9. Arenkiel BR, Peca J, Davison IG, Feliciano C, Deisseroth K, Augustine GJ, Ehlers MD, Feng G (2007) In vivo light-induced activation of neural circuitry in transgenic mice expressing channelrhodopsin-2. *Neuron*. 2007 Apr 19;54(2):205-18.

10. Baldwin TO (1996) Firefly luciferase: the structure is known, but the mystery remains. *Structure*. 1996 Mar 15; 4(3):223-8.

11. Bass J, Takahashi JS (2010) Circadian integration of metabolism and energetics. *Science*. 2010 Dec 3; 330(6009):1349-54.

12. Bedut S, Seminatore-Nole C, Lamamy V, Caignard S, Boutin JA, Nosjean O, Stephan JP, Coge F (2016) High-throughput drug profiling with voltage- and calcium-sensitive fluorescent probes in human iPSC-derived cardiomyocytes. *Am J Physiol Heart Circ Physiol*. 2016 Jul 1;311(1):H44-53.

13. Belas R, Mileham A, Cohn D, Hilman M, Simon M, Silverman M (1982) Bacterial bioluminescence: isolation and expression of the luciferase genes from *Vibrio harveyi*. *Science*. 1982 Nov 19; 218(4574):791-3.

14. Benninger RK, Piston DW (2013) Two-photon excitation microscopy for the study of living cells and tissues. *Curr Protoc Cell Biol.* 2013 Jun; Chapter 4: Unit 4.11.1-24.

15. Benninger RK, Hutchens T, Head WS, McCaughey MJ, Zhang M, Le Marchand SJ, Satin LS, Piston DW (2014) Intrinsic islet heterogeneity and gap junction coupling determine spatiotemporal Ca^{2+} wave dynamics. *Biophys J*. 2014 Dec 2; 107(11):2723-33.

16. Boyden ES, Zhang F, Bamberg E, Nagel G, Deisseroth K (2005) Millisecond-timescale, genetically targeted optical control of neural activity. *Nat Neurosci*. 2005 Sep;8(9):1263-8.

17. Branchini BR, Southworth TL, Khattak NF, Michelini E, Roda A (2005) Red- and green-emitting firefly luciferase mutants for bioluminescent reporter applications. *Anal Biochem*. 2005 Oct 1; 345(1):140-8.

18. Brandes C, Plautz JD, Stanewsky R, Jamison CF, Straume M, Wood KV, Kay SA, Hall JC (1996) Novel features of drosophila period Transcription revealed by real-time luciferase reporting. *Neuron*. 1996 Apr; 16(4):687-92.

19. Brenner S (1974) The genetics of *Caenorhabditis elegans*. *Genetics*. 1974 May;77(1):71-94.

20. Chalfie M, Tu Y, Euskirchen G, Ward WW, Prasher DC (1994) Green Fluorescent Protein as a Marker for Gene Expression. *Science* 263(5148):802-805.

21. Changenet-Barret P, Kovács L, Markovitsi D, Gustavsson T (2016). Xanthines Studied via Femtosecond Fluorescence Spectroscopy. *Molecules* 2016, 21, 1668.

22. Chearwae W, Shukla S, Limtrakul P, Ambudkar SV (2006). Modulation of the function of the multidrug resistance–linked ATP-binding cassette transporter ABCG2 by the cancer chemopreventive agent curcumin. *Mol Cancer Ther* 2006;5(8). August 2006.

23. Chen C, Chmelova H, Cohrs CM, Chouinard JA, Jahn SR, Stertmann J, Uphues I, Speier S (2016) Alterations in β-Cell Calcium Dynamics and Efficacy Outweigh Islet Mass Adaptation in Compensation of Insulin Resistance and Prediabetes Onset. *Diabetes*. 2016 Sep;65(9):2676-85.

24. Chen TW, Wardill TJ, Sun Y, Pulver SR, Renninger SL, Baohan A, Schreiter ER, Kerr RA, Orger MB, Jayaraman V, Looger LL, Svoboda K, Kim DS (2013) Ultrasensitive fluorescent proteins for imaging neuronal activity. *Nature* 2013 Jul 18;499(7458):295-300.

25. Chignell CF, Bilski P, Reszka KJ, Motten AG, Sik RH, Dahl TA (1994). Spectral and photochemical properties of curcumin. *Photochem Photobiol*. 1994 Mar;59(3):295-302.

26. Chu J, Haynes RD, Corbel SY, Li P, González-González E, Burg JS, Ataie NJ, Lam AJ, Cranfill PJ, Baird MA, Davidson MW, Ng HL, Garcia KC, Contag CH, Shen K, Blau HM, Lin MZ (2014) Non-invasive intravital imaging of cellular differentiation with a bright red-excitable fluorescent protein. *Nat Methods*. 2014 May; 11(5):572-8.

27. Chu J, Oh Y, Sens A, Ataie N, Dana H, Macklin JJ, Laviv T, Welf ES, Dean KM, Zhang F, Kim BB, Tang CT, Hu M, Baird MA, Davidson MW, Kay M, Fiolka R, Yasuda R, Kim DS, Ng HL, Lin MZ (2016) A bright cyan-excitable orange fluorescent protein facilitates dual-emission microscopy and enhances bioluminescence imaging in vivo. *Nat Biotechnol*. 2016 Jul;34(7):760-7.

28. Church J, Fletcher EJ, Abdel-Hamid K, MacDonald JF (1994) Loperamide blocks high-voltage-activated calcium channels and N-methyl-D-aspartate-evoked responses in rat and mouse cultured hippocampal pyramidal neurons. *Mol Pharmacol*. 1994 Apr;45(4):747-57.

29. Conti E, Franks NP, Brick P (1996) Crystal structure of firefly luciferase throws light on a superfamily of adenylate-forming enzymes. *Structure*. 1996 Mar 15;4(3):287-98.

30. Craig AT, Gavrilova O, Dwyer NK, Jou W, Pack S, Liu E, Pechhold K, Schmidt M, McAlister VJ, Chiorini JA, Blanchette-Mackie EJ, Harlan DM, Owens RA (2009) Transduction of rat pancreatic islets with pseudotyped adeno-associated virus vectors. *Virol J*. 2009 May 18;6:61.

31. Crivat G, Taraska JW (2012) Imaging proteins inside cells with fluorescent tags. *Trends Biotechnol*. 2012 Jan; 30(1):8-16.

32. Dadi PK, Vierra NC, Ustione A, Piston DW, Colbran RJ, Jacobson DA (2014) Inhibition of pancreatic β-cell Ca^{2+}/calmodulin-dependent protein kinase II reduces glucose-stimulated calcium influx and insulin secretion, impairing glucose tolerance. *J Biol Chem*. 2014 May 2;289(18):12435-45.

33. Dal Santo P, Logan MA, Chisholm AD, Jorgensen EM (1999) The inositol trisphosphate receptor regulates a 50-second behavioral rhythm in *C. elegans*. *Cell*. 1999 Sep 17;98(6):757-67.

34. Day RN, Davidson MW (2009) The fluorescent protein palette: tools for cellular imaging. *Chem Soc Rev.* 2009 Oct;38(10):2887-921.

35. Deisseroth K, Feng G, Majewska AK, Miesenböck G, Ting A, Schnitzer MJ (2006) Next-generation optical technologies for illuminating genetically targeted brain circuits. *J Neurosci.* 2006 Oct 11;26(41):10380-6.

36. DeLuca M and McElroy WD (1974) Kinetics of the Firefly Luciferase Catalyzed Reactions. *Biochemistry*. 1974 Feb 26;13(5):921-5.

37. Denk W, Strickler JH, Webb WW (1990) Two-Photon Laser Scanning Fluorescence Microscopy.

38. de Wet JR, Wood KV, Helinski DR, DeLuca M (1985) Cloning of firefly luciferase cDNA and the expression of active luciferase in *Escherichia coli*. *Proc Natl Acad Sci USA*. 1985 Dec;82(23):7870-3.

39. DiMenna FJ, Arad AD (2018) Exercise as 'precision medicine' for insulin resistance and its progression to type 2 diabetes: a research review. *BMC Sports Sci Med Rehabil*. 2018 Nov 23; 10:21.

40. Dreosti E, Odermatt B, Dorostkar MM, Lagnado L (2009) A genetically encoded reporter of synaptic activity in vivo. *Nat Methods*. 2009 Dec;6(12):883-9.

41. Eberhard M, Erne P (1991) Calcium binding to fluorescent calcium indicators: calcium green, calcium orange and calcium crimson. *Biochem Biophys Res Commun*. 1991 Oct 15;180(1):209-15.

42. Ebert AD, Liang P, Wu JC (2012) Induced pluripotent stem cells as a disease modeling and drug screening platform. *J Cardiovasc Pharmacol*. 2012 Oct;60(4):408-16.

43. Ebert AD, Diecke S, Chen IY, Wu JC (2015) Reprogramming and transdifferentiation for cardiovascular development and regenerative medicine: where do we stand? *EMBO Mol Med*. 2015 Sep;7(9):1090-103.

44. Fearnley CJ, Roderick HL, Bootman MD (2011) Calcium signaling in cardiac myocytes. *Cold Spring Harb Perspect Biol.* 2011 Nov 1;3(11): a004242.

45. Ferreira-Martins J, Rondon-Clavo C, Tugal D, Korn JA, Rizzi R, Padin-Iruegas ME, Ottolenghi S, De Angelis A, Urbanek K, Ide-Iwata N, D'Amario D, Hosoda T, Leri A, Kajstura J, Anversa P, Rota M (2009) Spontaneous calcium oscillations regulate human cardiac progenitor cell growth. *Circ Res*. 2009 Oct 9;105(8):764-74.

46. Flavin SA, Matthews RT, Wang Q, Muly EC, Winder DG (2014) α_{2A}-adrenergic receptors filter parabrachial inputs to the bed nucleus of the stria terminalis. *J Neurosci*. 2014 Jul 9;34(28):9319-31.

47. Fluhler E, Burnham VG, Loew LM (1985) Spectra, membrane binding, and potentiometric responses of new charge shift probes. *Biochemistry*. 1985 Oct 8; 24(21):5749-55.

48. Flytzanis NC, Bedbrook CN, Chiu H, Engqvist MK, Xiao C, Chan KY, Sternberg PW, Arnold FH, Gradinaru V (2014) Archaerhodopsin variants with enhanced voltage-sensitive fluorescence in mammalian and Caenorhabditis elegans neurons. *Nat Commun*. 2014 Sep 15; 5:4894.

49. Gee KR, Brown KA, Chen WN, Bishop-Stewart J, Gray D, Johnson I (2000) Chemical and physiological characterization of fluo-4 Ca^{2+}-indicator dyes. *Cell Calcium*. 2000 Feb;27(2):97-106.

50. Gilkey JC, Jaffe LF, Ridgway EB, Reynolds GT (1978) A free calcium wave traverses the activating egg of the Medaka, *Oryzias latipes*. *J Cell Biol.* 1978 Feb;76(2):448-66.

51. Gilpin W, Uppaluri S, Brangwynne CP (2015) Worms under Pressure: Bulk Mechanical Properties of *C. elegans* Are Independent of the Cuticle. *Biophys J*. 2015 Apr 21;108(8):1887-98.

52. Gooch VD, Mehra A, Larrondo LF, Fox J, Touroutoutoudis M, Loros JJ, Dunlap JC (2008) Fully codon-optimized luciferase uncovers novel temperature characteristics of the Neurospora clock. *Eukaryot Cell*. 2008 Jan;7(1):28-37.

53. Groskreutz DJ, Sherf BA, Wood KV Schenborn ET (1995) Increased expression and convenience with the new pGL3 luciferase reporter vectors, Promega Notes, 1995, 50, 2–6.

54. Grynkiewicz G, Poenie M, Tsien RY (1985) A new generation of Ca^{2+} indicators with greatly improved fluorescence properties. *J Biol Chem*. 1985 Mar 25; 260(6):3440-50.

55. Haddock SHD, Moline MA, Case JF (2010) Bioluminescence in the Sea. *Annu. Rev. Mar. Sci.* 2010. 2:443–93.

56. Hall MP, Unch J, Binkowski BF, Valley MP, Butler BL, Wood MG, Otto P, Zimmerman K, Vidugiris G, Machleidt T, Robers MB, Benink HA, Eggers CT, Slater MR, Meisenheimer PL, Klaubert DH, Fan F, Encell LP, Wood KV (2012) Engineered luciferase reporter from a deep sea shrimp utilizing a novel imidazopyrazinone substrate. *ACS Chem Biol*. 2012 Nov 16;7(11):1848-57.

57. Han C, Chatterjee A, Noetzel MJ, Panarese JD, Smith E, Chase P, Hodder P, Niswender C, Conn PJ, Lindsley CW, Stauffer SR (2015) Discovery and SAR of muscarinic receptor subtype 1 (M_1) allosteric activators from a molecular libraries high throughput screen. Part 1: 2,5-dibenzyl-*2H*-pyrazolo[4,3-c]quinolin-3(*5H*)-ones as positive allosteric modulators. *Bioorg Med Chem Lett*. 2015 Jan 15;25(2):384-8.

58. Hastings JW, Johnson CH (2003) Bioluminescence and chemiluminescence. *Methods Enzymol*. 2003; 360:75-104.

59. Head JF, Inouye S, Teranishi K, Shimomura O (2000) The crystal structure of the photoprotein aequorin at 2.3 Å resolution. *Nature* 2000 May 18;405(6784):372-6.

60. Heim R, Prasher DC, Tsien RY (1994) Wavelength mutations and posttranslational autoxidation of green fluorescent protein. *Proc Natl Acad Sci USA*. 1994 Dec 20;91(26):12501-4.

61. Hochbaum DR, Zhao Y, Farhi SL, Klapoetke N, Werley CA, Kapoor V, Zou P, Kralj JM, Maclaurin D, Smedemark-Margulies N, Saulnier JL, Boulting GL, Straub C, Cho YK, Melkonian M, Wong GK, Harrison DJ, Murthy VN, Sabatini BL, Boyden ES, Campbell RE, Cohen AE (2014) All-optical electrophysiology in mammalian neurons using engineered microbial rhodopsins. *Nat Methods*. 2014 Aug;11(8):825-33.

62. Imamura H, Nhat KP, Togawa H, Saito K, Iino R, Kato-Yamada Y, Nagai T, Noji H (2009) Visualization of ATP levels inside single living cells with fluorescence resonance energy transfer-based genetically encoded indicators. *Proc Natl Acad Sci USA*. 2009 Sep 15; 106(37):15651-6.

63. Inoue R, Sakurai A, Tsuga H, Oishi K, Uchida MK (1995) Carbachol-induced desensitization of rat basophilic leukemia (RBL-2H3) cells transfected with human m3 muscarinic acetylcholine receptors. *Gen Pharmacol*. 1995 Sep;26(5):1125-31.

64. Inoue S, Rahoi R, Goto T (1976) Squid Bioluminescence III. Isolation and structure of Watasenia luciferin. *Tetrahedron Letters* 1976; 34: 2971-2974.

65. Inouye S, Noguchi M, Sakaki Y, Takagi Y, Miyata T, Iwanaga S, Miyata T, Tsuji FI (1985) Cloning and sequence analysis of cDNA for the luminescent protein aequorin. *Proc. Natl Acad. Sci. USA* 82:3154 –3158.

66. Inouye S, Watanabe K, Nakamura H, Shimomura O (2000) Secretional luciferase of the luminous shrimp *Oplophorus gracilirostris*: cDNA cloning of a novel imidazopyrazinone luciferase. *FEBS Lett.* 2000 Sep 8; 481(1):19-25.

67. Inouye S, Sasaki S (2007) Overexpression, purification and characterization of the catalytic component of Oplophorus luciferase in the deep-sea shrimp, *Oplophorus gracilirostris*. *Protein Expr Purif*. 2007 Dec; 56(2):261-8.

68. Inouye S, Sato J, Sahara-Miura Y, Yoshida S, Kurakata H, Hosoya T (2013) C6-Deoxy coelenterazine analogues as an efficient substrate for glow luminescence reaction of nanoKAZ: the mutated catalytic 19 kDa component of Oplophorus luciferase. *Biochem Biophys Res Commun*. 2013 Jul 19; 437(1):23-8.

69. Ishiura M, Kutsuna S, Aoki S, Iwasaki H, Andersson CR, Tanabe A, Golden SS, Johnson CH, Kondo T (1998) Expression of a gene cluster kaiABC as a circadian feedback process in cyanobacteria. *Science*. 1998 Sep 4; 281(5382):1519-23.

70. Iwasaki K, Staunton J, Saifee O, Nonet M, Thomas JH (1997) Aex-3 encodes a novel regulator of presynaptic activity in C. elegans. *Neuron*. 1997 Apr;18(4):613-22.

71. Jabloński A (1933) Efficiency of anti-stokes fluorescence in dyes. *Nature* 131: 839–840 (10 June 1933).

72. Jiang M, Chen G (2006) High Ca^{2+}-phosphate transfection efficiency in low-density neuronal cultures. *Nat Protoc*. 2006;1(2):695-700.

73. Johnson CH, Knight MR, Kondo T, Masson P, Sedbrook J, Haley A, Trewavas A (1995) Circadian oscillations of cytosolic and chloroplastic free calcium in plants. *Science*. 1995 Sep 29;269(5232):1863-5.

74. Johnson CH, Zhao C, Xu Y, Mori T (2017) Timing the day: what makes bacterial clocks tick? *Nat Rev Microbiol*. 2017 Apr;15(4):232-242.

75. Kaech S, Banker G (2006) Culturing hippocampal neurons. *Nat Protoc*. 2006;1(5):2406-15.

76. Kahn SE (2003) The relative contributions of insulin resistance and beta-cell dysfunction to the pathophysiology of Type 2 diabetes. *Diabetologia*. 2003 Jan;46(1):3-19.

77. Kaneko M, Cahill GM (2005) Light-dependent development of circadian gene expression in transgenic zebrafish. *PLoS Biol*. 2005 Feb; 3(2):e34.

78. Kash TL, Winder DG (2006) Neuropeptide Y and corticotropin-releasing factor bi-directionally modulate inhibitory synaptic transmission in the bed nucleus of the stria terminalis. *Neuropharmacology*. 2006 Oct;51(5):1013-22.

79. Kato HE, Zhang F, Yizhar O, Ramakrishnan C, Nishizawa T, Hirata K, Ito J, Aita Y, Tsukazaki T, Hayashi S, Hegemann P, Maturana AD, Ishitani R, Deisseroth K, Nureki O (2012) Crystal structure of the channelrhodopsin light-gated cation channel. *Nature*. 2012 Jan 22; 482(7385):369-74.

80. Kennedy ED, Rizzuto R, Theler JM, Pralong WF, Bastianutto C, Pozzan T, Wollheim CB (1996) Glucose-stimulated insulin secretion correlates with changes in mitochondrial and cytosolic Ca^{2+} in aequorin-expressing INS-1 cells. *J Clin Invest*. 1996 Dec 1;98(11):2524-38.

81. Kenty JH, Melton DA (2015) Testing pancreatic islet function at the single cell level by calcium influx with associated marker expression. *PLoS One*. 2015 Apr 8;10(4):e0122044.

82. Kerr R, Lev-Ram V, Baird G, Vincent P, Tsien RY, Schafer WR (2000) Optical imaging of calcium transients in neurons and pharyngeal muscle of *C. elegans*. *Neuron*. 2000 Jun;26(3):583-94.

83. Kim D, Jun HS (2018) *In Vivo* Imaging of Transplanted Pancreatic Islets. *Front Endocrinol (Lausanne)*. 2018 Jan 22;8:382.

84. Kim JH, Lee SR, Li LH, Park HJ, Park JH, Lee KY, Kim MK, Shin BA, Choi SY (2011) High cleavage efficiency of a 2A peptide derived from porcine teschovirus-1 in human cell lines, zebrafish and mice. *PLoS One*. 2011;6(4):e18556.

85. Klinkenberg I, Blokland A (2010) The validity of scopolamine as a pharmacological model for cognitive impairment: a review of animal behavioral studies. *Neurosci Biobehav Rev*. 2010 Jul;34(8):1307-50.

86. Kondo T, Strayer CA, Kulkarni RD, Taylor W, Ishiura M, Golden SS, Johnson CH (1993) Circadian rhythms in prokaryotes: luciferase as a reporter of circadian gene expression in cyanobacteria. *Proc Natl Acad Sci USA*. 1993 Jun 15; 90(12):5672-6.

87. Kondo T, Tsinoremas NF, Golden SS, Johnson CH, Kutsuna S, Ishiura M (1994) Circadian clock mutants of cyanobacteria. *Science*. 1994 Nov 18; 266(5188):1233-6.

88. Kozak M (1986) Point mutations define a sequence flanking the AUG initiator codon that modulates translation by eukaryotic ribosomes. *Cell*. 1986 Jan 31;44(2):283-92.

89. Kremers GJ, Goedhart J, van Munster EB, Gadella TW Jr (2006) Cyan and yellow super fluorescent proteins with improved brightness, protein folding, and FRET Förster radius. *Biochemistry* 2006 May 30;45(21):6570-80.

90. Kumbalasiri T1, Rollag MD, Isoldi MC, Castrucci AM, Provencio I (2007) Melanopsin triggers the release of internal calcium stores in response to light. *Photochem Photobiol*. 2007 Mar-Apr;83(2):273-9.

91. Kurebayashi N, Harkins AB, Baylor SM (1993) Use of fura red as an intracellular calcium indicator in frog skeletal muscle fibers. *Biophys J*. 1993 Jun;64(6):1934-60.

92. Lam AJ, St-Pierre F, Gong Y, Marshall JD, Cranfill PJ, Baird MA, McKeown MR, Wiedenmann J, Davidson MW, Schnitzer MJ, Tsien RY, Lin MZ (2012) Improving FRET

dynamic range with bright green and red fluorescent proteins. *Nat Methods*. 2012 Oct;9(10):1005-12.

93. Levi J, De A, Cheng Z, Gambhir SS (2007) Bisdeoxycoelenterazine derivatives for improvement of bioluminescence resonance energy transfer assays. *J Am Chem Soc*. 2007 Oct 3;129(39):11900-1.

94. Lewis RS (2007) The molecular choreography of a store-operated calcium channel. *Nature*. 2007 Mar 15;446(7133):284-7.

95. Li G, Wu B, Ward MG, Chong AC, Mukherjee S, Chen S, Hao M (2016) Multifunctional in vivo imaging of pancreatic islets during diabetes development. *J Cell Sci*. 2016 Jul 15;129(14):2865-75.

96. Li X, Gutierrez DV, Hanson MG, Han J, Mark MD, Chiel H, Hegemann P, Landmesser LT, Herlitze S (2005) Fast noninvasive activation and inhibition of neural and network activity by vertebrate rhodopsin and green algae channelrhodopsin. *Proc Natl Acad Sci USA*. 2005 Dec 6;102(49):17816-21.

97. Liang Y, Walczak P, Bulte JW (2012) Comparison of red-shifted firefly luciferase Ppy RE9 and conventional Luc2 as bioluminescence imaging reporter genes for in vivo imaging of stem cells. *J Biomed Opt.* 2012 Jan;17(1):016004.

98. Lin WH, Nebhan CA, Anderson BR, Webb DJ (2010) Vasodilator-stimulated phosphoprotein (VASP) induces actin assembly in dendritic spines to promote their development and potentiate synaptic strength. *J Biol Chem*. 2010 Nov 12;285(46):36010-20.

99. Lipinski CA, Lombardo F, Dominy BW, Feeney PJ (2001) Experimental and computational approaches to estimate solubility and permeability in drug discovery and development settings. *Adv Drug Deliv Rev*. 2001 Mar 1;46(1-3):3-26.

100. Liu Y, Tsinoremas NF, Johnson CH, Lebedeva NV, Golden SS, Ishiura M, Kondo T (1995) Circadian orchestration of gene expression in cyanobacteria. *Genes Dev.* 1995 Jun 15; 9(12):1469-78.

101. Loening AM, Fenn TD, Wu AM, Gambhir SS (2006) Consensus guided mutagenesis of Renilla luciferase yields enhanced stability and light output. *Protein Eng Des Sel*. 2006 Sep; 19(9):391-400.

102. Loening AM, Fenn TD, Gambhir SS (2007) Crystal structures of the luciferase and green fluorescent protein from *Renilla reniformis*. *J Mol Biol*. 2007 Dec 7;374(4):1017-28.

103. Loening AM, Wu AM, Gambhir SS (2007) Red-shifted *Renilla reniformis* luciferase variants for imaging in living subjects. *Nat Methods*. 2007 Aug; 4(8):641-3.

104. Lundin A, Thore A (1975) Analytical information obtainable by evaluation of the time course of firefly bioluminescence in the assay of ATP. *Anal Biochem*. 1975 May 26; 66(1):47-63.

105. Macarron R, Banks MN, Bojanic D, Burns DJ, Cirovic DA, Garyantes T, Green DV, Hertzberg RP, Janzen WP, Paslay JW, Schopfer U, Sittampalam GS (2011) Impact of high-throughput screening in biomedical research. *Nat Rev Drug Discov*. 2011 Mar;10(3):188-95.

106. Magidson V, Khodjakov A (2013) Circumventing photodamage in live-cell microscopy. *Methods Cell Biol*. 2013; 114:545-60.

107. Mank M, Reiff DF, Heim N, Friedrich MW, Borst A, Griesbeck O (2006) A FRET-based calcium biosensor with fast signal kinetics and high fluorescence change. *Biophys J*. 2006 Mar 1;90(5):1790-6.

108. Meighen EA (1991) Molecular biology of bacterial bioluminescence. *Microbiol Rev*. 1991 Mar; 55(1):123-42.

109. Miesenböck G, De Angelis DA, Rothman JE (1998) Visualizing secretion and synaptic transmission with pH-sensitive green fluorescent proteins. *Nature* 1998 Jul 9; 394(6689):192-5.

110. Miesenböck G (2009) The optogenetic catechism. *Science*. 2009 Oct 16;326(5951):395-9.

111. Minta A, Kao JP, Tsien RY (1989) Fluorescent indicators for cytosolic calcium based on rhodamine and fluorescein chromophores. *J Biol Chem*. 1989 May 15;264(14):8171-8.

112. Miyawaki A, Llopis J, Heim R, McCaffery JM, Adams JA, Ikura M, Tsien RY (1997) Fluorescent indicators for Ca^{2+} based on green fluorescent proteins and calmodulin. *Nature*. 1997 Aug 28; 388(6645):882-7.

113. Miyawaki A, Griesbeck O, Heim R, Tsien RY (1999) Dynamic and quantitative Ca^{2+} measurements using improved cameleons. *Proc Natl Acad Sci USA*. 1999 Mar 2;96(5):2135-40.

114. Minsky M (1988) Memoir on inventing the confocal scanning microscope. *Scanning* 10:128-138.

115. Monteiro JP, Alves MG, Oliveira PF, Silva BM (2016). Structure-Bioactivity Relationships of Methylxanthines: Trying to Make Sense of All the Promises and the Drawbacks. *Molecules* 2016, 21, 974.

116. Montminy MR, Bilezikjian LM (1987) Binding of a nuclear protein to the cyclic-AMP response element of the somatostatin gene. *Nature* 328: 175-178.

117. Morin JG, Hastings JW (1971) Energy transfer in a bioluminescent system. *J. Cell Physiol.* 77: 313-316.

118. Murata Y, Iwasaki H, Sasaki M, Inaba K, Okamura Y (2005) Phosphoinositide phosphatase activity coupled to an intrinsic voltage sensor. *Nature* 2005 Jun 30;435(7046):1239-43.

119. Musa MA, Cooperwood JS, Khan MOF (2008). A Review of Coumarin Derivatives in Pharmacotherapy of Breast Cancer. *Curr Med Chem*. 2008, 15, 2664-2679.

120. Nagai T, Ibata K, Park ES, Kubota M, Mikoshiba K, Miyawaki A (2002) A variant of yellow fluorescent protein with fast and efficient maturation for cell-biological applications. *Nat Biotechnol*. 2002 Jan;20(1):87-90.

121. Nagai T, Yamada S, Tominaga T, Ichikawa M, Miyawaki A (2004) Expanded dynamic range of fluorescent indicators for Ca^{2+} by circularly permuted yellow fluorescent proteins. *Proc Natl Acad Sci USA*. 2004 Jul 20;101(29):10554-9.

122. Nagel G, Ollig D, Fuhrmann M, Kateriya S, Musti AM, Bamberg E, Hegemann P (2002) Channelrhodopsin-1: a light-gated proton channel in green algae. *Science*. 2002 Jun 28; 296(5577):2395-8.

123. Nagel G, Szellas T, Huhn W, Kateriya S, Adeishvili N, Berthold P, Ollig D, Hegemann P, Bamberg E (2003) Channelrhodopsin-2, a directly light-gated cation-selective membrane channel. *Proc Natl Acad Sci USA*. 2003 Nov 25; 100(24):13940-5.

124. Nagel G, Brauner M, Liewald JF, Adeishvili N, Bamberg E, Gottschalk A (2005) Light activation of channelrhodopsin-2 in excitable cells of Caenorhabditis elegans triggers rapid behavioral responses. *Curr Biol.* 2005 Dec 20; 15(24):2279-84.

125. Naumann EA, Kampff AR, Prober DA, Schier AF, Engert F (2010) Monitoring neural activity with bioluminescence during natural behavior. *Nat Neurosci*. 2010 Apr;13(4):513-20.

126. Nguyen AW, Daugherty PS (2005) Evolutionary optimization of fluorescent proteins for intracellular FRET. *Nat Biotechnol*. 2005 Mar;23(3):355-60.

127. Nguyen JP, Shipley FB, Linder AN, Plummer GS, Liu M, Setru SU, Shaevitz JW, Leifer AM (2016) Whole-brain calcium imaging with cellular resolution in freely behaving *Caenorhabditis elegans*. *Proc Natl Acad Sci USA*. 2016 Feb 23;113(8):E1074-81.

128. Niwa H, Yamamura K, Miyazaki J (1991) Efficient selection for high-expression transfectants with a novel eukaryotic vector. *Gene*. 1991 Dec 15;108(2):193-9.

129. Niwa K, Ichino Y, Kumata S, Nakajima Y, Hiraishi Y, Kato D, Viviani VR, Ohmiya Y (2010) Quantum yields and kinetics of the firefly bioluminescence reaction of beetle luciferases. *Photochem Photobiol*. 2010 Sep-Oct;86(5):1046-9.

130. Nolan EM, Lippard SJ (2009) Small-molecule fluorescent sensors for investigating zinc metalloneurochemistry. *Acc Chem Res*. 2009 Jan 20; 42(1):193-203.

131. Okkema PG, Harrison SW, Plunger V, Aryana A, Fire A (1993) Sequence requirements for myosin gene expression and regulation in *Caenorhabditis elegans*. *Genetics*. 1993 Oct;135(2):385-404.

132. Ono D, Honma S, Honma K (2013) Cryptochromes are critical for the development of coherent circadian rhythms in the mouse suprachiasmatic nucleus. *Nat Commun*. 2013; 4:1666.

133. Ono D, Honma K, Honma S (2015) Circadian and ultradian rhythms of clock gene expression in the suprachiasmatic nucleus of freely moving mice. *Sci Rep*. 2015 Jul 21;5:12310.

134. Otto-Duessel M, Khankaldyyan V, Gonzalez-Gomez I, Jensen MC, Laug WE, Rosol M (2006) In vivo testing of Renilla luciferase substrate analogs in an orthotopic murine model of human glioblastoma. *Mol Imaging*. 2006 Apr-Jun; 5(2):57-64.

135. Ouyang Y, Andersson CR, Kondo T, Golden SS, Johnson CH (1998) Resonating circadian clocks enhance fitness in cyanobacteria. *Proc Natl Acad Sci USA*. 1998 Jul 21; 95(15):8660-4.

136. Parikh SS, Blackwell DJ, Gomez-Hurtado N, Frisk M, Wang L, Kim K, Dahl CP, Fiane A, Tønnessen T, Kryshtal DO, Louch WE, Knollmann BC (2017) Thyroid and Glucocorticoid Hormones Promote Functional T-Tubule Development in Human-Induced Pluripotent Stem Cell-Derived Cardiomyocytes. *Circ Res*. 2017 Dec 8;121(12):1323-1330.

137. Patterson GH, Lippincott-Schwartz J (2002) A photoactivatable GFP for selective photolabeling of proteins and cells. *Science* 2002 Sep 13;297(5588):1873-7.

138. Patterson M, Chan DN, Ha I, Case D, Cui Y, Van Handel B, Mikkola HK, Lowry WE (2012) Defining the nature of human pluripotent stem cell progeny. *Cell Res*. 2012 Jan;22(1):178-93.

139. Pfleger KD, Dromey JR, Dalrymple MB, Lim EM, Thomas WG, Eidne KA (2006) Extended bioluminescence resonance energy transfer (eBRET) for monitoring prolonged protein-protein interactions in live cells. *Cell Signal*. 2006 Oct;18(10):1664-70.

140. Philipson LH, Rosenberg MP, Kuznetsov A, Lancaster ME, Worley JF 3rd, Roe MW, Dukes ID (1994) Delayed rectifier K^+ channel overexpression in transgenic islets and beta-cells associated with impaired glucose responsiveness. *J Biol Chem*. 1994 Nov 11;269(45):27787-90.

141. Piatkevich KD, Malashkevich VN, Morozova KS, Nemkovich NA, Almo SC, Verkhusha VV (2013) Extended Stokes shift in fluorescent proteins: chromophore-protein interactions in a near-infrared TagRFP675 variant. *Sci Rep*. 2013;3:1847.

142. Pincus Z, Mazer TC, Slack FJ (2016) Autofluorescence as a measure of senescence in *C. elegans*: look to red, not blue or green. *Aging (Albany NY)*. 2016 May;8(5):889-98.

143. Piston DW, Kremers GJ (2007) Fluorescent protein FRET: the good, the bad and the ugly. *Trends Biochem Sci*. 2007 Sep; 32(9):407-14.

144. Prasher D, McCann RO, Cormier MJ (1985) Cloning and expression of the cDNA coding for aequorin, a bioluminescent calcium-binding protein. *Biochem Biophys Res Commun.* 1985 Feb 15;126(3):1259-68.

145. Prasher DC, Eckenrode VK, Ward WW, Prendergast FG, Cormier MJ (1992) Primary structure of the Aequorea victoria green-fluorescent protein. *Gene* 11:229-233.

146. Qiu X, Kumbalasiri T, Carlson SM, Wong KY, Krishna V, Provencio I, Berson DM (2005) Induction of photosensitivity by heterologous expression of melanopsin. *Nature*. 2005 Feb 17;433(7027):745-9.

147. Reddy AR, Prasad DV, Darbarwar M (1986). Absorption and fluorescence spectra of 7-aminocoumarin derivatives. *J Photochem*. 32, 1, 69-80.

148. Ridgway EB, Ashley CC (1967) Calcium transients in single muscle fibers. *Biochem. Biophys. Res. Commun.* 29(2): 229-34.

149. Ridgway EB, Gilkey JC, Jaffe LF (1977) Free calcium increases explosively in activating medaka eggs. Proc. Natl. Acad. Sci. USA 72(2): 623-627.

150. Rizzo MA, Springer GH, Granada B, Piston DW (2004) An improved cyan fluorescent protein variant useful for FRET. *Nat Biotechnol.* 2004 Apr;22(4):445-9.

151. Rodriguez EA, Campbell RE, Lin JY, Lin MZ, Miyawaki A, Palmer AE, Shu X, Zhang J, Tsien RY (2017). The Growing and Glowing Toolbox of Fluorescent and Photoactive Proteins. *Trends Biochem Sci*. 42: 111-129.

152. Rodriguez JF, Rodriguez D, Rodriguez JR, McGowan EB, Esteban M (1988) Expression of the firefly luciferase gene in vaccinia virus: a highly sensitive gene marker to follow virus dissemination in tissues of infected animals. *Proc Natl Acad Sci USA*. 1988 Mar;85(5):1667-71.

153. Rogers KL, Stinnakre J, Agulhon C, Jublot D, Shorte SL, Kremer EJ, Brûlet P (2005) Visualization of local Ca^{2+} dynamics with genetically encoded bioluminescent reporters. *Eur J Neurosci*. 2005 Feb; 21(3):597-610.

154. Rutter GA, Hodson DJ, Chabosseau P, Haythorne E, Pullen TJ, Leclerc I (2017) Local and regional control of calcium dynamics in the pancreatic islet. *Diabetes Obes Metab*. 2017 Sep;19 Suppl 1:30-41.

155. Saito K, Hatsugai N, Horikawa K, Kobayashi K, Matsu-Ura T, Mikoshiba K, Nagai T (2010) Auto-luminescent genetically-encoded ratiometric indicator for real-time Ca^{2+} imaging at the single cell level. *PLoS One*. 2010 Apr 1;5(4):e9935.

156. Saito K, Chang YF, Horikawa K, Hatsugai N, Higuchi Y, Hashida M, Yoshida Y, Matsuda T, Arai Y, Nagai T (2012) Luminescent proteins for high-speed single-cell and whole-body imaging. *Nat Commun*. 2012; 3:1262.

157. Sauvé R, Diarra A, Chahine M, Simoneau C, Garneau L, Roy G (1990) Single-channel and Fura-2 analysis of internal Ca^{2+} oscillations in HeLa cells: contribution of the receptor-evoked Ca^{2+} influx and effect of internal pH. *Pflugers Arch*. 1990 Apr;416(1-2):43-52.

158. Shaner NC, Campbell RE, Steinbach PA, Giepmans BN, Palmer AE, Tsien RY (2004) Improved monomeric red, orange and yellow fluorescent proteins derived from *Discosoma* sp. red fluorescent protein. *Nat Biotechnol*. 2004 Dec;22(12):1567-72.

159. Shaner NC, Lambert GG, Chammas A, Ni Y, Cranfill PJ, Baird MA, Sell BR, Allen JR, Day RN, Israelsson M, Davidson MW, Wang J (2013) A bright monomeric green fluorescent protein derived from *Branchiostoma lanceolatum*. *Nat Methods*. 2013 May;10(5):407-9.

160. Shimomura O, Johnson FH, Saiga Y (1962) Extraction, purification and properties of aequorin, a bioluminescent protein from the luminous hydromedusan, Aequorea. *J Cell Comp Physiol.* 1962 Jun;59:223-39.

161. Shimomura O, Masugi T, Johnson FH, Haneda Y (1978) Properties and reaction mechanism of the bioluminescence system of the deep-sea shrimp *Oplophorus gracilorostris*. *Biochemistry* 1978 Mar 21; 17(6):994-8.

162. Shimomura O (2005) The discovery of aequorin and green fluorescent protein. *J Microsc.* 2005 Jan;217(Pt 1):1-15.

163. Shukla MK, Mishra PC. (1994). Electronic spectra and structures of some biologically important xanthines. *J Mol Struct.* 324, (1994) 241-249.

164. Siebring-van Olst E, van Beusechem VW. (2018). High-throughput Firefly Luciferase Reporter Assays. *Methods Mol Biol*. 2018, 1755:19-29.

165. Suzuki K, Kimura T, Shinoda H, Bai G, Daniels MJ, Arai Y, Nakano M, Nagai T (2016) Five colour variants of bright luminescent protein for real-time multicolour bioimaging. *Nat Commun*. 2016 Dec 14;7:13718.

166. Tackenberg MC, McMahon DG (2018) Photoperiodic Programming of the SCN and Its Role in Photoperiodic Output. *Neural Plast*. 2018 Jan 9; 2018:8217345.

167. Takahashi K, Yamanaka S (2006) Induction of pluripotent stem cells from mouse embryonic and adult fibroblast cultures by defined factors. *Cell*. 2006 Aug 25;126(4):663-76.

168. Tannous BA, Kim DE, Fernandez JL, Weissleder R, Breakefield XO (2005) Codon-optimized Gaussia luciferase cDNA for mammalian gene expression in culture and in vivo. *Mol Ther*. 2005 Mar;11(3):435-43.

169. Teuscher AC, Ewald CY (2018) Overcoming Autofluorescence to Assess GFP Expression During Normal Physiology and Aging in *Caenorhabditis elegans*. *Bio Protoc*. 2018 Jul 20;8(14). pii: e2940.

170. Thestrup T, Litzlbauer J, Bartholomäus I, Mues M, Russo L, Dana H, Kovalchuk Y, Liang Y, Kalamakis G, Laukat Y, Becker S, Witte G, Geiger A, Allen T, Rome LC, Chen TW, Kim DS, Garaschuk O, Griesinger C, Griesbeck O (2014) Optimized ratiometric calcium

sensors for functional in vivo imaging of neurons and T lymphocytes. *Nat Methods*. 2014 Feb;11(2):175-82.

171. Thorn P (1995) Ca^{2+} influx during agonist and Ins(2,4,5)P3-evoked Ca^{2+} oscillations in HeLa epithelial cells. *J Physiol*. 1995 Jan 15;482 (Pt 2):275-81.

172. Tomabechi Y, Hosoya T, Ehara H, Sekine SI, Shirouzu M, Inouye S (2016) Crystal structure of nanoKAZ: The mutated 19 kDa component of Oplophorus luciferase catalyzing the bioluminescent reaction with coelenterazine. *Biochem Biophys Res Commun*. 2016 Jan 29; 470(1):88-93.

173. Tong J, Du GG, Chen SR, MacLennan DH (1999) HEK-293 cells possess a carbachol- and thapsigargin-sensitive intracellular Ca^{2+} store that is responsive to stop-flow medium changes and insensitive to caffeine and ryanodine. *Biochem J*. 1999 Oct 1;343 Pt 1:39-44.

174. Tsien RY, Rink TJ, Poenie M (1985) Measurement of cytosolic free Ca^{2+} in individual small cells using fluorescence microscopy with dual excitation wavelengths. *Cell Calcium*. 1985 Apr;6(1-2):145-57.

175. Tsien RY (1998) The green fluorescent protein. *Annu. Rev. Biochem*. 1998. 67:509–44.

176. Ugarova NN, Maloshenok LG, Uporov IV, Koksharov MI (2005) Bioluminescence Spectra of Native and Mutant Firefly Luciferases as a Function of pH. *Biochemistry (Mosc).* 2005 Nov;70(11):1262-7.

177. Ustione A, Piston DW (2011) A simple introduction to multiphoton microscopy. *J Microsc*. 2011 Sep; 243(3):221-6.

178. Vetter I (2012) Development and optimization of FLIPR high throughput calcium assays for ion channels and GPCRs. *Adv Exp Med Biol*. 2012;740:45-82.

179. Viatchenko-Karpinski S, Fleischmann BK, Liu Q, Sauer H, Gryshchenko O, Ji GJ, Hescheler J (1999) Intracellular Ca^{2+} oscillations drive spontaneous contractions in cardiomyocytes during early development. *Proc Natl Acad Sci USA*. 1999 Jul 6;96(14):8259-64.

180. Viviani VR (2002) The origin, diversity, and structure function relationships of insect luciferases. *Cell Mol Life Sci.* 2002 Nov;59(11):1833-50.

181. Virostko J, Jansen ED, Powers AC (2006) Current status of imaging pancreatic islets. *Curr Diab Rep*. 2006 Aug;6(4):328-32.

182. Wäldchen S, Lehmann J, Klein T, van de Linde S, Sauer M (2015) Light-induced cell damage in live-cell super-resolution microscopy. *Sci Rep.* 2015 Oct 20;5:15348.

183. Wang Q, Shui B, Kotlikoff MI, Sondermann H (2008) Structural basis for calcium sensing by GCaMP2. *Structure*. 2008 Dec 10;16(12):1817-27.

184. Webb DJ, Brown CM (2013) Epi-fluorescence microscopy. *Methods Mol Biol*. 2013;931:29-59.

185. Wegner AM, Nebhan CA, Hu L, Majumdar D, Meier KM, Weaver AM, Webb DJ (2008) N-wasp and the arp2/3 complex are critical regulators of actin in the development of dendritic spines and synapses. *J Biol Chem*. 2008 Jun 6;283(23):15912-20.

186. Widder EA (2010) Bioluminescence in the ocean: origins of biological, chemical, and ecological diversity. *Science*. 2010 May 7;328(5979):704-8.

187. Wilson T, Hastings JW (1998) Bioluminescence. *Annu. Rev. Cell. Dev. Biol.* 1998. 14: 197-230.

188. Wilson T, Hastings JW (2013) Bioluminescence: Living Lights, Lights for Living. Cambridge, MA: Harvard University Press.

189. Xu X, Soutto M, Xie Q, Servick S, Subramanian C, von Arnim AG, Johnson CH (2007) Imaging protein interactions with bioluminescence resonance energy transfer (BRET) in plant and mammalian cells and tissues. *Proc Natl Acad Sci USA*. 2007 Jun 12;104(24):10264-9.

190. Xu Y, Piston DW, Johnson CH (1999) A bioluminescence resonance energy transfer (BRET) system: application to interacting circadian clock proteins. *Proc Natl Acad Sci USA.* 1999 Jan 5;96(1):151-6.

191. Yamazaki S, Numano R, Abe M, Hida A, Takahashi R, Ueda M, Block GD, Sakaki Y, Menaker M, Tei H (2000) Resetting central and peripheral circadian oscillators in transgenic rats. *Science*. 2000 Apr 28;288(5466):682-5.

192. Yang J, Cumberbatch D, Centanni S, Shi SQ, Winder D, Webb D, Johnson CH (2016) Coupling optogenetic stimulation with NanoLuc-based luminescence (BRET) Ca^{++} sensing. *Nat Commun*. 2016 Oct 27;7:13268.

193. Yang TT, Cheng L, Kain SR (1996) Optimized codon usage and chromophore mutations provide enhanced sensitivity with the green fluorescent protein. *Nucleic Acids Res.* 1996 Nov 15;24(22):4592-3.

194. Yin DZ, Brunk UT (1991) Microfluorometric and fluorometric lipofuscin spectral discrepancies: a concentration-dependent metachromatic effect? *Mech Ageing Dev*. 1991 Jun 14;59(1-2):95-109.

195. Yin J, Wang J (2016) Renal drug transporters and their significance in drug-drug interactions. *Acta Pharm Sin B*. 2016 Sep;6(5):363-373.

196. Yoo SH, Yamazaki S, Lowrey PL, Shimomura K, Ko CH, Buhr ED, Siepka SM, Hong HK, Oh WJ, Yoo OJ, Menaker M, Takahashi JS (2004) PERIOD2::LUCIFERASE real-

time reporting of circadian dynamics reveals persistent circadian oscillations in mouse peripheral tissues. *Proc Natl Acad Sci USA*. 2004 Apr 13;101(15):5339-46.

197. Zhang F, Wang LP, Brauner M, Liewald JF, Kay K, Watzke N, Wood PG, Bamberg E, Nagel G, Gottschalk A, Deisseroth K (2007) Multimodal fast optical interrogation of neural circuitry. *Nature*. 2007 Apr 5;446(7136):633-9.

198. Zhang JH, Chung TD, Oldenburg KR (1999) A Simple Statistical Parameter for Use in Evaluation and Validation of High Throughput Screening Assays. *J Biomol Screen*. 1999;4(2):67-73.

199. Zhang R, Xie X (2012) Tools for GPCR drug discovery. *Acta Pharmacol Sin*. 2012 Mar;33(3):372-84.

200. Zhang Y, Xie Q, Robertson JB, Johnson CH (2012) pHlash: a new genetically encoded and ratiometric luminescence sensor of intracellular pH. *PLoS One*. 2012;7(8):e43072.

201. Zhao H, Doyle TC, Wong RJ, Cao Y, Stevenson DK, Piwnica-Worms D, Contag CH (2004) Characterization of coelenterazine analogs for measurements of Renilla luciferase activity in live cells and living animals. *Mol Imaging*. 2004 Jan; 3(1):43-54.

202. Zhao H, Doyle TC, Coquoz O, Kalish F, Rice BW, Contag CH (2005) Emission spectra of bioluminescent reporters and interaction with mammalian tissue determine the sensitivity of detection in vivo. *J Biomed Opt.* 2005 Jul-Aug;10(4):41210.

203. Zhao Y, Araki S, Wu J, Teramoto T, Chang YF, Nakano M, Abdelfattah AS, Fujiwara M, Ishihara T, Nagai T, Campbell RE (2011) An expanded palette of genetically encoded Ca^{2+} indicators. *Science*. 2011 Sep 30;333(6051):1888-91.

204. Zhong W, Maradit-Kremers H, St Sauver JL, Yawn BP, Ebbert JO, Roger VL, Jacobson DJ, McGree ME, Brue SM, Rocca WA (2013) Age and sex patterns of drug prescribing in a defined American population. *Mayo Clin Proc*. 2013 Jul;88(7):697-707.